October 2006
Research Report: UCPRC-RR-2006-08

Reflective Cracking Study: First-Level Report on Laboratory Fatigue Testing

Authors:
B. Tsai, D. Jones, J. Harvey, and C. Monismith

Partnered Pavement Research Program (PPRC) Contract Strategic Plan Element 4.10:
Development of Improved Rehabilitation Designs for Reflective Cracking

PREPARED FOR:

California Department of Transportation
Division of Research and Innovation
Office of Roadway Research

PREPARED BY:

University of California
Pavement Research Center
UC Davis, UC Berkeley

DOCUMENT RETRIEVAL PAGE		**Research Report: UCPRC-RR-2006-08**
Title: Reflective Cracking Study: First-Level Report on Laboratory Fatigue Testing		
Authors: B. Tsai, D. Jones, J. Harvey and C Monismith		
Prepared for: Caltrans	**FHWA No:** CA091073E	**Date**: October 2006
Contract No: 65A0172	**Client Reference No:** SPE 4.10	**Status:** Stage 6, Approved Version

Abstract:

This report contains a summary of the laboratory fatigue tests on mixes used as overlays on the Reflective Cracking Study Test Track at the Richmond Field Station. Evaluation of the results of the laboratory study on fatigue response of the overlay mixes reported herein included the effects of mix temperatures, air-void content, aging, mixing and compaction conditions, aggregate gradation, and time of loading. Five binders were assessed, namely AR4000, asphalt rubber (Type G), and three modified binders, termed MB4, MB15, and MAC15. A full factorial considering all the variables required a total of 1,440 tests. This was reduced to 172 tests to accommodate time and fund constraints. Based on the fatigue test results for the mixes used in the overlay experiment, mix rankings for initial stiffness and fatigue life are, from highest to lowest, as follows:

Initial stiffness	**Fatigue life**
AR4000-D	MB4-G
RAC-G	MB15-G and MAC15-G
MAC15-G	RAC-G
MB4-G and MB15-G	AR4000-D

Until a range of pavement types and environments are evaluated in the 2nd Level Analysis, only a general indication of the relative performance of the modified binders can be deduced. It would appear that the MB4, MB15, and MAC15 binders used in gap-graded mixes as overlays on existing cracked asphalt concrete pavements should provide comparable lives (at least) to RAC-G mixes when used in comparable thicknesses in thin layers (less than about 60 mm). Recommendations for the use of MB4, MB15 and MAC15 binders in thicker layers and as dense-graded mixes await the results of the shear test results and pavement performance analyses.

Keywords:
Reflective cracking, overlay, modified binder, fatigue testing, HVS test, MB Road

Proposals for implementation:

Related documents:
UCPRC-RR-2005-03, UCPRC-RR-2006-09

Signatures:

B. Tsai 1st Author	C Monismith Technical Review	D. Spinner Editor	J. Harvey Principal Investigator	M Samadian Caltrans Contract Manager

DISCLAIMER

The contents of this report reflect the views of the authors who are responsible for the facts and accuracy of the data presented herein. The contents do not necessarily reflect the official views or policies of the State of California or the Federal Highway Administration. This report does not constitute a standard, specification, or regulation.

PROJECT OBJECTIVES

The objective of this project is to develop improved rehabilitation designs for reflective cracking for California.

This objective will be met after completion of four tasks identified by the Caltrans/Industry Rubber Asphalt Concrete Task Group (RACTG):

1. Develop improved mechanistic models of reflective cracking in California,
2. Calibrate and verify these models using laboratory and HVS testing,
3. Evaluate the most effective strategies for reflective cracking, and
4. Provide recommendations for reflective cracking strategies

This document is one of a series addressing Tasks 2 and 3.

ACKNOWLEDGEMENTS

The University of California Pavement Research Center acknowledges the assistance of the Rubber Pavements Association, Valero Energy Corporation, and Paramount Petroleum which contributed funds and asphalt binders for the construction of the Heavy Vehicle Simulator test track discussed in this study.

REFLECTIVE CRACKING STUDY REPORTS

The reports prepared during the reflective cracking study document data from construction, Heavy Vehicle Simulator (HVS) tests, laboratory tests, and subsequent analyses. These include a series of first- and second-level analysis reports and two summary reports. On completion of the study this suite of documents will include:

1. Reflective Cracking Study: Summary of Construction Activities, Phase 1 HVS testing and Overlay Construction (UCPRC-RR-2005-03).
2. Reflective Cracking Study: First-level Report on the HVS Rutting Experiment (UCPRC-RR-2007-06).
3. Reflective Cracking Study: First-level Report on HVS Testing on Section 590RF — 90 mm MB4-G Overlay (UCPRC-RR-2006-04).
4. Reflective Cracking Study: First-level Report on HVS Testing on Section 589RF — 45 mm MB4-G Overlay (UCPRC-RR-2006-05).
5. Reflective Cracking Study: First-level Report on HVS Testing on Section 587RF — 45 mm RAC-G Overlay (UCPRC-RR-2006-06).
6. Reflective Cracking Study: First-level Report on HVS Testing on Section 588RF — 90 mm AR4000-D Overlay (UCPRC-RR-2006-07).
7. Reflective Cracking Study: First-level Report on HVS Testing on Section 586RF — 45 mm MB15-G Overlay (UCPRC-RR-2006-12).
8. Reflective Cracking Study: First-level Report on HVS Testing on Section 591RF — 45 mm MAC15-G Overlay (UCPRC-RR-2007-04).
9. Reflective Cracking Study: HVS Test Section Forensic Report (UCPRC-RR-2007-05).
10. Reflective Cracking Study: First-level Report on Laboratory Fatigue Testing (UCPRC-RR-2006-08).
11. Reflective Cracking Study: First-level Report on Laboratory Shear Testing (UCPRC-RR-2006-11).
12. Reflective Cracking Study: Backcalculation of FWD Data from HVS Test Sections (UCPRC-RR-2007-08).
13. Reflective Cracking Study: Second-level Analysis Report (UCPRC-RR-2007-09).
14. Reflective Cracking Study: Summary Report (UCPRC-SR-2007-01). Detailed summary report.
15. Reflective Cracking Study: Summary Report (UCPRC-SR-2007-03). Four-page summary report.

CONVERSION FACTORS

SI* (MODERN METRIC) CONVERSION FACTORS				
APPROXIMATE CONVERSIONS TO SI UNITS				
Symbol	**Convert From**	**Multiply By**	**Convert To**	**Symbol**
LENGTH				
in	inches	25.4	millimeters	mm
ft	feet	0.305	meters	m
AREA				
in^2	square inches	645.2	square millimeters	mm^2
ft^2	square feet	0.093	square meters	m2
VOLUME				
ft^3	cubic feet	0.028	cubic meters	m^3
MASS				
lb	pounds	0.454	kilograms	kg
TEMPERATURE (exact degrees)				
°F	Fahrenheit	5 (F-32)/9 or (F-32)/1.8	Celsius	C
FORCE and PRESSURE or STRESS				
lbf	poundforce	4.45	newtons	N
lbf/in^2	poundforce/square inch	6.89	kilopascals	kPa
APPROXIMATE CONVERSIONS FROM SI UNITS				
Symbol	**Convert From**	**Multiply By**	**Convert To**	**Symbol**
LENGTH				
mm	millimeters	0.039	inches	in
m	meters	3.28	feet	ft
AREA				
mm^2	square millimeters	0.0016	square inches	in^2
m^2	square meters	10.764	square feet	ft^2
VOLUME				
m^3	cubic meters	35.314	cubic feet	ft^3
MASS				
kg	kilograms	2.202	pounds	lb
TEMPERATURE (exact degrees)				
C	Celsius	1.8C+32	Fahrenheit	F
FORCE and PRESSURE or STRESS				
N	newtons	0.225	poundforce	lbf
kPa	kilopascals	0.145	poundforce/square inch	lbf/in^2

*SI is the symbol for the International System of Units. Appropriate rounding should be made to comply with Section 4 of ASTM E380. (Revised March 2003)

GLOSSARY OF TERMS

av	Percent air-void content
BBR	Bending Beam Rheometer
binder	Binder types including AR4000, ARB, MB4, MB15, and MAC15
comp	Compaction including FMFC, FMLC, and LMLC
cond	Conditioning, either aging or non-aging
DSR	Dynamic Shear Rheometer
E^*	Dynamic mix elastic complex modulus in MPa
G*	Dynamic binder shear complex modulus in kPa
grad	Gradation
FMFC	Field-mixed field-compacted
FMLC	Field-mixed laboratory-compacted
LMLC	Laboratory-mixed laboratory-compacted
lnaT	Natural logarithm of temperature shift factor
lnα_1 and β_1	Intercept and slope of Stage I of a three-stage fatigue/shear Weibull curve
lnα_2 and β_2	Intercept and slope of Stage II of a three-stage fatigue/shear Weibull curve
lnα_3 and β_3	Intercept and slope of Stage III of a three-stage fatigue/shear Weibull curve
ln$G$	Initial resilient shear modulus (MPa) in natural logarithm
ln*kcy5*	Permanent shear strain after 5,000 loading cycles
lnn_1	Separation point between Stage I and Stage II of a three-stage fatigue/shear Weibull curve
lnn_2	Separation point between Stage II and Stage III of a three-stage fatigue/shear Weibull curve
ln*Nf*	Traditional fatigue life (repetitions at 50 percent loss of initial stiffness) in natural logarithm
ln*pct5*	Cycles to 5 percent permanent shear strain (in natural logarithm)
ln*stif*	Initial stiffness (MPa) in natural logarithm
ln*stn*	Strain level in natural logarithm
ln*sts*	Stress level (kPa) in natural logarithm
nf	Fatigue life
pa	Phase angle
PAV	Pressure Aging Vessel
PSS	Permanent shear strain
RSS	Residual sum of squares
RTFO	Rolling Thin Film Oven
SR	Stiffness ratio
srn_1	Stage I stiffness ratio in a three-stage fatigue Weibull curve
srn_2	Stage II stiffness ratio in a three-stage fatigue Weibull curve
temp	Temperature in °C
γ_1	Parameter that determines the degree of slope change from Stage I to Stage II of a three-stage fatigue/shear Weibull curve
γ_2	Parameter that determines the degree of slope change from Stage II to Stage III of a three-stage fatigue/shear Weibull curve

EXECUTIVE SUMMARY

This report contains a summary of the laboratory fatigue tests on mixes used as overlays on the Reflective Cracking Study Test Road at the Richmond Field Station. The laboratory mix fatigue study is one phase of the overall program to evaluate reflective cracking performance of conventional asphalt and modified binder mixes used as overlays for the rehabilitation of cracked asphalt concrete pavements in California. The study is a part of the Partnered Pavement Research Center (PPRC) Strategic Plan Element (SPE) 4.10 entitled, "Development of Improved Rehabilitation Designs for Reflective Cracking." The SPE includes:

- Development of an improved analytical methodology for analysis and design of structural overlays;
- Laboratory studies to define the fatigue and permanent deformation characteristics of the overlay mixes; and
- Heavy Vehicle Simulator (HVS) accelerated pavement tests on a full-scale pavement structure containing overlays including both a conventional asphalt mix and mixes containing binders modified with crumb rubber and polymers.

The overlays and the underlying pavement structure for the full scale tests were designed and constructed according to standard Caltrans specifications and procedures. HVS testing was divided into two phases:

- Phase 1: the specially constructed test pavement was trafficked on six different sections to induce fatigue cracking in the asphalt concrete layer; and
- Phase 2: the overlay mixes containing the conventional and modified binders were placed to evaluate both their reflective cracking response on the cracked existing pavement sections and their rutting response on the uncracked adjacent portions of the underlying asphalt concrete.

Evaluation of the results of the laboratory study on fatigue response of the overlay mixes reported herein included the effects of the following variables:

- Mix temperatures
- Air-void content,
- Aging,
- Mixing and compaction conditions,
- Aggregate gradation, and
- Time of loading (load frequency)

Five binders were included in this study: AR4000, asphalt rubber (Type G), and three modified binders, termed MB4, MB15, and MAC15. The modified binders were used in all gap-graded mixes, the AR4000 was used in a dense-graded asphalt concrete (DGAC) mix, and the asphalt rubber Type G binder (ARB) was used in a gap-graded rubber asphalt concrete (RAC-G) mix. The modified binders were terminal-blended, rubber modified binders whereas the Type G asphalt rubber binder was blended on site prior to mixing with aggregate to produce the RAC-G mix. The mixes containing the five binders comprised the overlay sections for the accelerated loading tests using the HVS.

A comprehensive experimental design was prepared for the study. To test the full factorial considering all the variables, a total of 1,440 tests would have been required. Because of time and fund constraints, a partial factorial experiment was completed with 172 tests.

Laboratory fatigue testing was carried out on beams cut from slabs prepared using rolling wheel compaction. Materials were sampled from:

- Loose mix collected from the paver during construction and stored in sealed containers until ready for compaction and testing, referred to as field-mixed, laboratory-compacted (FMLC) samples in the report, and
- Binder and aggregate stockpiles at the asphalt plant, referred to as laboratory-mixed, laboratory-compacted (LMLC) samples in the report. These samples were included in the study to assess the potential for using the modified binders in dense-graded as well as in gap-graded mixes.

The binder contents for the AR4000-D and RAC-G mixes were based on Caltrans mix design requirements (Section 39 of the Standard Specifications for the DGAC and Section 39-10 of the Standard Special Provisions for the RAC-G). Binder contents for the gap-graded mixes with the MB4, MB15 and MAC15 binders were recommended by the binder suppliers.

Flexural fatigue testing and stiffness (frequency sweep) determinations followed the AASHTO T321 procedure (four point bending). Fatigue tests were all conducted at 10 Hz. Stiffness measurements were conducted over the range of 15 Hz to 0.01 Hz and at temperatures of 10°C (50°F), 20°C (68°F), and 30°C (86°F) to define the effect of time-of-loading and temperature on this mix characteristic. These mix stiffnesses are essential for the performance evaluation to be presented in the 2nd Level Analysis report.

For the LMLC dense-graded mixes containing the modified binders, the standard California procedure for mix design (Section 39 of the Standard Specifications) was followed to define the binder contents used for the beam specimens.

Binder tests on the AR4000, MB4, MB15, and MAC15 were performed by the Federal Highway Administration and included the Bending Beam Rheometer (BBR) and the Dynamic Shear Rheometer (DSR) over a range of loading times (BBR) and frequencies (DSR). The asphalt rubber binder was not tested due to limitations of the equipment used with respect to crumb rubber. Specimens were tested in their original condition, short-term aged using the Rolling Thin Film Oven Test, and long-term aged using the Pressure Aging Vessel Test. Based on the current specification requirements, binder rankings considering low-temperature cracking, fatigue, and rutting are as follows, ranked from least to highest susceptibility:

Low Temperature Cracking	Fatigue	Permanent Deformation
MB4	MB4	AR4000
MB15	MB15	MB4 and MB15
MAC15	MAC15	MAC15
AR4000	AR4000	

Significant factors affecting fatigue response were identified using:

- A correlation matrix
- Analysis of variance (ANOVA)
- Design plots, and
- Pairs diagrams.

This approach was deemed essential since a partial factor experiment (172 tests) rather than a full factorial (1,440 tests) was conducted. By using this approach, greater confidence can be achieved that the major effects were included in any performance equation resulting from the experiment to predict the performance of a mix containing a specific binder in pavement structures subjected to a range in traffic and environmental conditions.

Test Effects

The binder type had an overall effect on all the response variables including initial phase angle, initial stiffness, and fatigue life. As expected, the temperature effect on all three response variables was immediately apparent. The other effects assessed at 20°C (68°F)(for comparison with HVS testing) revealed that:

- Air-void content had a significant effect for some parts of the experiment, such as the FMLC mixes at 20°C, but the effect was not significant for many of the mixes and test conditions for all of the response variables.
- The aging effect was only significant for initial phase angle and stiffness but not for fatigue life.

- All the response variables were significantly affected by the change from a gap-gradation to a dense-gradation for the MAC15-G, MB15-G, and MB4-G mixes.

Ranking of Initial Stiffness and Fatigue Performance

The ranking of predicted initial stiffness and fatigue life under various specimen preparation and testing conditions, and specifically for the controlled strain mode of loading used in this experiment, was normally in the order listed below. For initial stiffness, no apparent differences existed between the MB15-G and MB4-G mixes, while for fatigue life, no apparent differences existed between the MAC15-G and MB15-G mixes. As expected, the two orders are reversed.

Initial Stiffness	Fatigue Life
1. AR4000-D	1. MB4-G
2. RAC-G	2. MB15-G and MAC15-G
3. MAC15-G	3. RAC-G
4. MB4-G and MB15-G	4. AR4000-D

While the fatigue tests on the dense-graded mixes containing the three modified binders were limited, the initial stiffnesses of these three dense-graded mixes were generally greater than those of the corresponding gap-graded mixes but less than those of the AR4000-D and RAC-G mixes. Beam fatigue lives at a given tensile strain of the dense-graded mixes were generally less than those of the corresponding gap-graded mixes, but greater than those of the AR4000-D and RAC-G mixes. Any improvement in rutting resistance from increased stiffnesses of the dense-graded mixes with MB4, MB15, and MAC15 binders over those of the corresponding gap-graded mixes will be discussed in the report on laboratory shear testing.

Fatigue test results indicated that initial stiffness and fatigue life were moderately negative-correlated (ρ = -0.604), confirming a general observation that lower stiffnesses equate to higher fatigue life at a given tensile strain under controlled-strain testing when ranking fatigue life performance against initial stiffness or vice versa. However, when using this observation, consideration must also be given to rutting, as mixes with low stiffness are generally susceptible to this distress.

Preliminary analysis of stiffness versus strain repetition curves using three-stage Weibull analysis indicated differences in crack initiation and propagation. The AR4000-D mix had different behavior from that of the RAC-G mix, while the RAC-G mix performed differently than the MB4-G, MB15-G, and MAC15-G mixes. The results indicate that damage may slow during the propagation phase of the latter four mixes, while it accelerates for the AR4000-D mix.

Dense-Graded versus Gap-Graded Mixes (laboratory-mix, laboratory compact)

The optimum binder contents used in the mix designs for the MAC15, MB15, and MB4 dense-graded mixes (6.0, 6.0, and 6.3 percent respectively) were lower than the optimum binder contents used in the mix designs of the gap-graded mixes (7.4, 7.1, and 7.2 percent respectively).

Limited fatigue testing of modified binders in dense-graded mixes led to the following observations:

- The initial stiffness of the dense-graded mixes was generally greater than those of the corresponding gap-graded mixes but less than those of the AR4000-D and RAC-G mixes. The beam fatigue life at a given tensile strain of the dense-graded mixes was generally less than those of the corresponding gap-graded mixes, but greater than those of the AR4000-D and RAC-G mixes.
- The mix ranking of initial stiffness, from most to least stiff, for laboratory mixed, laboratory compacted specimens at 6 percent air-voids was:
    1. AR4000-D
    2. MAC15-D
    3. RAC-G
    4. MB15-D
    5. MB4-D
    6. MAC15-G
    7. MB15-G
    8. MB4-G
- The mix ranking for the same conditions for beam fatigue life at 400 microstrain showed exactly the reverse trend from the above except that MAC15-D and RAC-G changed places:
    1. MAC15-G
    2. MB4-G
    3. MB15-G
    4. MB4-D
    5. MB15-D
    6. MAC15-D
    7. RAC-G

Complex Modulus Master Curves of Mixes (laboratory-mix, laboratory compact)

Complex modulus master curves from flexural frequency sweep tests showed mix stiffnesses for a wide range of temperature and time of loading conditions. These curves allow a stiffness modulus for a particular mix to be selected for times of loading other than the 10 Hz value associated with the fatigue test data, allowing the effect of vehicle speed to be incorporated in pavement performance analyses. The mix ranking of the complex modulus master curves under various combinations of material properties and testing conditions was generally in the order listed below, and is comparable to the overall general ranking of beam fatigue performance in the controlled-strain testing. The MB4-G and MB15-G mixes showed no significant difference in master curves.

Master curve stiffness	Beam fatigue life
1. AR4000-D	1. MB4-G
2. RAC-G	2. MB15-G
3. MAC15-G	3. MAC15-G
4. MB15-G	4. RAC-G
5. MB4-G	5. AR4000-D

- The ranking of complex modulus master curves for dense-graded mixes considering the effect of gradation was in the order below, with no significant difference between the MB4-D and MB15-D mixes:
    1. MAC15-D
    2. MB4-D
    3. MB15-D

In conclusion, it must be emphasized that until a range of pavement types and environments are evaluated in the 2nd Level Analysis, only a general indication of the relative performance of the modified binders can be deduced. It would appear that the MB4, MB15, and MAC15 binders used in gap-graded mixes as overlays on existing cracked asphalt concrete pavements should provide comparable lives (at least) to RAC-G mixes when used in comparable thicknesses in thin layers (less than about 60 mm). Recommendations for the use of MB4, MB15 and MAC15 binders in thicker layers and as dense-graded mixes await the results of the shear test results and pavement performance analyses.

TABLE OF CONTENTS

LIST OF TABLES

LIST OF FIGURES

1. INTRODUCTION

1.1. Objectives

The first-level analysis presented in this report is part of Partnered Pavement Research Center Strategic Plan Element 4.10 (PPRC SPE 4.10) being undertaken for the California Department of Transportation (Caltrans) by the University of California Pavement Research Center (UCPRC). The objective of the study is to evaluate the reflective cracking performance of asphalt binder mixes used in overlays for rehabilitating cracked asphalt concrete pavements in California. The study includes mixes modified with rubber and polymers, and it will develop tests, analysis methods, and design procedures for mitigating reflective cracking in overlays. This work is part of a larger study on modified binder (MB) mixes being carried out under the guidance of the Caltrans Pavement Standards Team (PST) (1) that includes laboratory and accelerated pavement testing using the Heavy Vehicle Simulator (carried out by the UCPRC), and the construction and monitoring of field test sections (carried out by Caltrans).

1.2. Overall Project Organization

This UCPRC project is a comprehensive study, carried out in three phases, involving the following primary elements (2):

- Phase 1
  - The construction of a test pavement and subsequent overlays;
  - Six separate Heavy Vehicle Simulator (HVS) tests to crack the pavement structure;
  - Placing of six different overlays on the cracked pavement;
- Phase 2
  - Six HVS tests to assess the susceptibility of the overlays to high-temperature rutting (Phase 2a);
  - Six HVS tests to determine the low-temperature reflective cracking performance of the overlays (Phase 2b);
  - Laboratory shear and fatigue testing of the various hot-mix asphalts (Phase 2c);
  - Falling Weight Deflectometer (FWD) testing of the test pavement before and after construction and before and after each HVS test;
  - Forensic evaluation of each HVS test section;
- Phase 3
  - Performance modeling and simulation of the various mixes using models calibrated with data from the primary elements listed above.

Phase 1

In this phase, a conventional dense-graded asphalt concrete (DGAC) test pavement was constructed at the Richmond Field Station (RFS) in the summer of 2001. The pavement was divided into six cells, and within each cell a section of the pavement was trafficked with the HVS until the pavement failed by either fatigue (2.5 m/m^2 [0.76 ft/ft^2]) or rutting (12.5 mm [0.5 in]). This period of testing began in the summer of 2001 and was concluded in the spring of 2003. In June 2003 each test cell was overlaid with either conventional DGAC or asphalt concrete with modified binders as follows:

- Full-thickness (90 mm) AR4000-D dense-graded asphalt concrete overlay, included as a control for performance comparison purposes (AR-4000 is approximately equivalent to a PG64-16 performance grade binder);
- Full-thickness (90 mm) MB4-G gap-graded overlay;
- Half-thickness (45 mm) rubberized asphalt concrete gap-graded overlay (RAC-G), included as a control for performance comparison purposes;
- Half-thickness (45 mm) MB4-G gap-graded overlay;
- Half-thickness (45 mm) MB4-G gap-graded overlay with minimum 15 percent recycled tire rubber (MB15-G), and
- Half-thickness (45 mm) MAC15-G gap-graded overlay with minimum 15 percent recycled tire rubber.

The conventional overlay was designed using the current (2003) Caltrans overlay design process. The various modified overlays were either full (90 mm) or half thickness (45 mm). Mixes were designed by Caltrans. The overlays were constructed in one day.

Phase 2

Phase 2 included high-temperature rutting and low-temperature fatigue testing with the HVS as well as laboratory shear and fatigue testing. The rutting tests were started and completed in the fall of 2003. For these tests, the HVS was placed above a section of the underlying pavement that had not been trafficked during Phase 1. A fatigue test was next conducted on each overlay from the winter of 2003-2004 to the summer of 2007. For these tests, the HVS was positioned precisely on top of the sections of failed pavement from the Phase 1 HVS tests to investigate the extent and rate of crack propagation through the overlay.

In conjunction with Phase 2 HVS testing, a full suite of laboratory testing, including shear and fatigue testing, was carried out on field-mixed, field-compacted (FMFC); field-mixed, laboratory-compacted (FMLC); and laboratory-mixed, laboratory-compacted (LMLC) specimens.

Phase 3

Phase 3 entails a second-level analysis that will be carried out on completion of HVS and laboratory testing. This includes extensive analysis and characterization of the mix fatigue and mix shear data, backcalculation of the FWD data, performance modeling of each HVS test, and a detailed series of pavement simulations carried out using the combined data.

An overview of the project timeline is shown in Figure 1.1.

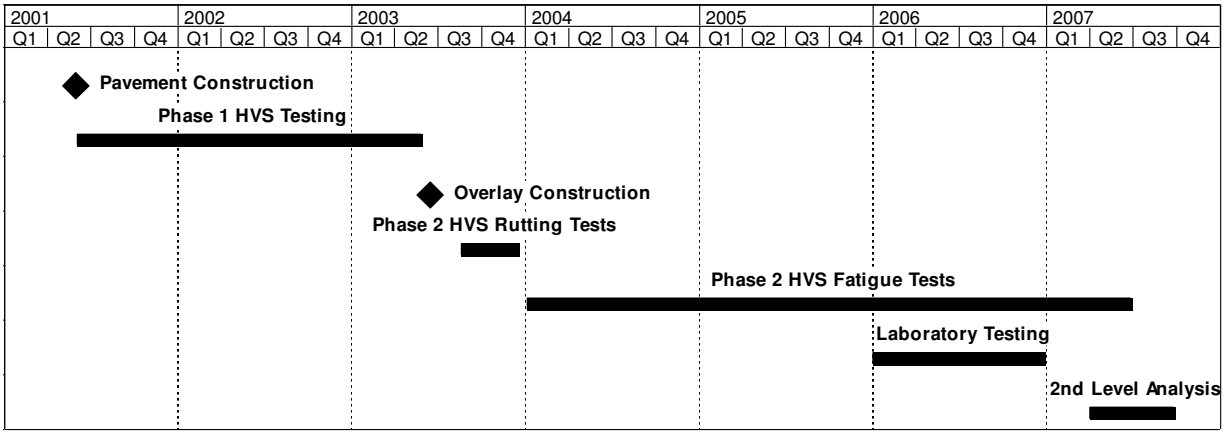

Figure 1.1: Timeline for the Reflective Cracking Study.

Reports

The reports prepared during the reflective cracking study document data from construction, HVS tests, laboratory tests, and subsequent analyses. These include a series of first- and second-level analysis reports and two summary reports. On completion of the study this suite of documents will include:

- One first-level report covering the initial pavement construction, the six initial HVS tests, and the overlay construction (Phase 1);
- One first-level report covering the six Phase 2 rutting tests (but offering no detailed explanations or conclusions on the performance of the pavements);
- Six first-level reports, each of which covers a single Phase 2 fatigue test (containing summaries and trends of the measured environmental conditions, pavement responses, and pavement performance but offering no detailed explanations or conclusions on the performance of the pavement);
- One first-level report covering laboratory shear testing;
- One first-level report covering laboratory fatigue testing;
- One report summarizing the HVS test section forensic investigation;
- One report summarizing the backcalculation analysis of deflection tests,

- One second-level analysis report detailing the characterization of shear and fatigue data, pavement modeling analysis, comparisons of the various overlays, and simulations using various scenarios (Phase 3), and
- One four-page summary report capturing the entire study's conclusions and one longer, more detailed summary report that covers the findings and conclusions from the research conducted by the UCPRC.

1.3. Structure and Content of this Report

This report presents the results of a first-level analysis of laboratory fatigue testing results. The laboratory flexural beam test results are available in the University of California Pavement Research Center (UCPRC) relational database, and are documented in detail in a related document (3). This report is organized as follows:

- Chapter 2 details the test plan and describes specimen preparation and conditioning.
- Chapter 3 provides information on the binders used in the study.
- Chapter 4 presents and discusses the results of fatigue testing in terms of the effects of the variables listed above.
- Chapter 5 presents and discusses the results of flexural frequency sweep testing.
- Chapter 6 provides conclusions.

1.4. Measurement Units

Metric units have always been used in the design and layout of HVS test tracks, all the measurements and data storage, and all associated laboratory testing at the eight HVS facilities worldwide (as well as all other international accelerated pavement testing facilities). Use of the metric system facilitates consistency in analysis, reporting, and data sharing.

In this report, metric and English units (provided in parentheses after the metric units) are used in the Executive Summary, Chapter 1 and 2, and the Conclusion. In keeping with convention, only metric units are used in Chapters 3, 4, and 5. A conversion table is provided on Page iv at the beginning of this report.

2. EXPERIMENT DESIGN

2.1. Introduction

The laboratory fatigue study was undertaken in conjunction with HVS testing, which was carried out on the following sections:

1. Full-thickness (90 mm) AR4000 dense-graded asphalt concrete (DGAC), included as a control for performance comparison purposes
2. Half-thickness rubberized asphalt concrete gap-graded (RAC-G) overlay, included as a control for performance comparison purposes
3. Full-thickness (90 mm) MB4 gap-graded (MB4-G) overlay
4. Half-thickness (45 mm) MB4 gap-graded (MB4-G) overlay
5. Half-thickness MB4 gap-graded overlay with minimum 15 percent recycled tire rubber (MB15-G)
6 Half-thickness MAC15TR gap-graded overlay with minimum 15 percent recycled tire rubber (MAC15-G)

Samples of loose asphalt mix were collected from the HVS test site during construction of the test sections. In addition, samples of the asphalt binders and aggregates were obtained at the hot-mix site. Both sets of materials were used to prepare laboratory mixed, laboratory compacted (LMLC) specimens for the laboratory fatigue study reported herein. The resulting specimens were used to evaluate the influence on fatigue performance of the binders considering the effects of temperature, relative compaction (air-void content), aging, aggregate gradation, and loading frequency and amplitude.

This chapter discusses the test protocols, experimental design, and specimen preparation.

2.2. Test Protocols

The laboratory fatigue study followed the AASHTO T321 test procedures, developed by the Strategic Highway Research Program (SHRP) A-003A project. It should be noted that this test procedure is included as a part of the characterization process for asphalt mixes for use in the New Design Guide. The test consists of flexural controlled-deformation fatigue tests and frequency sweep tests.

2.2.1 Flexural Controlled-Deformation Fatigue Test (AASHTO T321)

Beam test specimens, 50 mm thick by 63 mm wide by 380 mm long, are subjected to four-point bending using a sinusoidal waveform at a loading frequency of 10 Hz. While the majority of testing is performed at

20°C, temperatures in the range 5°C to 30°C can be used. A major advantage of this form of loading test is that the middle one-third of the beam is theoretically subjected to "pure" flexural bending and the size of the specimen has been set to minimize shear deformations.

2.2.2 Flexural Controlled-Deformation Frequency Sweep (Modified AASHTO T321)

The flexural frequency sweep test establishes the relationship between complex modulus and load frequency. The same sinusoidal waveform as in fatigue testing is used in the frequency sweep testing in the controlled deformation mode and at frequencies of 15, 10, 5, 2, 1, 0.5, 0.2, 0.1, 0.05, 0.02, and 0.01 Hz. The upper limit of 15 Hz is a constraint imposed by the capabilities of the test machine. To ensure that the specimen is tested in a nondestructive manner, the frequency sweep test is conducted at a small strain amplitude level (200 microstrain), proceeding from the highest frequency to the lowest in the sequence noted above.

2.3. Experiment Design

The experiment design was formulated to quantify the effects of:

- Temperature,
- Relative compaction (air voids),
- Aging, and
- Gradation.

Table 2.1 shows the overall experiment design including fatigue and frequency sweep testing. Table 2.2 provides the detailed experiment designs for the study. The following sections briefly discuss the effects mentioned, and the motivation and application for the study. With each effect, the type of specimen tested [laboratory-mixed laboratory-compacted (LMLC) or field-mixed laboratory-compacted (FMLC)] is noted in parentheses. LMLC specimens were prepared from the aggregate and asphalt samples taken at the plant and refinery during construction, and later mixed and compacted in the laboratory. FMLC specimens were compacted in the laboratory using mix collected from the plant during construction of the HVS test section overlays.

In order to test a full factorial, a total of 1,440 tests (three replicates of five binder types, two compaction types, two condition types, two gradations, two air-void contents, three temperatures, and two strain levels) would need to have been undertaken. This quantity was unrealistic in terms of time and resources. A partial factorial was therefore tested (Table 2.1), and where possible, the same tests under different effects were not repeated. In addition, results were extrapolated where required.

Table 2.1: Overall Laboratory Testing Test Plan including Fatigue and Frequency Sweep

Mix/Compaction[1,2]	Air-Voids (%)	Binder Content (%)[4]	Grad.	Test Type	Variables	Total
FMLC (Temperature susceptibility and 20°C fatigue)	Design AV (6±0.5%)	Field binder content	Gap-graded and dense-graded	Fatigue	3 temperatures (10,20,30°C) 2 strain levels (400,700 με) 3 replicates	18
				Frequency sweep	3 temperatures (10,20,30°C) 1 strain level (200 με) 2 replicates	6
	Field AV (9±1%)	Field binder content	Gap-graded and dense-graded	Fatigue	1 temperature (20°C) 2 strain levels (400, 700 με) 3 replicates	6
				Frequency sweep	3 temperatures (10,20,30°C) 1 strain level (200 με) 1 replicates	3
FMLC (Aging)	Design AV (6±0.5%)	Field binder content	Gap-graded and dense-graded	Fatigue	1 temperature (20°C) LTOA (6 days) 2 strain levels (400, 700 με) 2 replicates	4
				Frequency sweep	3 temperatures (10,20,30°C) LTOA (6 days) 1 strain level (200 με) 1 replicates	3
LMLC[3] (20°C fatigue)	Design AV (6±0.5%)	Design binder content	Gap-graded	Fatigue	1 temperature (20°C) 2 strain levels (400,700 με) 2 replicates	4
				Frequency sweep	3 temperatures (10,20,30°C) 1 strain levels (200 με) 1 replicates	3
LMLC[3] (20°C fatigue)	Design AV (6±0.5%)	Design binder content	Dense-graded	Fatigue	1 temperatures (20°C) 2 strain levels (400,700 με) 2 replicates	4
				Frequency sweep	3 temperatures (10,20,30°C) 1 strain level (200 με) 1 replicates	3
					Total tests per mix type	**54**
					5 mixes	**256***

1. FMLC: field-mixed laboratory-compacted; LMLC: laboratory-mixed laboratory-compacted.
2. Binders: AR4000, ARB (asphalt rubber binder), MAC15, MB15, and MB4.
3. LMLC gap-graded tests consider MB4, MB15, MAC15, and Asphalt Rubber binders. LMLC dense-graded tests consider MB4, MB15, MAC15, and AR4000 binders.
4. Design binder content for dense gradations and MB binders performed by UCPRC; other design binder contents performed by producer or Caltrans.

Table 2.2: Experimental Design for Laboratory Fatigue Testing

Type of Fatigue Study (Total number of specimens tested)	Mix[1]	Condition[2]	Binder	Gradation	Design Binder Content (%)[4]	Air-voids (%)	Temperature (°C)	Strain (με)	Replicates	Number of Tests
Temperature effect (90)	FMLC	none	AR4000	Dense	5.0	6 ± 0.5	10, 20, 30	400 and 700	3	3 x 2 x 3 = 18
			ARB	Gap	8.0					3 x 2 x 3 = 18
			MAC15		7.4					3 x 2 x 3 = 18
			MB15		7.1					3 x 2 x 3 = 18
			MB4		7.2					3 x 2 x 3 = 18
Air-void content effect (60)	FMLC	none	AR4000	Dense	5.0	6 ± 0.5	20	400 and 700	3	1 x 2 x 3 = 6
						9 ± 1				1 x 2 x 3 = 6
			ARB	Gap	8.0	6 ± 0.5				1 x 2 x 3 = 6
						9 ± 1				1 x 2 x 3 = 6
			MAC15		7.4	6 ± 0.5				1 x 2 x 3 = 6
						9 ± 1				1 x 2 x 3 = 6
			MB15		7.1	6 ± 0.5				1 x 2 x 3 = 6
						9 ± 1				1 x 2 x 3 = 6
			MB4		7.2	6 ± 0.5				1 x 2 x 3 = 6
						9 ± 1				1 x 2 x 3 = 6
Aging effect (50)	FMLC	none	AR4000	Dense	5.0	6 ± 0.5	20	400 and 700	3	1 x 2 x 3 = 6
			ARB	Gap	8.0					1 x 2 x 3 = 6
			MAC15		7.4					1 x 2 x 3 = 6
			MB15		7.1					1 x 2 x 3 = 6
			MB4		7.2					1 x 2 x 3 = 6
		aging	AR4000	Dense	5.0				2	1 x 2 x 2 = 4
			ARB	Gap	8.0					1 x 2 x 2 = 4
			MAC15		7.4					1 x 2 x 2 = 4
			MB15		7.1					1 x 2 x 2 = 4
			MB4		7.2					1 x 2 x 2 = 4

1. FMLC: field-mixed laboratory-compacted; LMLC: laboratory-mixed laboratory-compacted.
2. Aging is 6 days at 85°C for compacted beam.
3. The shaded area in "Total Runs" column represents the tests borrowed from the other effects.
4. Percent by mass of aggregate.

Table 2.2: Experimental Design for Laboratory Fatigue Testing *(cont.)*

Type of Fatigue Study (Total number of specimens tested)	Mix[1]	Condition[2]	Binder	Gradation	Design Binder Content (%)[4]	Air-voids (%)	Temperature (°C)	Strain (με)	Replicates	Number of Tests
Mixing and compaction effect (50)	FMLC	none	ARB	Gap	8.0	6 ± 0.5	20	400 and 700	3	1 x 2 x 3 = 6
			MAC15		7.4					1 x 2 x 3 = 6
			MB15		7.1					1 x 2 x 3 = 6
			MB4		7.2					1 x 2 x 3 = 6
			AR4000	Dense	5.0					1 x 2 x 3 = 6
	LMLC		ARB	Gap	8.0				2	1 x 2 x 2 = 4
			MAC15		7.4					1 x 2 x 2 = 4
			MB15		7.1					1 x 2 x 2 = 4
			MB4		7.2					1 x 2 x 2 = 4
			AR4000	Dense	5.0					1 x 2 x 2 = 4
Gradation effect (24)	LMLC	none	MAC15	Dense	6.0	6 ± 0.5	20	400 and 700	2	1 x 2 x 2 = 4
			MB15		6.0					1 x 2 x 2 = 4
			MB4		6.3					1 x 2 x 2 = 4
			MAC15	Gap	7.4					1 x 2 x 2 = 4
			MB15		7.1					1 x 2 x 2 = 4
			MB4		7.2					1 x 2 x 2 = 4

1. FMLC: field-mixed laboratory-compacted; LMLC: laboratory-mixed laboratory-compacted.
2. Aging is 6 days at 85°C for compacted beam.
3. The shaded area in "Total Runs" column represents the tests borrowed from the other effects.
4. Percent by mass of aggregate.

2.3.1 Temperature Effect (FMLC)

This part of the experiment evaluated the temperature susceptibility of the mixes in the field-mixed, laboratory-compacted (FMLC) specimens. Testing was carried out at three temperatures (10°C, 20°C, and 30°C) and two strain levels (400 and 700 microstrain). Three replicates were tested.

2.3.2 Air-Void Content Effect (FMLC)

The effect of construction quality in terms of compaction on pavement performance was considered by conducting tests on specimens at two different air-void contents, 6.0 ± 0.5 percent and 9.0 ± 1.0 percent. Three replicates of fatigue tests were run at one temperature (20°C) and two strain levels (400 and 700 microstrain).

2.3.3 Aging Effect (FMLC)

The aging effect simulates extended environmental exposure, primarily oxidizing of the binder. For conventional asphalt binders (steam refined, no modifiers), fatigue resistance is generally reduced as a more brittle binder is more susceptible to cracking. The AASHTO PP2-94 protocol, which conditions a compacted specimen for five days at 85°C, is typically followed for long-term oven aging. In the SHRP-A-390 protocol, long-term oven aging at 85°C for eight days represents (conservatively) approximate aging at sites nine years or older in the dry-freeze zone, and eighteen years or older in the wet no-freeze zone (4). For this experiment, an aging period of six days at 85°C was used, based on previous experience (5). Specimens are aged in a forced-draft oven for the six days, cooled to room temperature, then conditioned at 20°C for two hours prior to testing.

To evaluate the aging effect of the asphalt binder on the fatigue performance each binder, the test plan compared four aged beams (two strain levels, two replicates) with six non-aged beams (two strain levels, three replicates) for temperature effect with the same air-void content (6.0 ± 0.5%) and the same test temperature (20°C).

2.3.4 Mixing and Compaction Effect (FMLC and LMLC)

In this test, twenty LMLC beams (two replicates of five binder types at two strain levels) and thirty FMLC beams (three replicates of five binder types at two strain levels) were compared. Air-void content (6.0 ± 0.5%) and test temperature (20°C) were constant.

2.3.5 Gradation Effect (LMLC)

HVS testing is being conducted only on gap-graded mixes containing the MAC15, MB15, and MB4 binders. However, the laboratory study was extended to assess the use of these three modified binders in

both gap- and dense-graded mixes. The dense-graded mix designs were performed by the UCPRC according to the CTM 304, 366, and 367 procedures. These mixes were compared with the dense-graded mix containing the AR4000 binder (DGAC) and the gap-graded mix with the rubber asphalt (RA) binder (ARB).

2.4. Specimen Preparation

2.4.1 Laboratory-Mixed, Laboratory-Compacted Specimens

Gradation and Binder Contents

Laboratory mix aggregate gradations and binder contents are shown in Tables 2.3 and 2.4 and in Figures 2.1 and 2.2. The aggregate gradations conform to the requirements specified by Caltrans Specification Section 39. The dense gradation is a 19 mm Type A Coarse and the gap gradation conforms to the special provisions for Type G-MB. The target gradation was determined from the field samples collected and tested by Caltrans. For the gap gradation, several different field samples were tested and the average gradation was calculated and set as the laboratory target. For the dense gradation, only one material and two samples were tested. The target dense gradation was set as the average of these two test results.

Table 2.3: Summary of Gradation Curves

Sieve Size (mm)	Gap-graded (% passing)			Dense-graded (% passing)		
	Design (Caltrans)	Field (Caltrans)	LMLC (UCB)	Design (Caltrans)	Field (Caltrans)	LMLC (UCB)
25.4	100.0	100.0	100.0	100.0	100.0	100.0
19.0	98.0	96.3	96.7	98.0	93.0	91.5
12.7	82.0	78.2	78.2	85.0	72.0	72.4
9.5	69.0	64.8	64.6	79.0	63.0	63.8
4.75	36.0	32.3	32.5	49.0	44.0	41.4
2.38	21.0	20.5	20.2	35.0	31.5	28.8
1.19	13.0	15.7	15.8	23.0	24.0	23.7
0.59	10.0	12.3	12.6	16.0	19.0	19.2
0.23	7.0	9.2	9.2	11.0	13.0	13.4
0.15	5.0	5.0	5.5	6.0	6.0	6.4
0.075	3.1	3.6	3.8	4.0	3.7	4.3

Table 2.4: Design Binder Contents of Laboratory Mixes

Gap-graded[1]		Dense-graded[2]	
Binder	Binder Content	Binder	Binder Content
ARB	8.0	AR4000	5.0
MAC15	7.4	MAC15	6.3
MB15	7.1	MB15	6.2
MB4	7.2	MB4	6.4

1. Gap-graded mix designs determined by Caltrans.
2. Dense-graded mix designs for MAC15, MB15, and MB4 binders determined by UC Pavement Research Center.

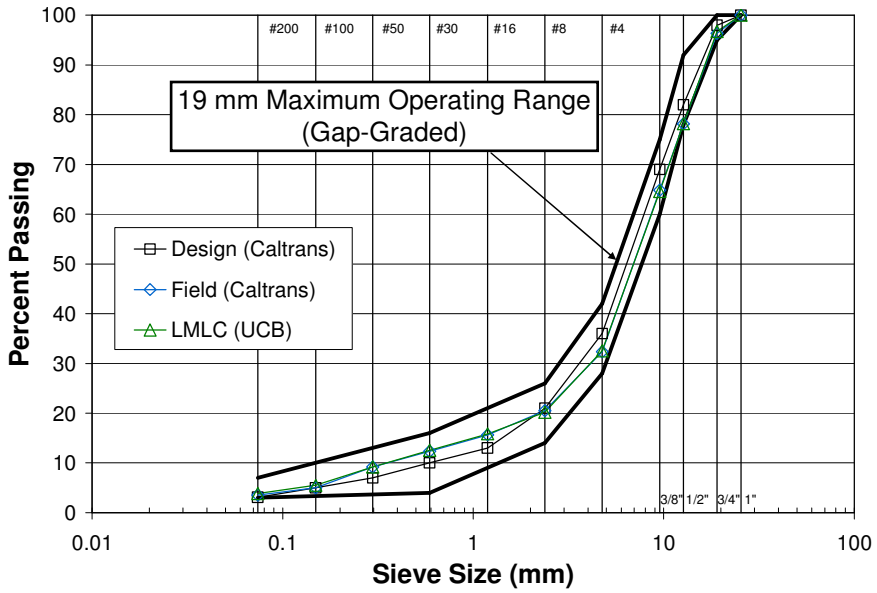

Figure 2.1: Gradation curves for gap-graded mixes.

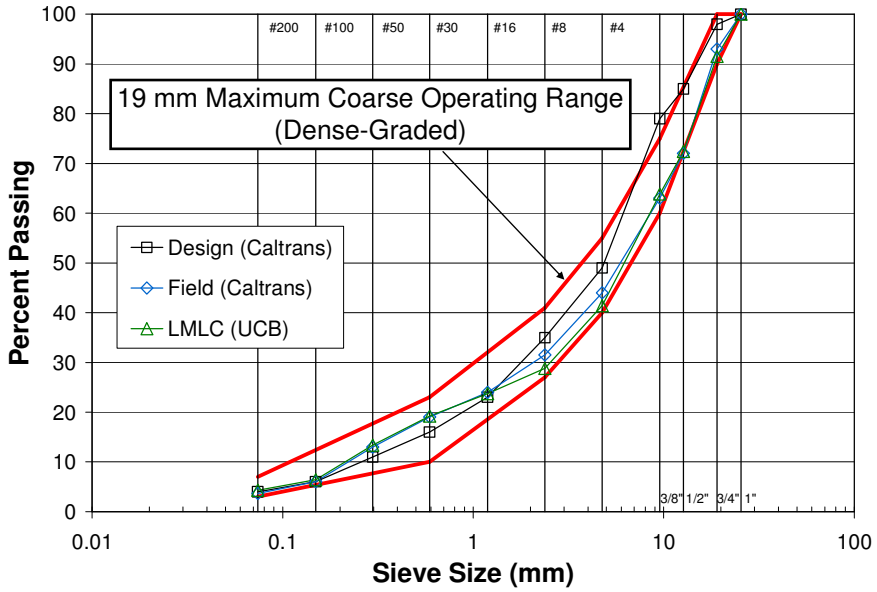

Figure 2.2: Gradation curves for dense-graded mixes.

Preparation

Specimens were prepared from raw materials supplied by the contractor constructing the HVS Test Track, Syar Industries, Inc. The aggregate, a basalt, was obtained from Syar's Lake Herman quarry, located near Vallejo, CA. The aggregate blend was obtained from four bins with size ranges as follows: 19 mm x 12.5mm, 12.5 mm x 9.5 mm, 9.5 mm x dust, and 4.75 mm x dust. Binders produced for the HVS Test Track were obtained from a number of California refineries.

The production of fatigue beams involved:

- Checking the aggregate gradings using AASHTO T11 (wet sieving, passing No. 200 sieve) and AASHTO T27 (dry sieving fine and coarse aggregate)
- Batching of aggregates and mixing with binder
- Short-term oven aging (AASHTO PP2-94)
- Specific gravity testing (AASHTO T209)
- Rolling wheel compaction to produce slabs
- Sawing to size of beams for flexural fatigue and frequency sweep tests
- Target air-void content [AASHTO T275 (Caltrans CTM 308)]

In the batching and mixing processes, 7.0 kg batches were heated to the binder-specific mixing temperature for at least two hours before mixing. The asphalt binder was heated to the same temperature for approximately one hour, or until consistently pourable, and then mixed with the aggregate until the aggregates were fully coated (typically about five minutes). The mixing bowl and blades were preheated to prevent adhesion of the binder. The binder mixing temperatures are shown in Table 2.5.

Table 2.5: LMLC Binder Mixing Temperatures

Mix	Binder Mix Temperatures	Temperature Specification Range
MB4	163°C	150–163°C
MB15	163°C	150–163°C
MAC15	163°C	150–163°C
ARB	163°C	149–163°C
AR4000	163°C	–

The short-term oven aging procedure used in this investigation (AASHTO PP2-94) attempts to replicate aging that occurs in the mixing and compaction process. In this procedure, oven-aging involves conditioning the loose mix at 145°C for four hours with periodic stirring. Following the short-term oven-aging procedure, compaction of the LMLC and FMLC mixes were performed at the temperatures shown in Table 2.6.

Table 2.6: Compaction Temperatures for LMLC and FMLC

Mix	Compaction Temperature	Temperature Specification Range
MB4	Comp. at 150°C	143–150°C
MB15	Comp. at 150°C	143–150°C
MAC	Comp. at 150°C	143–150°C
ARB	Comp. at 145°C	143–149°C
AR4000	Comp. at 145°C	–

2.4.2 Field-Mixed, Laboratory Compacted Specimens

The field-mixed laboratory-compacted specimens were prepared using the loose mix collected during construction of the HVS test road. After construction, this material was stored in five-gallon sealed metal cans at room temperature in a warehouse without temperature control for up to several years before compaction. Some further aging may have occurred during the time between site sampling and specimen production. For specimen production, the mix was tested for its maximum specific gravity and compacted following the procedures described above.

The compaction temperatures for field-mixed, lab-compacted specimens were the same as for the LMLC mixes.

2.5. Ignition Oven Tests

2.5.1 Test Method

California Test CTM382 (Determination of Asphalt Binder Content of Bituminous Mixtures by the Ignition Method) was used to determine binder contents for the field mix collected during construction of the HVS test sections. The ignition oven values were corrected for ignition of the aggregate using aggregate samples also collected during construction. Mixes tested for binder content were RAC-G, MAC15-G, MB15-G, and MB4-G.

2.5.2 Results

Table 2.7 summarizes the results of the ignition oven test on the selected mixes. Table 2.8 lists revised 95 percent confidence intervals based on a pooled standard deviation. The results show that the mean field binder contents were approximately 0.5, 0.15, 0.4, and 0.3 percent above the design binder contents for the ARB, MAC15, MB15, and MB4 gap-graded mixes, respectively.

Table 2.7: Summary of Binder Ignition Tests

Mix Type	Design Binder Content (%)	Ignition Oven Correction Factor	Test Results of Field Mixes					Mean	Standard Error	95% Confidence Interval
			1	2	3	4	5			
RAC-G	8.0	1.86	8.79	8.35	8.54	8.26	-	8.485	0.117	(8.112, 8.857)
MAC15-G	7.4	1.86	7.64	7.42	7.65	7.48	-	7.548	0.058	(7.363, 7.733)
MB15-G	7.1	1.76	7.89	7.66	7.41	7.08	7.58	7.524	0.135	(7.149, 7.899)
MB4-G	7.2	2.15	7.84	7.84	7.62	6.71	-	7.503	0.269	(6.647, 8.359)

Table 2.8: Summary of Binder Ignition Tests (pooled standard deviation)

Mix Type	Design Binder Content (%)	Ignition Oven Correction Factor	Test Results of Field Mixes					Mean	Standard Error	95% Confidence Interval
			1	2	3	4	5			
RAC-G	8.0	1.86	8.79	8.35	8.54	8.26	-	8.485	0.166	(7.957, 9.013)
MAC15-G	7.4	1.86	7.64	7.42	7.65	7.48	-	7.548	0.166	(7.020, 8.076)
MB15-G	7.1	1.76	7.89	7.66	7.41	7.08	7.58	7.524	0.148	(7.053, 7.995)
MB4-G	7.2	2.15	7.84	7.84	7.62	6.71	-	7.503	0.166	(6.974, 8.031)

3. BINDER TESTING

3.1. Introduction

A total of five binders have been used in this investigation including: a conventional AR4000 asphalt cement, asphalt rubber (ARB), and three modified binders designated MB4, MB15, and MAC15. This chapter provides a summary of the Bending Beam Rheometer (BBR) and Dynamic Shear Rheometer (DSR) tests conducted at the Turner-Fairbank Highway Research Center of the Federal Highway Administration (FHWA) as part of this study. Tests were conducted on binders in their original condition and after the Rolling Thin Film Oven (RTFO) and Pressure Aging Vessel (PAV) conditioning. These five binders were used in the HVS test program and the laboratory fatigue study; all but the AR binder were tested by the FHWA using tests associated with the AASTHO PG Binder Specification M320.

3.2. Bending Beam Rheometer

3.2.1 Test Method

AASHTO T313 was used to assess the propensity of the binders to develop thermal stresses at low pavement temperature. The two values obtained from the Bending Beam Rheometer are the creep stiffness and the m-value (the rate of change of the creep stiffness versus time of loading). The PG binder specification M320 includes limiting values for these two parameters associated with the low temperature of the PG binder grade. The allowable maximum creep stiffness value is 300 MPa and the minimum m-value is 0.3, both determined at a loading time of 60 seconds.

3.2.2 Results

Table 3.1 lists the temperatures at which creep stiffnesses reached 300 MPa, and m-values reached 0.3. Figures 3.1 and 3.2 plot the creep stiffnesses and m-values versus temperature for the un-aged condition and after RTFO and PAV aging. According to the test results and the Superpave specification for thermal cracking, the ranking of susceptibility of the binders to low-temperature thermal cracking is (from highest to lowest susceptibility):

1. AR4000
2. MAC15
3. MB15
4. MB4

Table 3.1: Summary of Bending Beam Rheometer Test Results

Binder Type	Binder Status*	Temp@S=300 MPa (°C)	Temp@m=0.3 (°C)
AR4000	ORG	-11.5	-15.7
	RTFO	-11.3	-15.3
	PAV	-7.7	-11.3
MAC15	ORG	-20.5	-23.9
	RTFO	-18.8	-22.3
	PAV	-18.0	-19.3
MB15	ORG	-26.7	-28.3
	RTFO	-25.6	-26.7
	PAV	-24.0	-22.5
MB4	ORG	-31.7	-31.3
	RTFO	-28.3	-27.8
	PAV	-25.7	-22.0

* ORG: original
RTFO: rolling thin film oven
PAV: pressure aging vessel

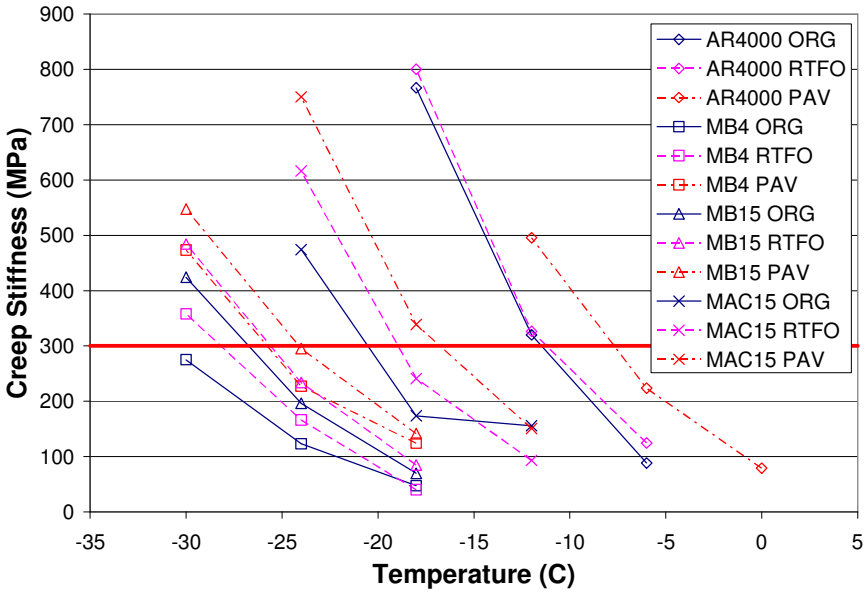

Figure 3.1: Creep stiffness summary of BBR test results.

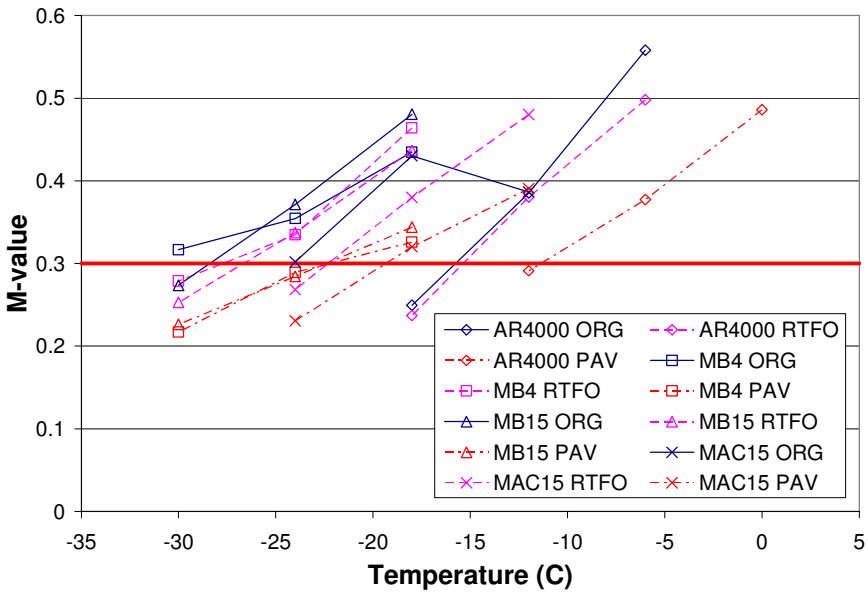

Figure 3.2: m-value summary of BBR test results.

3.3. Dynamic Shear Rheometer

3.3.1 Test Method

AASHTO T315 method was followed to assess the rutting ($G^*/\sin\delta$) and long-term fatigue performance ($G^*\sin\delta$) of the binders.

3.3.2 Results

Rutting Resistance

AASHTO M320 defines and places requirements on a rutting factor of binder, $G^*/\sin\delta$, which represents a measure of high temperature rutting resistance of the asphalt binder. To minimize the rutting, the specification requires that $G^*/\sin\delta$ must be a minimum of 1.0 kPa for the original asphalt binder and 2.2 kPa after aging the binder using the RTFO procedure. Dynamic shear modulus G^* at 10 rad/s against the test temperatures and the specification requirements for the binders are shown in Figures 3.3 and 3.4 for these two conditions.

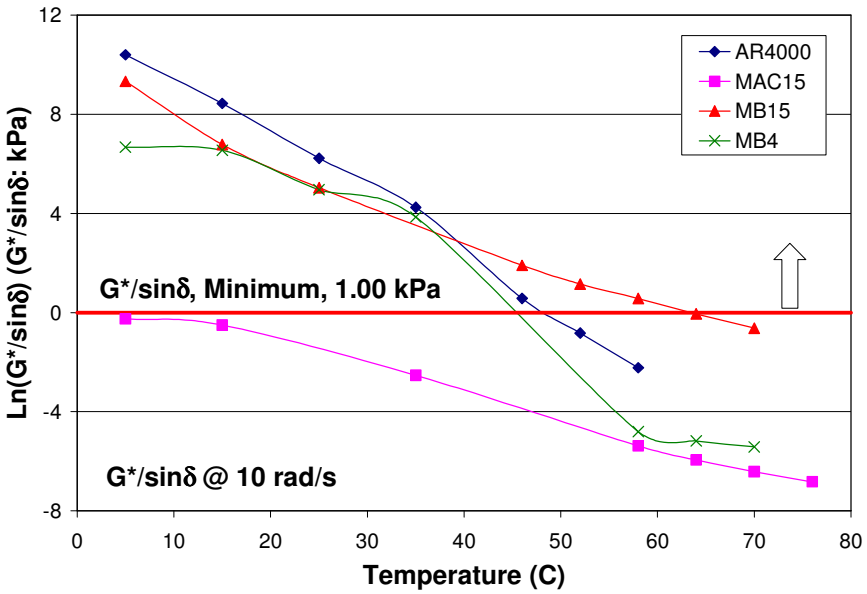

Figure 3.3: *G*/sinδ* summary of DSR test results on original binder.

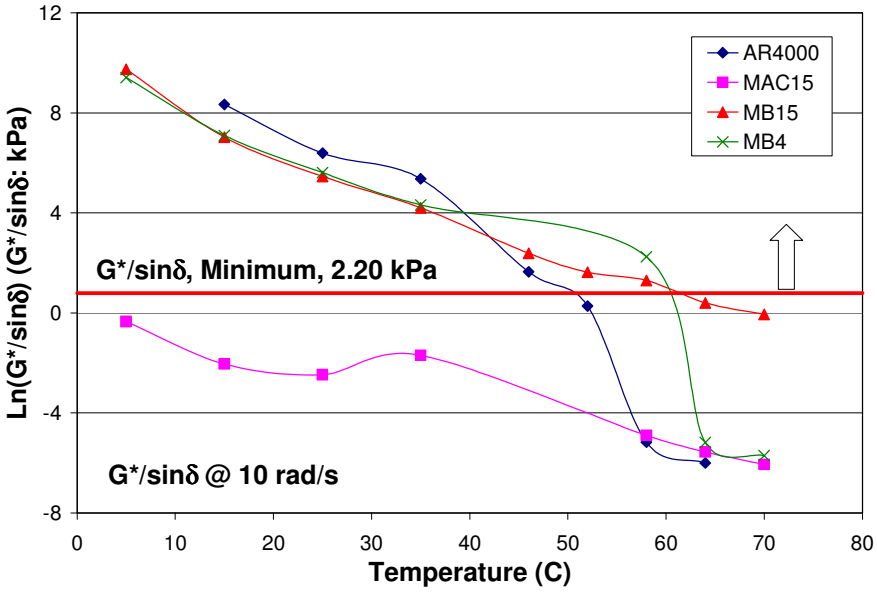

Figure 3.4: *G*/sinδ* summary of DSR test results on RTFO aged binder.

Fatigue Resistance

In the AASHTO M320 specification, the fatigue resistance of the binder is controlled by the parameter $G^*\sin\delta$. This parameter represents a measure of the cracking resistance of the asphalt binder in the intermediate temperature range. To minimize fatigue cracking, the specification requires that $G^*\sin\delta$ have a minimum value of 5,000 kPa after PAV aging.

Figure 3.5 illustrates the dynamic shear modulus G^* at 10 rad/s versus a range of temperatures and contains the specification requirement for $G^*\sin\delta$.

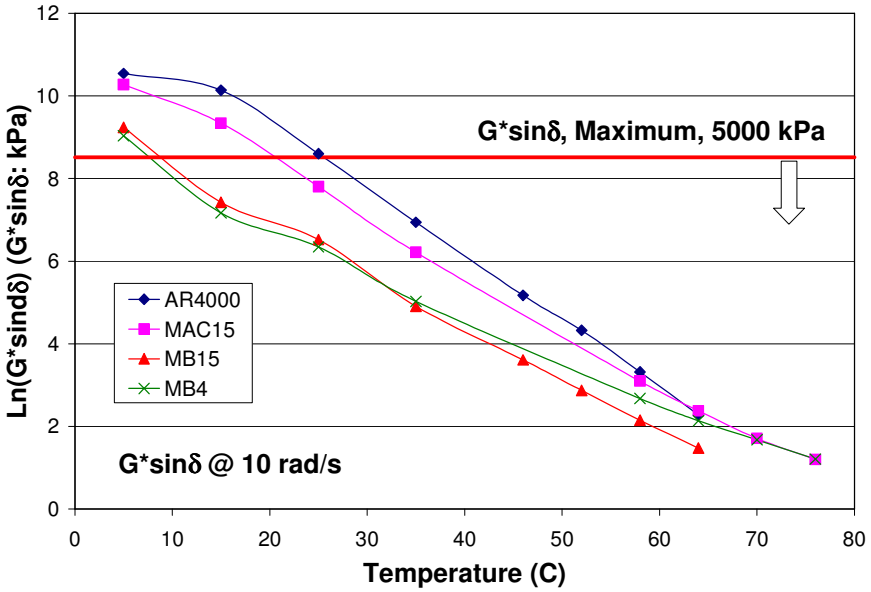

Figure 3.5: $G^*\sin\delta$ summary of DSR test results on PAV-aged binder.

Shear Susceptibility

The Shear Susceptibility of Viscosity (SSV) and Shear Susceptibility of Delta (SSD) are derived from DSR test results and are defined in California Test 381. Reese (5) further developed these parameters for Type G-MB asphalt concrete as follows:

$SSD \geq 30(0.6+SSV)^3$ for original binder @ 25°C

$SSD \geq -115(SSV) - 50.6$ for PAV-aged binder at @ 25°C

Table 3.2 summarizes the SSD and SSV values for the binders. All the binders satisfy the PAV-aged binder requirement, while only the MB4 binder satisfies the un-aged binder requirement.

Test Summary

According to the test results, the ranking of susceptibility of the binders to rutting is (from highest to lowest):

1. MAC15 (binder failed to meet minimum requirements of rutting)
2. MB4, MB15
3. AR4000

The ranking of susceptibility of the binders to fatigue cracking is (from highest to lowest):

1. AR4000
2. MAC15
3. MB15
4. MB4

The MB4 and MB15 binders had similar rutting and fatigue resistance capacities. The AR4000 binder appeared to have better rutting resistance below 40°C than the MB4 and MB15 binders.

Table 3.2: Summary of SSV and SSD Values from DSR Test Results

Binder	Binder Status*	SSV@25°C	SSD@25°C	SSD for ORG	SSD for PAV
AR4000	ORG	-0.2085	-12.848	No	
	RTFO	-0.4264	-4.454		
	PAV	-0.2983	-11.428		Yes
MB4	ORG	-0.4523	6.388	Yes	
	RTFO	-0.4369	2.944		
	PAV	-0.3059	-2.376		Yes
MB15	ORG	-0.2201	-2.742	No	
	RTFO	-0.2742	-2.013		
	PAV	-0.2490	-5.911		Yes
MAC15	ORG	-0.2289	-0.210	No	
	RTFO	-0.2585	2.358		
	PAV	-0.2623	-6.898		Yes

* ORG: original
RTFO: rolling thin film oven
PAV: pressure aging vessel.

3.3.3 Master Curve of Shear Complex Modulus

The master curves of the binder shear complex moduli were constructed using time-temperature superposition and a genetic algorithm (3). Figures 3.6 through 3.13 present the *G** master curves and temperature-shift relationships at various aging conditions for AR4000, MB4, MB15, and MAC15 binders respectively. Observations based on the results of this analysis are:

- For binders aged with the PAV procedure, the complex shear moduli increase across all frequencies for the four binders.
- The MB4 and MB15 binders show small-to-moderate changes between the various aging conditions.
- For original and RTFO aging conditions, the master curves of MAC15 binder are similar; however, the master curve at PAV stage exhibits some deviation from the other two curves. The reason is not clear at this time.
- In general, the temperature-shift relationship does not change significantly for different aging conditions. The only exception is the MAC15 binder. Its temperature sensitivity for the PAV-aged

condition increases rapidly at low temperatures and is greater than the temperature sensitivity in the original and RTFO conditions.

Figures 3.14 through 3.16 compare the master curves at various aging conditions, respectively. In the original and RTFO conditioning, the master curves of MAC15 binder are significantly lower than the master curves for the AR4000, MB4, and MB15 binders. The ranking of the master curves for PAV conditioning is changed with the order from highest to lowest as follows:

1. AR4000
2. MAC15
3. MB4
4. MB15

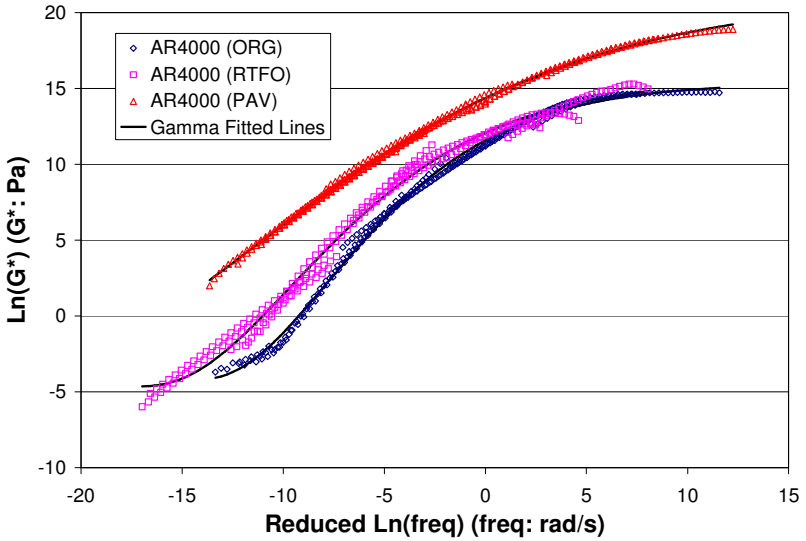

Figure 3.6: Master curves of shear complex modulus of AR4000.

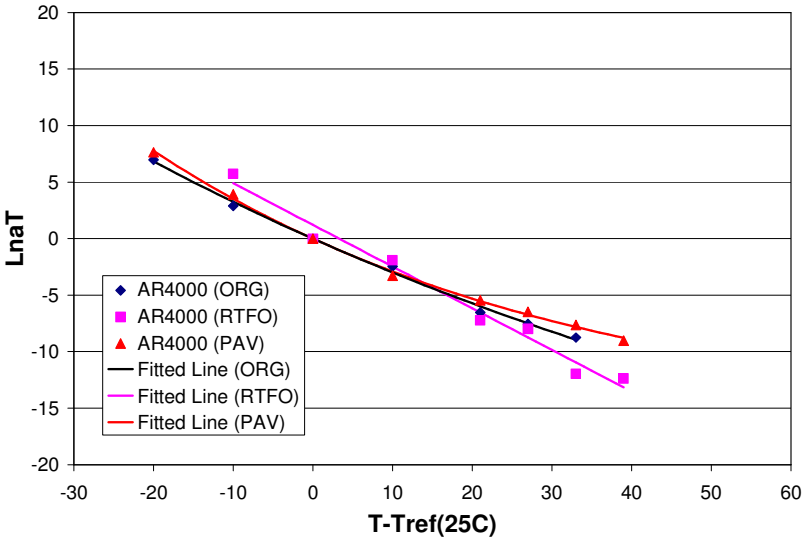

Figure 3.7: Temperature-shift relationships of AR4000.

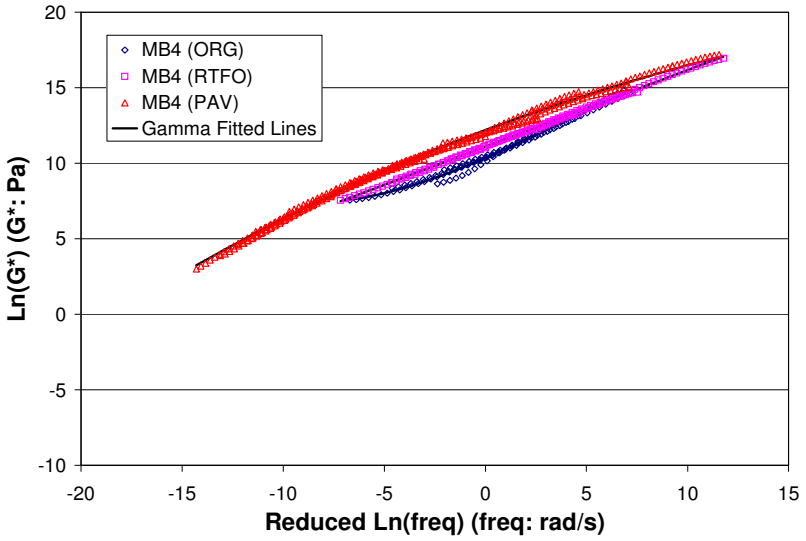

Figure 3.8: Master curves of shear complex modulus of MB4.

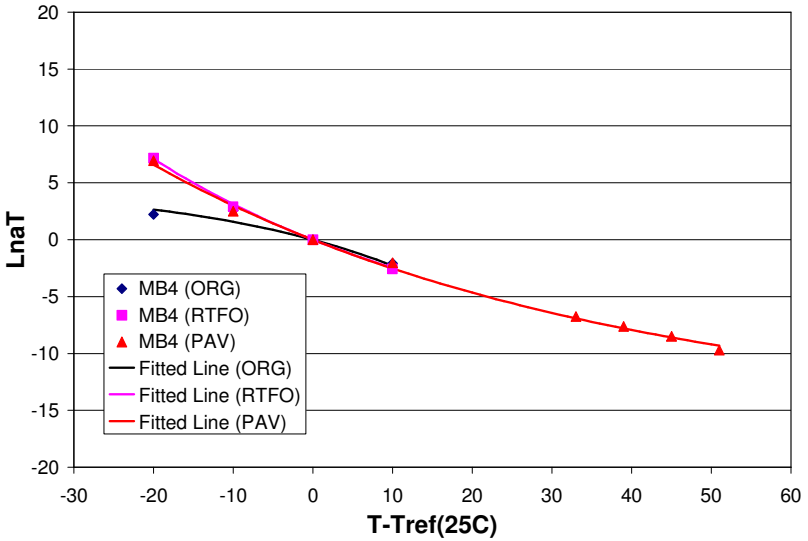

Figure 3.9: Temperature-shift relationships of MB4.

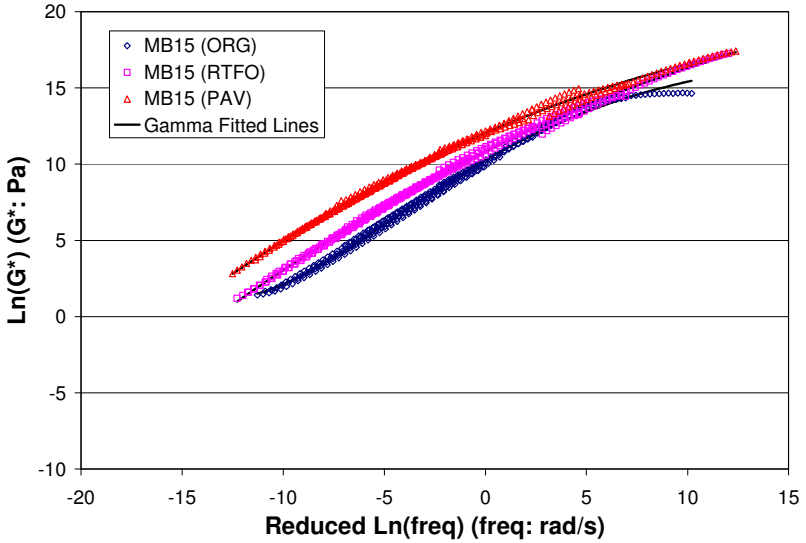

Figure 3.10: Master curves of shear complex modulus of MB15.

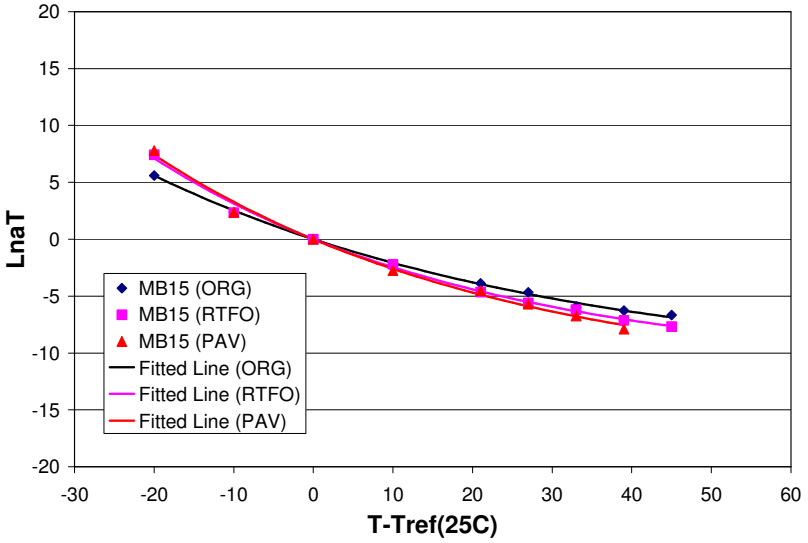

Figure 3.11: Temperature-shift relationships of MB15.

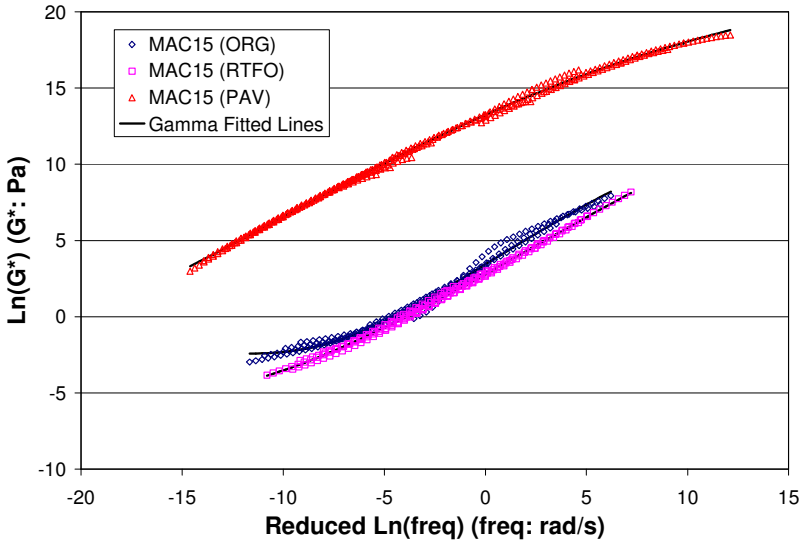

Figure 3.12: Master curves of shear complex modulus of MAC15.

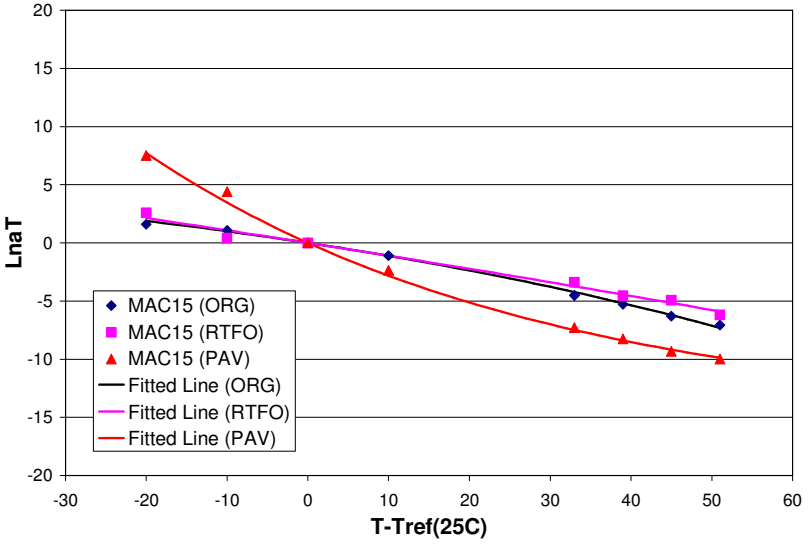

Figure 3.13: Temperature-shift relationships of MAC15.

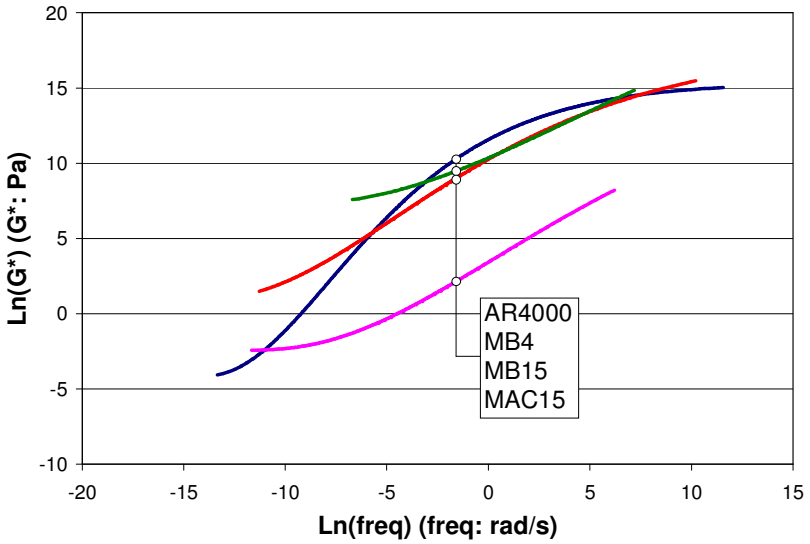

Figure 3.14: Comparison of *G Master curves (original).**

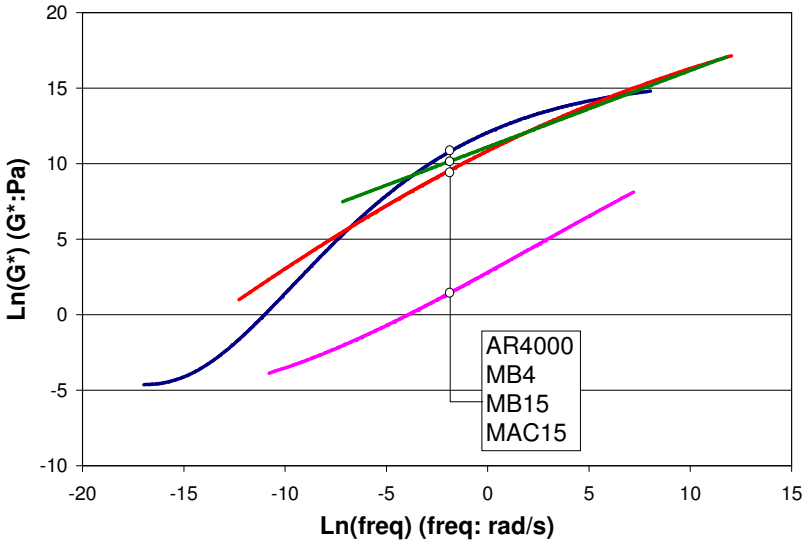

Figure 3.15: Comparison of *G Master curves (RTFO).**

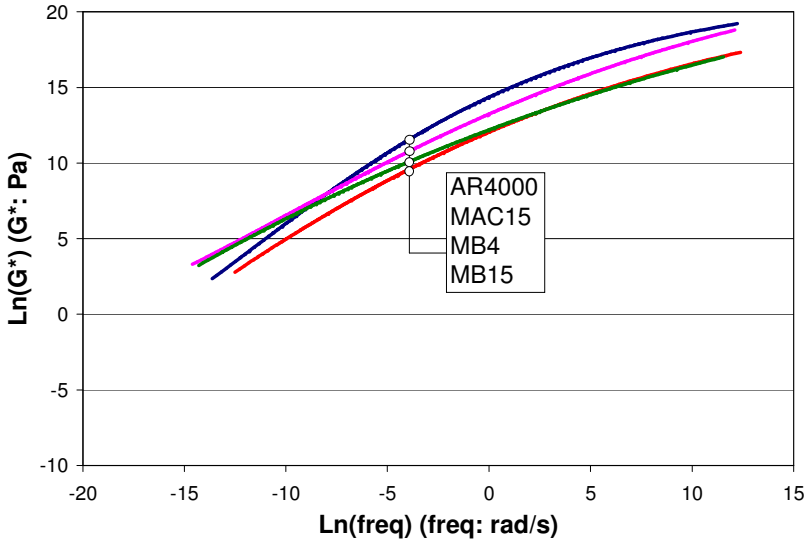

Figure 3.16: Comparison of *G Master curves (PAV).**

4. FATIGUE TESTING

4.1. Introduction

This chapter provides an overview of the laboratory fatigue testing study together with the analysis and interpretation of the results on field mixed, laboratory compacted (FMLC) and laboratory mixed, laboratory compacted (LMLC) materials. Included are:

- Summary of the flexural controlled-deformation fatigue test results
- Identification of the significant factors (or covariates) that affect fatigue performance
- Discussion of regression models of initial stiffness and fatigue life
- Summary of the collective dataset analysis and regression model

4.1.1 Definitions Used in Statistical Analyses

The factors investigated include:

- Temperature effect (on FMLC material)
- Air-void content effect (on FMLC material)
- Aging effect (on FMLC material)
- Compaction effect (on FMLC and LMLC material)
- Gradation effect (on LMLC material)

The response variables are:

- Initial phase angle (*pangle or pa*)
- Natural logarithm of the initial stiffness (*lnstif*)
- Natural logarithm of the fatigue life (*lnnf*)

The phase angle and initial stiffness were obtained taken after the first fifty repetitions; at this number of repetitions temperature stability and stabilization of the strain level in the fatigue beam are obtained. It should be noted that both the stiffness and tensile strain are calculated from the measured load and center beam deflections.

Fatigue life is defined for this analysis as the number of tensile strain repetitions to a 50 percent reduction in stiffness from the initial stiffness measured at 50 repetitions. This definition of fatigue life has been used extensively and correlates well with the initiation of cracking in fatigue beams for mixes with conventional binders. Its applicability to modified binders has been questioned and some alternative

definitions of flexural fatigue beam life recently have been proposed. Analyses that consider alternative definitions of fatigue life will be included in the second-level analysis report.

The category covariates and factor levels evaluated include:

- Binder type (*binder*)
  - AR4000 (*ar4000*)
  - ARB (*rac*)
  - MAC15 (*mac15*)
  - MB15 (*mb15*)
  - MB4 (*mb4*)
- Gradation (*grad*)
  - Dense-graded (*dg*)
  - Gap-graded (*gg*)
- Compaction (*comp*)
  - Field-mixed, laboratory-compacted (*fmlc*)
  - Laboratory-mixed, laboratory-compacted (*lmlc*)
- Conditioning (*cond*)
  - No conditioning (*none*)
  - Long-term oven aging for 6 days (*aging*)
- Air-void content (*av*)
  - 6 percent air-void content (*av6*)
  - 9 percent air-void content (*av9*)
- Test temperature (*temp*)
  - 10°C (*10C*)
  - 20°C (*20C*)
  - 30°C (*30C*)
- Test strain levels (*stn*)
  - 400 microstrain (*stn400*)
  - 700 microstrain (*stn700*).

The covariate *binder* has different meanings depending on the test, as follows:

- On all effects other than gradation, *binder* implies a binder type with a specific gradation type and corresponding design binder content as used in this experiment, regardless of compaction type (FMLC or LMLC). It should be noted that AR4000-D and RAC-G are defined by specification and hence a gap-graded mix with the AR4000 binder (AR4000-G) and a dense-graded mix with

the ARB binder (RAC-D) are not included in the experiment. The interpretations of *binder* include:

  - *ar4000* - AR4000 binder with dense-graded gradation and 5.0 percent design asphalt content
  - *rac* - AR binder with gap-graded gradation and 8.0 percent design asphalt content
  - *mac15* - MAC15 binder with gap-graded gradation and 7.4 percent design asphalt content
  - *mb15* - MB15 binder with gap-graded gradation and 7.1 percent design asphalt content
  - *mb4* - MB4 binder with gap-graded gradation and 7.2 percent design asphalt content

- When considering the gradation effect, *binder* implies a binder type with a specific design binder content. In this instance, *binder* is used as follows:
  - *mac15* - MAC15 binder with 6.0 percent asphalt content if dense-graded, or 7.4 percent asphalt content if gap-graded
  - *mb15* - MB15 binder with 6.0 asphalt content if dense-graded, or 7.1 percent asphalt content if gap-graded.
  - *mb4* - MB4 binder with 6.3 percent asphalt content if dense-graded, or 7.2 percent asphalt content if gap-graded
- When developing the comprehensive regression models with all fatigue tests, *binder* signifies a binder type with specific design asphalt content associated with its gradation (dense-graded or gap-graded).

4.1.2 Expected Effects of Response Variables on Performance

The expected effects of response variables from flexural fatigue beam tests on performance are summarized in Table 4.1. These are simplifications of complex distress mechanisms, particularly fatigue cracking. However, they provide a general guide to interpret the results presented in this chapter.

Phase angle is a measure of the time lag between the applied stress and the resulting strain when a sinusoidal wave is applied to a viscoelastic material, such as asphalt and mixes of asphalt and aggregate. Phase angle is included in the rutting, low temperature, and fatigue specification properties for PG binders, where it is referred to as delta (δ). A phase angle of zero degrees means that there is no time lag, and the material is therefore elastic. A low phase angle is good for rutting performance because it means that when the material is deformed it should return almost to its original condition when the load is removed, resulting in little permanent deformation. It is bad for low-temperature cracking performance because it means that the material will not relax tensile stresses that occur when the material contracts as it gets colder.

Table 4.1: Summary of Expected Effects of Response Variables on Performance

Flexural Beam Test Response Variable	Distress Mechanism in Field	Expected Effect on Field Performance
Phase angle	Rutting at high temperatures	High phase angle at high temperatures expected to result in more rutting.
	Low-temperature cracking	Low phase angle at low temperatures expected to increase risk of low-temperature cracking.
	Fatigue and Reflective Cracking	Phase angle effect highly correlated with stiffness, see Stiffness explanation.
Stiffness	Rutting at high temperatures	High stiffness at high temperatures expected to result in less rutting.
	Low-temperature cracking	High stiffness at low temperatures expected to increase risk of low-temperature cracking.
	Tensile strain (related to fatigue and reflective cracking)	Thin overlay: high stiffness has little influence on tensile strain.
		Thick overlay: high stiffness reduces tensile strains, which increases fatigue life.
Beam fatigue life (repetitions to cracking at a constant tensile strain)	Rutting at high temperatures	No effect.
	Low-temperature cracking	High fatigue life at low temperatures may indicate reduced risk of low-temperature cracking in areas without extremely cold temperatures.
	Fatigue cracking and reflective cracking	Thin overlay: High fatigue life indicates increased fatigue life
		Thick overlay: High fatigue life indicates increased fatigue life
Interaction of stiffness and beam fatigue life	Fatigue cracking and reflective cracking	Thin overlay: High stiffness causes short life in beam fatigue at a given tensile strain, and little change in tensile strain in the field. Net result is that high stiffness will usually result in short cracking life in the field.
		Thick overlay: High stiffness causes short life in beam fatigue at a given tensile strain, but reduces tensile strain in the pavement. Net result must be determined from mechanistic pavement structural analysis.

A phase angle of 90 degrees indicates that the material has the maximum time lag possible between stress and strain, and that the material is therefore completely viscous. A high phase angle is bad for rutting performance because it indicates that none of the deformation returns when the load is removed. However, a high phase angle is good for low-temperature cracking performance.

Phase angle is highly correlated with stiffness in asphalt mixes. Mixes having high stiffness typically have low phase angles. Therefore, in the general understanding of the effects of phase angle on rutting and low-temperature cracking discussed above, “low stiffness” can often be substituted for “high phase angle”. Modifiers in asphalt mixes can change phase angle and stiffness independently to some degree, and the assumption of a strong correlation between high phase angle and low stiffness is not always valid for these materials.

The effect of phase angle and stiffness on fatigue performance, whether for bottom up fatigue cracking in new structures or reflective cracking in overlays placed over cracked pavement, is dependent on the interaction of the mix properties (particularly stiffness and the sensitivity of fatigue life to tensile strain), crack dimensions, underlying pavement condition, load, and other factors. It is therefore difficult to make a generally applicable statement regarding the expected effect of stiffness and phase angle on expected reflective cracking life.

A general description of the expected interaction of stiffness and beam fatigue life for thin and thick overlays on cracked pavements, or new pavements with granular bases with a thin or thick asphalt layer is shown in Table 4.2 and Figure 4.1. It must be remembered that this is a qualitative example using hypothetical data. In actual practice, mechanistic analysis should be performed using actual laboratory beam test results and calculations of tensile strain in the pavement to quantify the expected performance. In the second-level analyses that will be carried out on completion of all laboratory and HVS tests, actual fatigue test data for the various mixes evaluated in this study together with mechanistic analyses of representative pavement structures will be used to estimate pavement performance for a range of traffic and environmental conditions.

Table 4.2: Example of Stiffness and Beam Fatigue Life Interaction in Predicting Field Performance

Pavement	Stiff Asphalt Mix		Soft Asphalt Mix	
	Tensile Strain (microstrain)	Predicted Pavement Fatigue Life	Tensile Strain (microstrain)	Predicted Pavement Fatigue Life
Thin overlay	400	122,860	450	770,651
Thick overlay	140	7,848,700	300	3,838,304

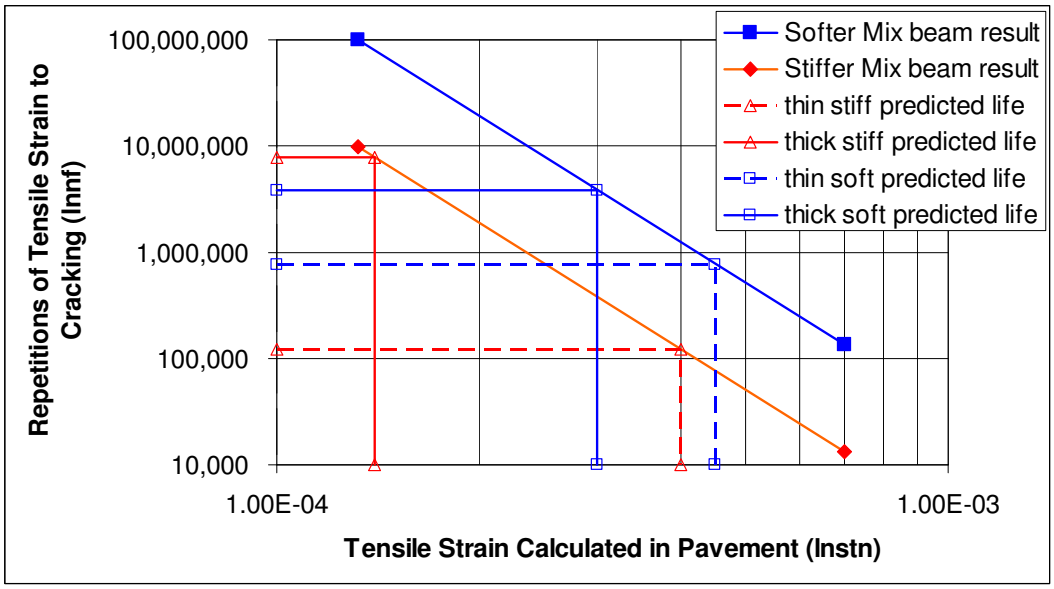

Figure 4.1: Example of stiffness and beam fatigue life interaction in predicting field performance

Figure 4.1 shows the calculated tensile strains versus repetitions to cracking for the thin and thick pavements together with fatigue life equations for the example:

Soft asphalt: $nf = 2.87\ (10^{-9})\ stn^{-3.960}$ **(4.1)**

Stiff asphalt beam: $nf = 2.87\ (10^{-10})\ stn^{-3.960}$ **(4.2)**

As can be seen in this figure, plots of these equations indicate that the softer asphalt mix has a longer beam fatigue life than the stiffer asphalt mix, for a given tensile strain. This is typical of most asphalt mixes. However, one cannot look only at the beam fatigue life to determine whether a given mix will have better fatigue performance. The change in tensile strain caused by the change of mix stiffness must also be considered.

In Table 4.2 and Figure 4.1, it can be seen that for the thin overlay the change from a soft to a stiff mix results in a comparatively small reduction in tensile strain (on the logarithmic scale). This is attributed to tensile strain in thin layers being controlled primarily by the underlying layers in the pavement. For the thick overlay, the change from the soft to the stiff mix results in a comparatively larger reduction in tensile strain, which is controlled by the thickness of the overlay. The reduction in tensile strain combined with the shift from the fatigue relation of the soft mix to the stiff mix still results in a net increase in the predicted fatigue life of the overlay.

Thus, an understanding of the interactions of mix stiffness and pavement structure is essential and will be used to comment on the laboratory results presented in this chapter.

4.1.3 Presentation of Results

The flexural fatigue test results are organized in three sections for each effect:

- Summary boxplots of test results, where each box contains three data points (the three replicates), two of which are the top (highest) and bottom (lowest) sides of the box and one, a white line, is the middle data point. The height of the box indicates the data variation across the three replicates.
- Identification of significant factors that affect the fatigue-response variables on an effect-categorized basis.
- Model selection using conventional regression analysis.

In the following discussion, brief explanations of the statistical analyses used in the chapter are provided in the section on temperature effect (Section 4.2). A more detailed discussion is provided in the detailed first-level source report (3). Additional information regarding the mixes, testing conditions, and detailed

test results are also provided in the first-level analysis report (3). Summary tables of the results of the fatigue tests for each mix are attached to this report as Appendix A.

4.2. Temperature Effect

This dataset includes the test results of ninety field-mixed, laboratory-compacted (FMLC) beams, tested with the following experiment design:

- Five binder types (AR4000, ARB, MAC15, MB15, and MB4)
- One air-void content (6.0 ± 0.5 percent)
- Three test temperatures (10°C, 20°C, and 30°C)
- Two strain levels (400 and 700 microstrain)
- Three replicates

The covariates investigated were:

- Binder type (*binder*)
- Temperature (*temp*)
- Strain level (*stn*)

4.2.1 Results

Figures 4.2 through 4.4 are boxplots summarizing the fatigue test results of temperature effect for phase angle, initial stiffness, and fatigue life. The boxplots are categorized by binder/mix type, strain level, and temperature.

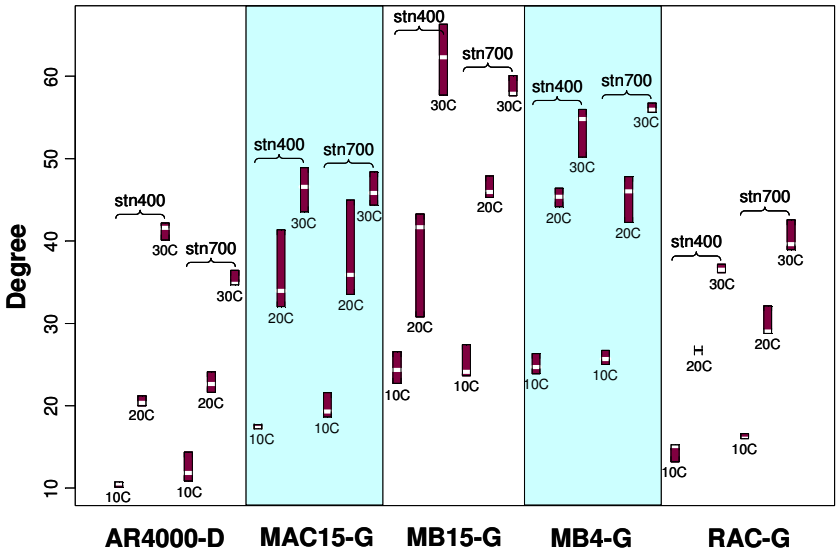

Figure 4.2: Summary plots of temperature effect and phase angle (6 percent AV).

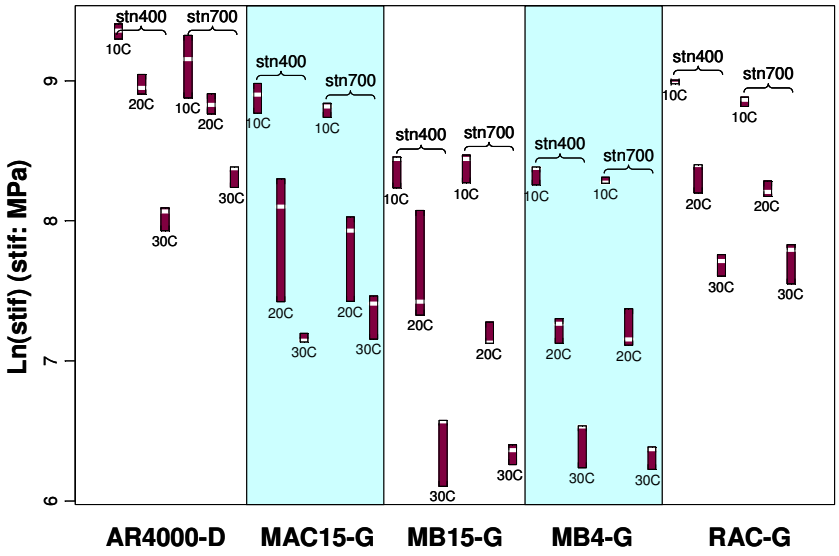

Figure 4.3: Summary plots of temperature effect and initial stiffness (6 percent AV).

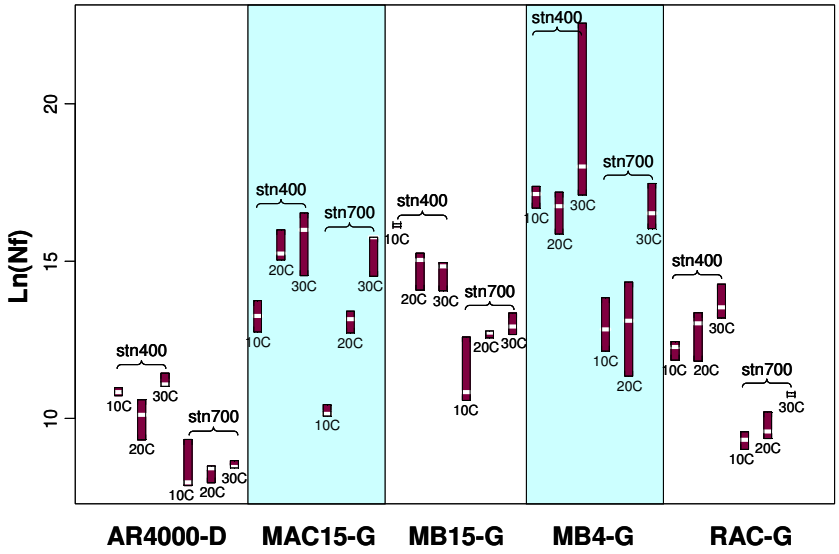

Figure 4.4: Summary plots temperature effect and fatigue life (6 percent AV).

The following statistical observations are made from the plots:

- Temperature is highly positive-correlated with phase angle and negative-correlated with initial stiffness per binder/mix type and strain level. An increase in temperature generally results in an increase in fatigue life per binder type and strain level. The only exception is the MB15-G mix at 400 microstrain, probably because the fatigue lives at this level and 10°C were obtained by extrapolation. The fatigue life values of MB4-G show some scatter at 400 microstrain and 30°C for the same reason.
- The strain level has no effect on phase angle and initial stiffness for binder type and temperature, but does have an effect on fatigue life.

- All three response variables are significantly affected by the binder/mix types.

The following observations are made regarding performance implications from the plots:

- The strain level has no effect on phase angle and initial stiffness for binder type and temperature, but does have an effect on fatigue life, as expected.
- Phase angles are lower and stiffnesses are larger at lower temperatures, as expected, and without exception.
- The beam fatigue lives at 700 microstrain are generally greater at higher temperatures, with few exceptions. However, at 400 microstrain the effect of temperature on beam fatigue life is less consistent. This is probably partly due to the larger number of specimens where the repetitions to failure had to be extrapolated because they never reached 50 percent loss of stiffness. It may also be partly due to the fact that asphalts from some crude sources do not show much temperature susceptibility of beam fatigue life, such as asphalt made from California Valley sources.
- In general, the MB4-G, MB15-G, and MAC15-G mixes have larger phase angles, lower stiffnesses, and longer beam fatigue lives at a given tensile strain than the RAC-G mix. The AR4000-D mix has even smaller phase angles, greater stiffness, and shorter beam fatigue lives at a given tensile strain compared with the RAC-G mix.

4.2.2 Identification of Significant Factors

Correlation Matrix

The correlation matrix (Table 4.3) shows the strength of linear relationship between the pairs of variables and was used as a quantitative method of identifying significant factors. Correlations that are significant based on an initial threshold correlation of 0.4 are highlighted in the table. The following is observed from the correlation matrix:

- Temperature is highly positive-correlated with phase angle, highly negative-correlated with initial stiffness, and has no apparent correlation with fatigue. This implies that higher temperatures result in higher initial phase angles and lower initial stiffness.
- Strain (*lnstn*) is negatively correlated with fatigue life, but does not correlate with phase angle and initial stiffness. This implies that fatigue life will decrease with increasing strain levels.
- Phase angle is highly negative-correlated with initial stiffness.
- All response variables appear to be somewhat affected by binder type.

Table 4.3: Correlation Matrix for Temperature Effect

	Binder	Temperature	Strain	Phase angle	Initial stiffness	Fatigue life
Binder	1.000000					
Temperature	-0.0008052731	1.000000				
Strain	0.0178554701	0.0537381228	1.000000			
Phase angle	0.1498805339	0.8154776111	0.10499028	1.000000		
Initial stiffness	-0.2621259643	-0.7245151231	-0.09380779	-0.9700557	1.000000	
Fatigue life	0.2829874359	0.2314169772	-0.43491147	0.5295507	-0.61930475	1.000000

Analysis of Variance (ANOVA)

The ANOVA results in Table 4.4 provide a second quantitative way to identify significant factors that affect the response variables. The criterion of assessing the importance of effect was set at a 5 percent significance level of P-value. Highlighted numbers in the table are considered significant.

Table 4.4: Analysis of Variance for Temperature Effect

Covariate	Statistic				
	Df	Sum of Sq	Mean Sq	F Value	Pr (F)
Phase angle					
binder	4	5086.28	1271.57	128.996	0.0000000
temp	1	12266.40	12266.40	1244.376	0.0000000
stn	1	33.51	33.51	3.399	0.0692335
binder:temp	4	226.10	56.52	5.734	0.0004474
binder:stn	4	28.81	7.20	0.731	0.5739031
temp:stn	1	38.08	38.08	3.863	0.0531171
Residuals	74	729.45	9.86		
Initial stiffness					
binder	4	27.65701	6.91425	199.916	0.0000000
temp	1	36.32274	36.32274	1050.220	0.0000000
stn	1	0.07740	.0.7740	2.238	0.1389228
binder:temp	4	2.12373	0.53093	15.351	0.0000000
binder:stn	4	0.05672	0.014118	0.410	0.8008904
temp:stn	1	0.18325	0.18325	5.298	0.0241614
Residuals	74	2.55935	0.03459		
Fatigue life					
binder	4	435.3588	108.8397	133.4643	0.00000000
temp	1	41.0334	41.0334	50.3170	0.00000000
stn	1	166.2617	166.2617	203.8779	0.00000000
binder:temp	4	31.7430	7.9358	9.7312	0.00000222
binder:stn	4	7.1785	1.7946	2.2007	0.07710575
temp:stn	1	8.5946	8.5946	10.5391	0.00175711
Residuals	74	60.3467	0.8155		

Design Plots

Design plots are used as a qualitative method to identify significant factors. A series of design plots based on the factor levels used in the study are presented in Figure 4.5 for phase angle, initial stiffness, and fatigue life, respectively. It should be emphasized at the outset that recognition of the importance of factor using design plots is a subjective judgment.

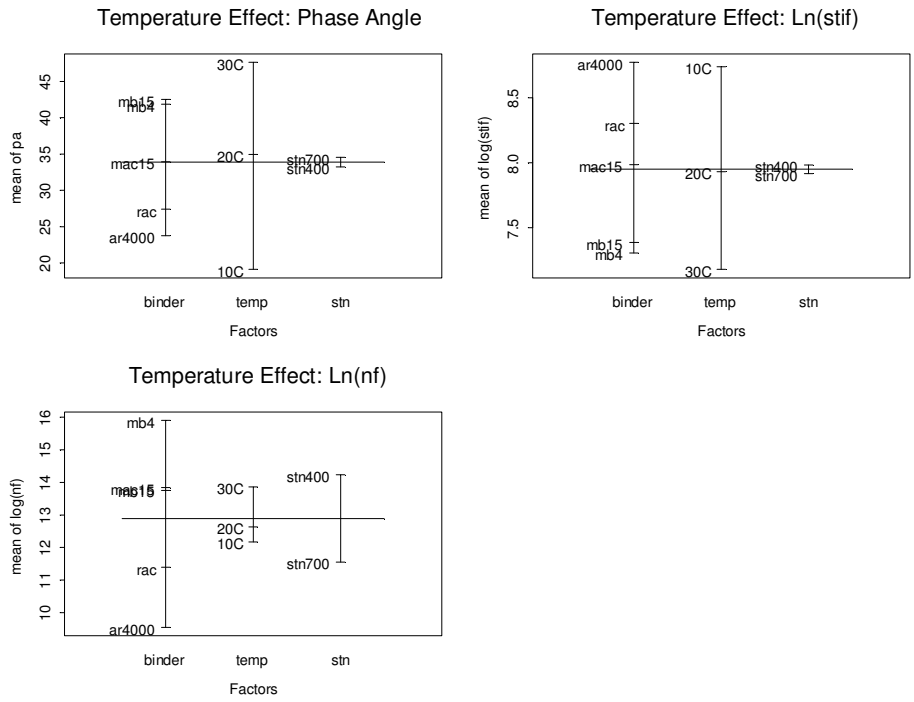

Figure 4.5: Design plots for temperature effect (6 percent AV).

In the figure, the horizontal line represents the overall mean of the response variable and the vertical lines indicate the means of the factor levels for a specific factor. The farther apart the marked factor levels in the vertical line, the more significant the effect of the factor on the response variable. The following was observed from the design plots:

- Phase angle is primarily affected by temperature and binder and is not affected by strain. Higher temperatures result in a larger initial phase angle.
- Initial stiffness is mainly affected by the binder and temperature but not by strain. The lower the temperature the higher the stiffness.
- Strain has a significantly greater effect on fatigue life than it does on stiffness.
- Temperature has a minor effect on fatigue life.
- The difference in beam fatigue performance is evident among the various binder/mix types.
- Higher mix stiffness results in lower fatigue life and vice versa.

Using the design plots, the controlled strain fatigue life of the various binders is ranked as follows, from best to worst:

1. MB4-G
2. MAC15-G, MB15-G
3. RAC-G
4. AR4000-D

The ranking of initial stiffness is generally reversed, going from stiffest to least stiff:

1. AR4000-D
2. RAC-G
3. MAC15-G
4. MB15-G
5. MB4-G

Pairs Diagram

A pairs diagram [contained in Reference (3)] was used as a second qualitative method of identifying the significance of correlation. This analysis confirmed the initial observations from the boxplots. *(N.B. An example of a pairs diagram is included subsequently in Figure 4.27.)*

Summary

The significant factors were identified from the correlation matrix, analysis of variance, design plot, and other plots (e.g., pairs diagram and interception plots). If all four criteria show significance in one independent variable, then this is considered as a "very important" factor. If three criteria are check-marked, the factor is considered as being "important". If only one or two criteria are checked, the variable is considered "less important."

Using this approach for the dataset of temperature effect, the following are noted:

- Binder is "important" to all three response variables (phase angle, initial stiffness, and fatigue life).
- Temperature is "very important" to both phase angle and initial stiffness and "important" to fatigue life.
- Strain is "very important" to fatigue life and has no impact on phase angle and initial stiffness.

The results indicate that the MB4-G, MB15-G, and MAC15-G mixes may have better reflective cracking performance than the RAC-G and AR4000-D mixes when used as thin overlays. They would also likely have better low-temperature cracking resistance, but would have a greater risk of rutting of the asphalt mix. They would also provide less structural protection to underlying layers because of their lower stiffnesses.

It should be emphasized, based on the discussion presented earlier, that the observations presented are directly related only to the use of thin overlays over cracked pavements. If these mixes are used as

structural overlays, analyses like that illustrated including individual layer thickness and stiffness, loads, temperature, and fatigue-versus-strain results, should be used.

4.2.3 Regression Analysis

Mallows' C_p criterion was used to identify the best subset of covariates for each regression equation, in addition to the analysis of the significance of variables described in much greater detail in Reference 3. The analysis of the significance of explanatory variables included the correlation matrix, Analysis of Variance, design plots, and pairs diagrams.

Initial Stiffness

Temperature and binder were identified as the two factors most influencing initial stiffness. The final model chosen for initial stiffness is therefore:

$$E(\ln stif) = \underset{(0.0682)}{9.5115} - \underset{(0.0407)}{0.3949}\,binder1 - \underset{(0.0235)}{0.3300}\,binder2 - \underset{(0.0166)}{0.1875}\,binder3 + \underset{(0.0129)}{0.0883}\,binder4 - \underset{(0.0031)}{0.0775}\,temp \qquad \textbf{(4.3)}$$

$R^2 = 0.93$

where initial stiffness (*stif*) has the unit MPa and temperature (*temp*) is in °C.

The term $E(\ln stif)$ is the expected value of $\ln stif$ and the number in parentheses shown under each regression coefficient is the standard error of the estimate of the regression coefficient. The residual standard error is 0.244 on 84 degrees of freedom and the regression line explains as high as 93 percent of the variation in the data.

The term *binder* in the formulation is a category covariate (or factor), which needs to be coded (or parameterized) by "contrasts" for use in the linear regression equation for stiffness. To find the stiffness for a given mix, the appropriate set of integers shown in Table 4.5 must be used in the equation.

Example

To determine the regression equation of initial stiffness (*lnstif*) for MB4, the factor values should be set as follows (from Table 4.5):

binder1 = 0, *binder2* = 0, *binder3* = 3, and *binder4* = -1.

This results in the following initial stiffness regression equation for the MB4 mixes:

$$E(\ln stif) = 8.8607 - 0.0775\,temp \qquad \textbf{(4.4)}$$

Table 4.5: Contrast Tables of Category Covariates Used in Regression Analyses

Factor *binder*: for all the effects other than gradation effect				
Binder	***binder1***	***binder2***	***binder3***	***binder4***
AR4000	-1	-1	-1	-1
MAC15	1	-1	-1	-1
MB15	0	2	-1	-1
MB4	0	0	3	-1
ARB	0	0	0	4
Factor *binder*: for gradation effect				
Binder	***binder1***	***binder2***		
MAC15	-1	-1		
MB15	1	-1		
MB4	0	2		
Factor *cond*: for aging effect				
Condition	***cond***			
aging	-1			
none	1			
Factor *comp*: for compaction effect				
Compaction	***comp***			
FMLC	-1			
LMLC	1			
Factor *grad*: for gradation effect				
Grading	***grad***			
DG	-1			
GG	1			

An analysis of the residuals of the fit was performed, and is described in detail in Reference 3. The results of the analysis showed that there was a slight parabolic trend in the residuals. Inclusion of the interaction term *binder*temp* would correct this; however, the increasing complexity of the model specification outweighs the increase of R^2. The assumption of homoscedasticity appeared reasonable. The Cook's distance accompanied with the normal probability plot, the quantile-quantile plot (QQ plot), and the histogram of residuals was used to identify the influential points and possible outliers. The distribution of estimated residuals was found to be close to a normal distribution, which is an assumption of the regression equation.

Fatigue Life

In evaluating the significance of variables affecting the beam fatigue life, strain was identified as "very important," while temperature and binder were identified as "important" in terms of influencing fatigue life. Using Mallows' C_p criterion, the same factors were identified as the best subset of covariates.

The final model chosen for fatigue life is:

$$E(\ln nf) = \underset{(2.8240)}{-22.7041} + \underset{(0.1629)}{2.1694}\,binder1 + \underset{(0.0941)}{0.7178}\,binder2 + \underset{(0.0696)}{0.8797}\,binder3 - \underset{(0.0517)}{0.3740}\,binder4 + \underset{(0.0127)}{0.0837}\,temp - \underset{(0.3711)}{4.5027}\ln stn$$

$$R^2 = 0.88 \qquad \textbf{(4.5)}$$

The residual standard error of the fit is 0.9774 on 81 degrees of freedom. It should be noted that two outliers (G9-MB4-14A and G9-MB4-20B) were eliminated according to the Cook's distance (3). The residuals analysis of the fatigue life fit showed no significant patterns, indicating that the suggested model is appropriate. Both the QQ plot and the histogram showed results that are considered acceptable.

As with the final regression equation for initial stiffness, care should be used when interpreting the coefficient of *binder*, and the contrast scheme in Table 4.5 should be followed.

Similar analysis procedures to that described above are followed in Sections 4.3 through 4.6 and only the results are presented. Additional information and data tables are provided in the first-level report (3).

4.3. Air-Void Content Effect

This test investigated the effect of degree of compaction (the air-void content effect) on fatigue performance at 20°C for various mixes. The experiment design contained a total of sixty tests comprising:

- Five binder types (AR4000, ARB, MAC15, MB15, and MB4),
- Two air-void contents (6.0 ± 0.5 percent and 9.0 ± 1.0 percent),
- Two strain levels (400 and 700 microstrain), and
- Three replicates.

The results of thirty tests from the temperature effect study (6.0 percent air void at 20 C) were included in this experiment.

The covariates investigated were primarily:

- Binder type (*binder*)
- Air-void content (*av*)
- Strain level (*stn*)

Example summary boxplots and design plots are shown in Figures 4.6 through 4.9. The other plots, correlation matrices, and analysis of variance results are provided in Reference (3).

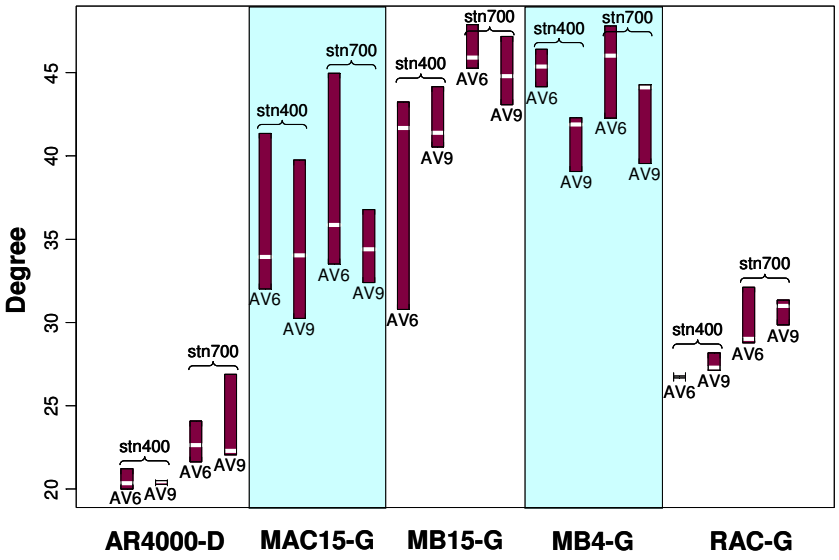

Figure 4.6: Summary boxplots of air-void content effect and phase angle (AV=9 percent).

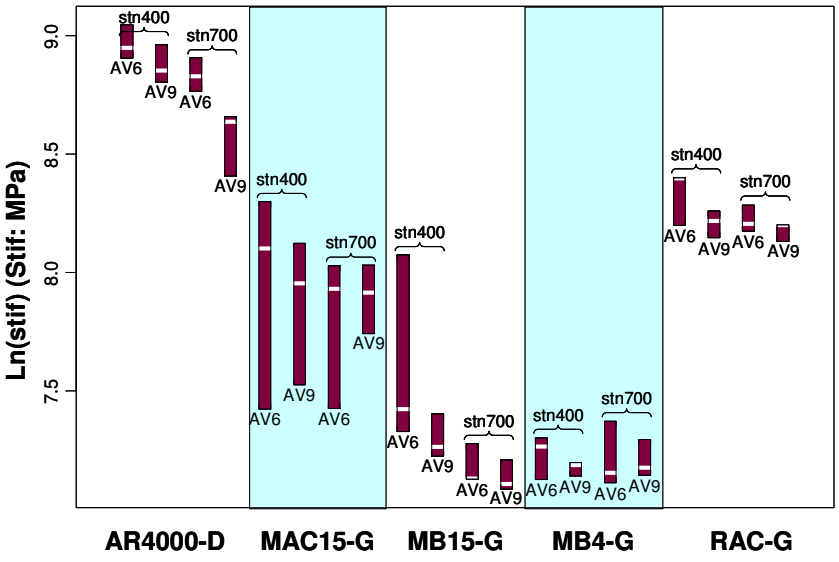

Figure 4.7: Summary boxplots of air-void content effect and initial stiffness (AV=9 percent).

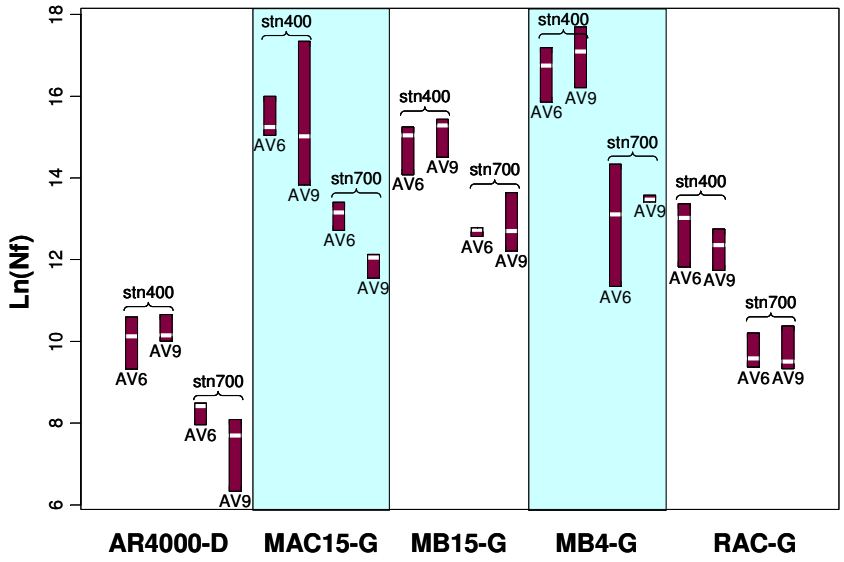

Figure 4.8: Summary boxplots of air-void content effect and fatigue life (AV=9 percent).

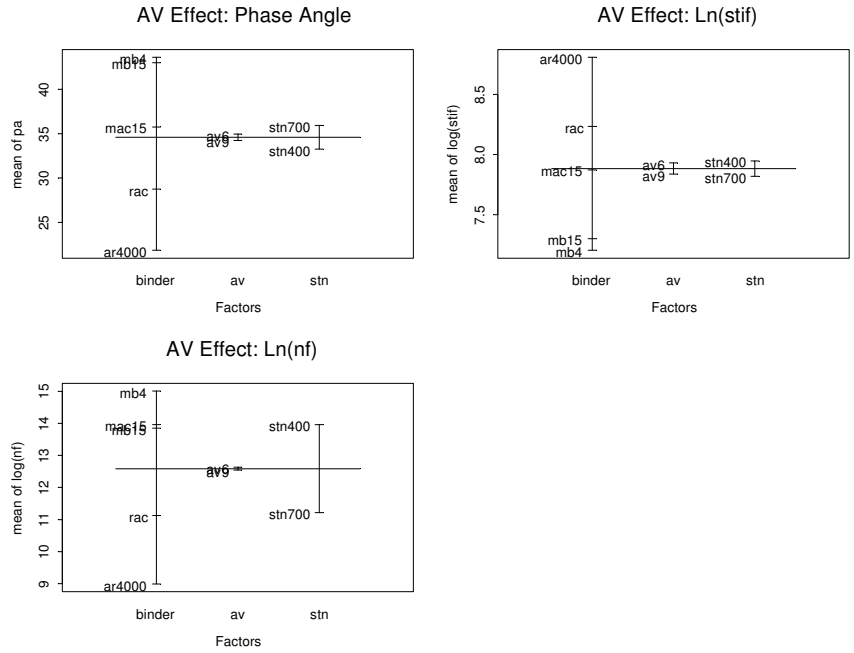

Figure 4.9: Design plots of air-void content effect (AV=9 percent).

A review of the data led to the following observations:

- From the summary boxplots, an apparent air-void content effect is only noted for:
  - MB4-G with regard to phase angle
  - AR4000-D and MB15-G with regard to initial stiffness
  - AR4000-D and MAC15-G with regard to beam fatigue life at 700 microstrain

- There is no air-void content effect on the response variables. Instead, the beam fatigue performance is mainly dominated by the binder type. The strain factor is "very important" to the beam fatigue life, but not phase angle and initial stiffness.
- In the analysis of variance, phase angle and initial stiffness are sensitive to the strain level, with the higher strain causing higher phase angle and lower stiffness. Overall, there are no obvious interaction effects on fatigue performance.
- The best subsets of covariates chosen by Mallows' C_p criterion are:
    - Binder and air-void content for initial stiffness
    - Binder and strain for fatigue life

The final regression models after the identification of significant factors and the iterative procedure of model building are:

$$E(\ln stif) = \underset{(0.0931)}{8.2053} - \underset{(0.0277)}{0.4120}\,binder1 - \underset{(0.0159)}{0.3850}\,binder2 - \underset{(0.0109)}{0.2007}\,binder3 + \underset{(0.0084)}{0.0897}\,binder4 - \underset{(0.0123)}{0.0425}\,av \qquad \textbf{(4.6)}$$

$R^2 = 0.96$

and

$$E(\ln nf) = \underset{(2.5359)}{-25.1119} + \underset{(0.1476)}{2.5119}\,binder1 + \underset{(0.0852)}{0.8216}\,binder2 + \underset{(0.0603)}{0.7180}\,binder3 - \underset{(0.0467)}{0.3696}\,binder4 - \underset{(0.3369)}{5.0109}\ln stn \qquad \textbf{(4.7)}$$

$R^2 = 0.94$

4.4. Aging Effect

This experiment investigated the effect of long-term oven aging (six days) on beam fatigue performance for the various mixes. The relative experiment design contained a total of fifty tests, thirty of which were taken as part of the temperature effect study (6.0 percent air void at 20 C). The experimental design for the other twenty tests included:

- Five binder types (AR4000, ARB, MAC15, MB15, and MB4)
- Two strain levels (400 and 700 microstrain)
- Two replicates

The compacted beam specimens were conditioned in a forced draft oven for six days at 85°C. The covariates investigated were:

- Binder type (*binder*)
- Conditioning (*cond*)
- Strain level (*stn*)

Example summary boxplots and design plots are shown in Figures 4.10 through 4.13. Additional statistical plots, correlation matrices, and analysis of variance results are provided in Reference (3).

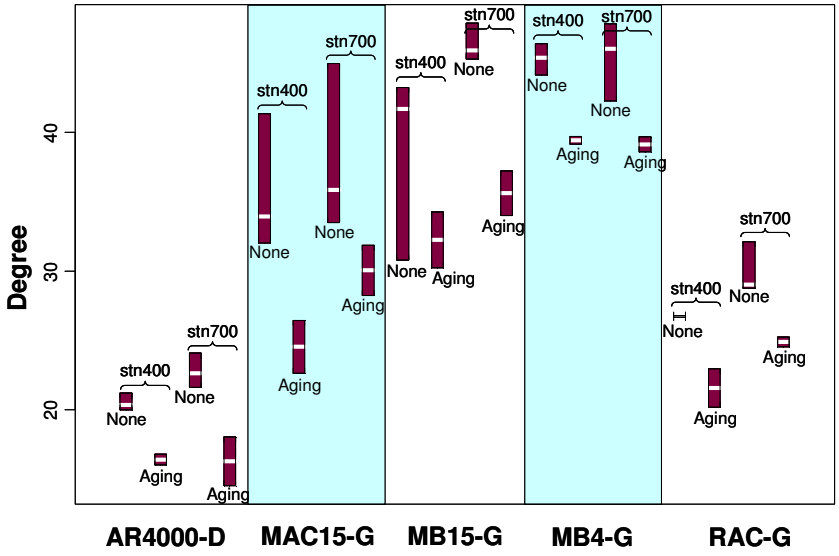

Figure 4.10: Summary boxplots of aging effect and phase angle (6 days aging, 6 percent AV, 20°C).

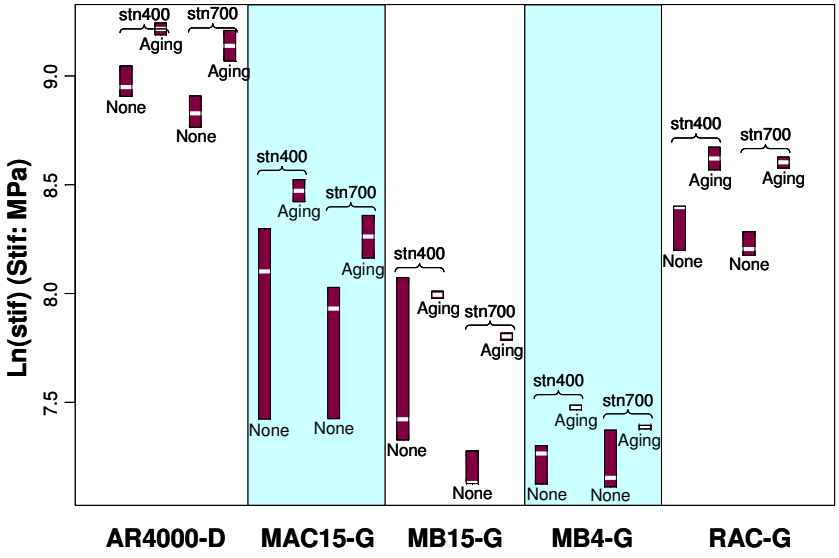

Figure 4.11: Summary boxplots aging effect and initial stiffness (6 days aging, 6 percent AV, 20°C).

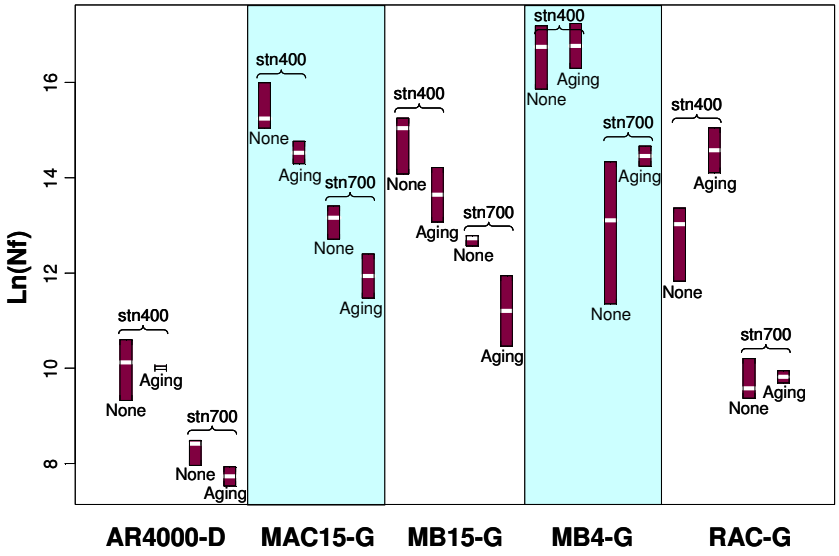

Figure 4.12: Summary boxplots of aging effect and fatigue life (6 days aging, 6 percent AV, 20°C).

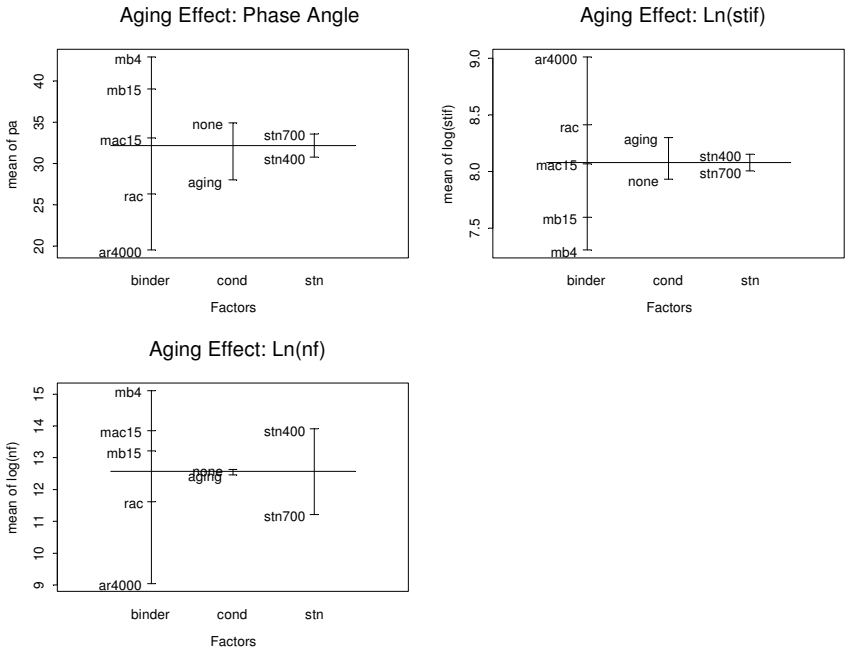

Figure 4.13: Design plots for aging effect (6 day aging, 6 percent AV, 20°C).

A review of the data led to the following observations regarding performance and the statistical significance of explanatory variables:

- From the summary boxplots, it is apparent that aging results in a decrease in initial phase angle and an increase in initial stiffness for all binder types and strain levels. In general, aging causes reduced beam fatigue life for each binder type and strain level, but opposite trends are noted for

MB4-G at 700 microstrain and RAC-G at 400 microstrain, implying that aging increases the fatigue life for these binders. This has been observed for some mixes in other experiments (5).

- From the design plots, it appears that aging [shown as "conditioning" *(cond)* in Figure 4.13] is "important" to phase angle and initial stiffness but appears to have no effect on beam fatigue life when evaluated across all of the mixes together. This reflects the fact that the aging had the opposite effect for the MB4-G and RAC-G compared to AR4000-D, MAC15-G, and MB15-G.
- The ranking of the mixes for beam fatigue life, stiffness, and phase angle is the same for the aged and un-aged tests.
- Strain is "very important" to fatigue life but has no effect on phase angle and initial stiffness.
- Beam fatigue performance is significantly affected by binder type.
- The interaction effect of binder and conditioning on fatigue life is apparent
- The best subsets of covariates chosen by Mallows' C_p criterion are:
    - Binder and conditioning for initial stiffness
    - Binder, conditioning, and strain for fatigue life

The final regression models after the identification of significant factors and the iterative procedure of model building are:

$$E(\ln stif) = \underset{(0.0254)}{8.1027} - \underset{(0.0390)}{0.4717}\,binder1 - \underset{(0.0234)}{0.3383}\,binder2 - \underset{(0.0160)}{0.2239}\,binder3 + \underset{(0.0124)}{0.0867}\,binder4 - \underset{(0.0254)}{0.1944}\,cond \qquad \textbf{(4.8)}$$

$R^2 = 0.94$

and

$$E(\ln nf) = \underset{(2.5566)}{-21.3729} + \underset{(0.1448)}{2.4274}\,binder1 + \underset{(0.0836)}{0.6077}\,binder2 + \underset{(0.0616)}{0.8821}\,binder3 - \underset{(0.0481)}{0.3062}\,binder4 + \underset{(0.0959)}{0.2001}\,cond - \underset{(0.3396)}{4.5051}\ln stn \qquad \textbf{(4.9)}$$

$R^2 = 0.95$

4.5. Mixing and Compaction Effect

This test investigated the effect of mixing and compaction methods on fatigue performance. The relative experiment design contained a total of fifty tests, thirty of which were undertaken as part of the temperature effect study (6.0 percent air void at 20 C) on field-mixed, laboratory-compacted specimens. The experimental design for the other twenty tests on laboratory-mixed, laboratory compacted beams included:

- Five binder types (AR4000-D, RAC-G, MAC15-G, MB15-G, and MB4-G),
- Two strain levels (400 and 700 microstrain), and
- Two replicates.

The covariates investigated were primarily:

- Binder type (*binder*)
- Compaction method (*comp*)
- Strain level (*stn*)

Summary boxplots and design plots are shown in Figures 4.14 through 4.17. Additional plots, correlation matrices, and analysis of variance results are provided in Reference (3).

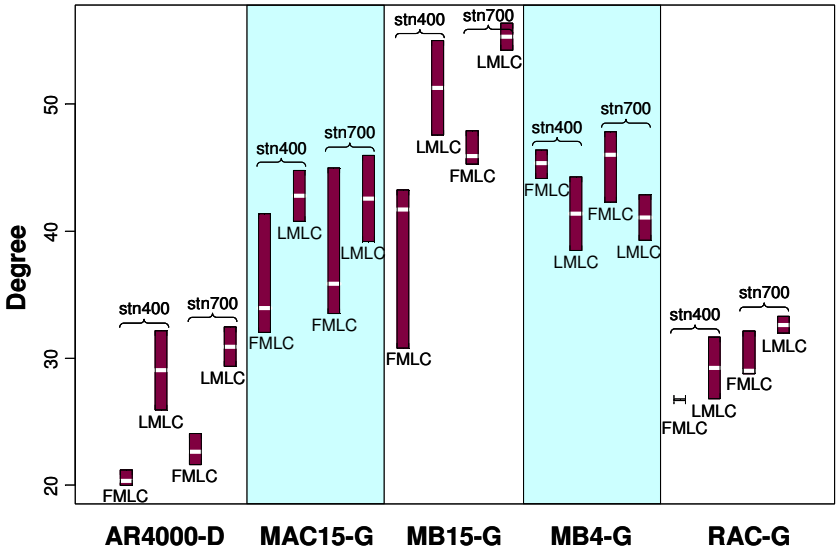

Figure 4.14: Summary boxplots of compaction effect and phase angle (6 percent AV, 20°C).

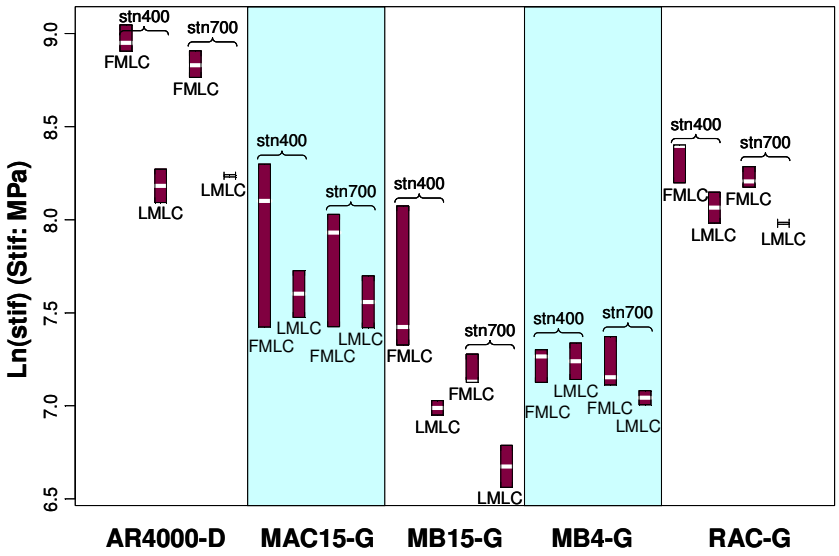

Figure 4.15: Summary boxplots of compaction effect and initial stiffness (6 percent AV, 20°C).

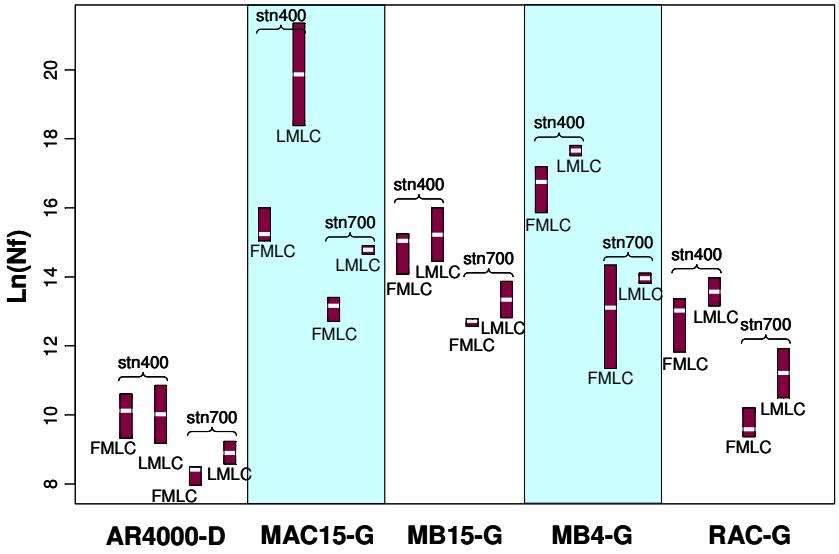

Figure 4.16: Summary boxplots of compaction effect and fatigue life (6 percent AV, 20°C).

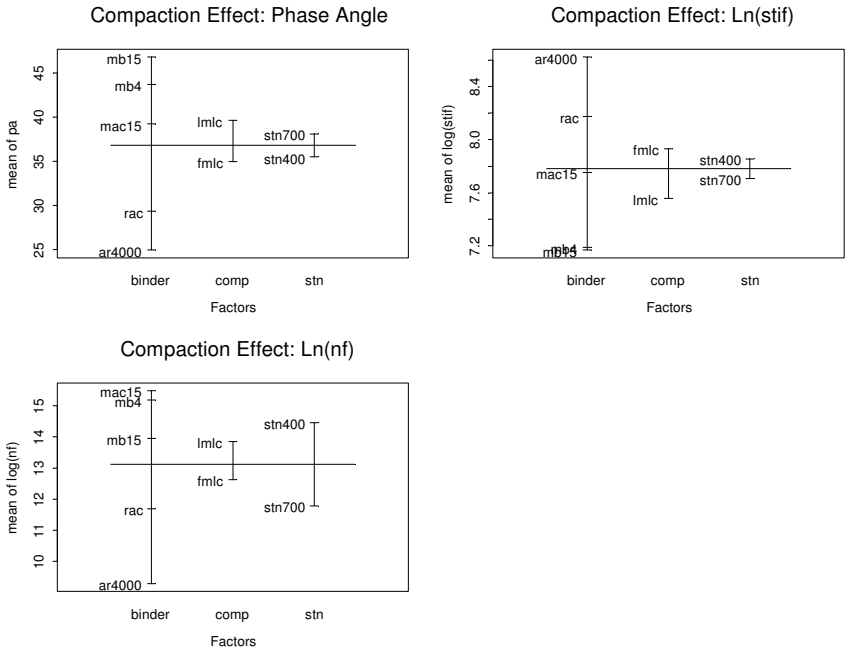

Figure 4.17: Design plots for compaction effect (6 percent AV, 20°C).

A review of the data led to the following observations regarding performance and statistical significance:

- The LMLC specimens had generally had greater phase angles, were less stiff, and had longer beam fatigue lives compared to the FMLC. These results are consistent with less aging of the LMLC specimens. This is to be expected considering that the FMLC mixes were mixed in the plant, stored in cans, and then reheated for laboratory compaction, while the LMLC specimens were mixed from binder that had been stored in sealed containers, short-term oven aged, then

immediately compacted. The LMLC specimens also generally spent less time on the shelf waiting for testing than did the FMLC specimens.

- The ranking of the mixes for phase angle for LMLC is the same as for FMLC, except that the MB4-G mix had a greater phase angle for the FMLC mix than for the LMLC mix, which changed its place in the rankings. The ranking for phase angle from highest to lowest is: AR4000-D > RAC-G > MB4-G, MB15-G, MAC15-G, with the latter three changing rank depending upon strain level.
- The ranking of the mixes for initial stiffness for LMLC is the same as for FMLC, except for some overlap between MAC15-G, MB4-G, and MB15-G at the low strain level. In general, the ranking from stiffest to least stiff is: AR4000-D > RAC-G > MAC15-G > MB4-G > MB15-G.
- The ranking of the mixes for beam fatigue life for LMLC and FMLC is the same as for FMLC, except for some overlap and interchange between MB15-G, MAC15-G, and MB4-G, depending on strain level and specimen preparation. In general, the ranking from best to worst beam fatigue life is: MAC15-G, MB4-G > MB15-G > RAC-G > AR4000-D. It must be remembered that this is the beam fatigue life under constant deformation testing, and that mechanistic analysis must be performed to determine which mix will have the best expected best fatigue life in the pavement structure.
- Compaction and binder are "important" to all three response variables.
- Strain is "very important" to beam fatigue life.
- The interaction of binder and compaction is significant at the 5 percent significance level. However, if the mean square in the analysis of variance is used for comparison, the interaction effects can be ignored (3).
- The best subsets of covariates chosen by Mallows' C_p criterion are:
    - Binder and compaction for initial stiffness
    - Binder, compaction, and strain for fatigue life

The final regression models after the identification of significant factors and the iterative procedure of model building are:

$$E(\ln stif) = \underset{(0.0288)}{7.7301} - \underset{(0.0442)}{0.4353}\,binder1 - \underset{(0.0265)}{0.3683}\,binder2 - \underset{(0.0181)}{0.1576}\,binder3 + \underset{(0.0140)}{0.1026}\,binder4 - \underset{(0.0288)}{0.1733}\,comp \qquad \textbf{(4.10)}$$

$R^2 = 0.92$

and

$$E(\ln nf) = \underset{(3.1749)}{-21.4758} + \underset{(0.1842)}{2.8998}\,binder1 + \underset{(0.1043)}{0.6178}\,binder2 + \underset{(0.0734)}{0.6478}\,binder3 - \underset{(0.0567)}{0.3345}\,binder4 + \underset{(0.1175)}{0.5082}\,comp - \underset{(0.4222)}{4.60001}\ln stn \qquad \textbf{(4.11)}$$

$R^2 = 0.92$

4.6. Gradation Effect

This experiment investigated the effect of dense- and gap-gradation on phase angle, initial stiffness, and beam fatigue life. The relative experiment design contained a total of twenty-four tests on laboratory-mixed, laboratory compacted beams as follows:

- Three binder types (MAC15, MB15, and MB4),
- Two gradations (dense and gap),
- Two strain levels (400 and 700 microstrain),
- One temperature (20°C), and
- One air-void content (6 percent).

In addition to these twenty-four beams, four AR4000-D (LMLC) and four RAC-G (LMLC) beams were tested for comparison.

The covariates investigated were primarily:

- Binder type (*binder*)
- Gradation (*grad*)
- Strain level (*stn*)

Summary boxplots and design plots are shown in Figures 4.18 through 4.21. The other plots, correlation matrices, and analysis of variance results are provided in Reference (3).

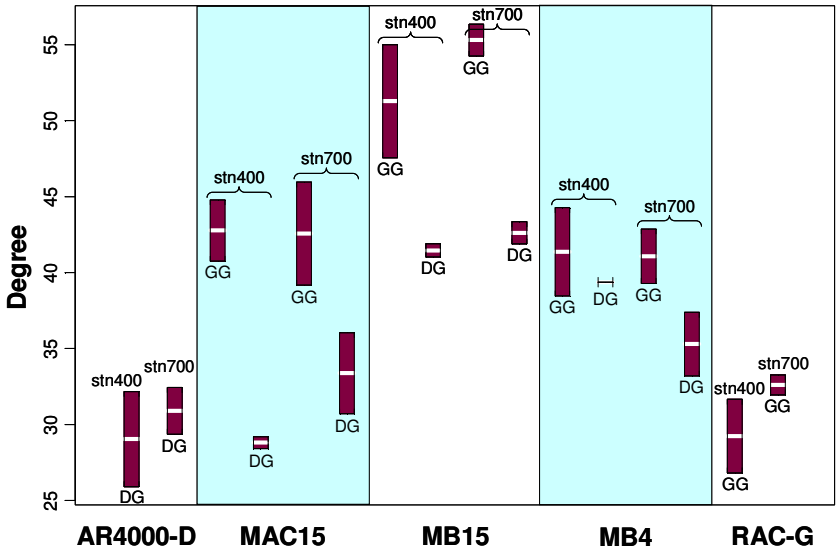

Figure 4.18: Summary boxplots of gradation effect and phase angle (6 percent AV).

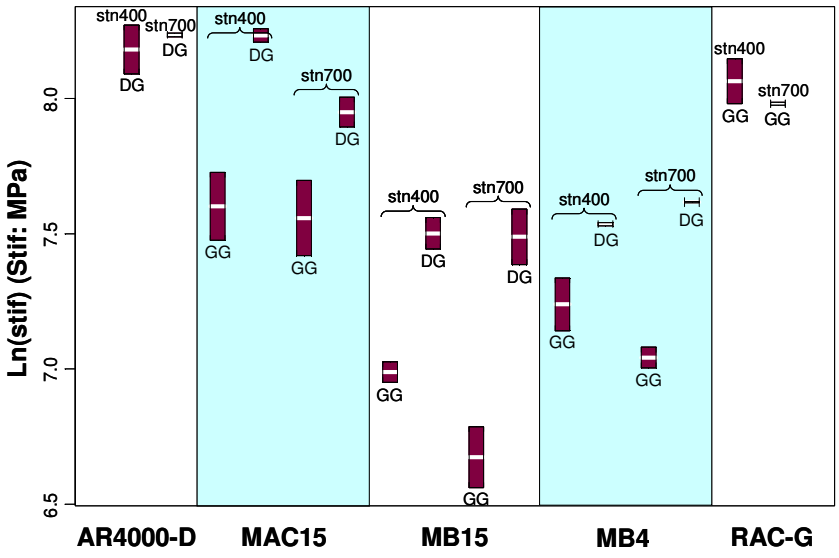

Figure 4.19: Summary boxplots of gradation effect and initial stiffness (6 percent AV).

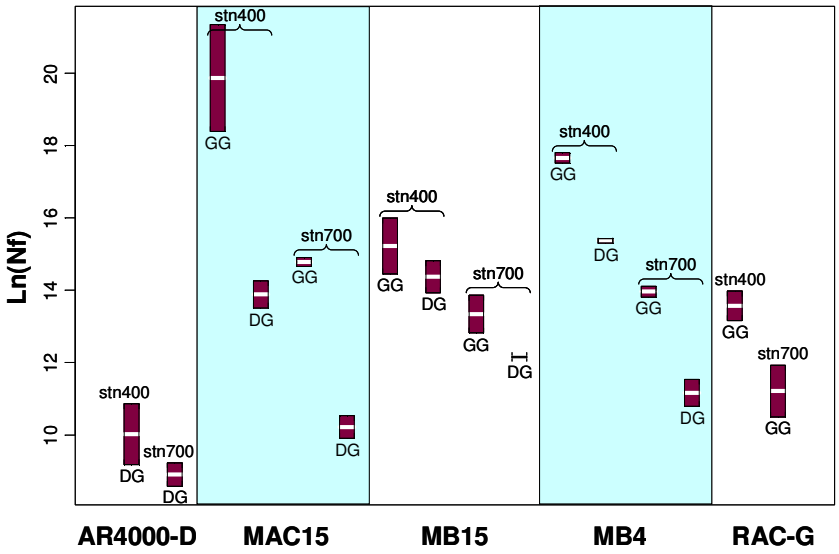

Figure 4.20: Summary boxplots of gradation effect and fatigue life (6 percent AV).

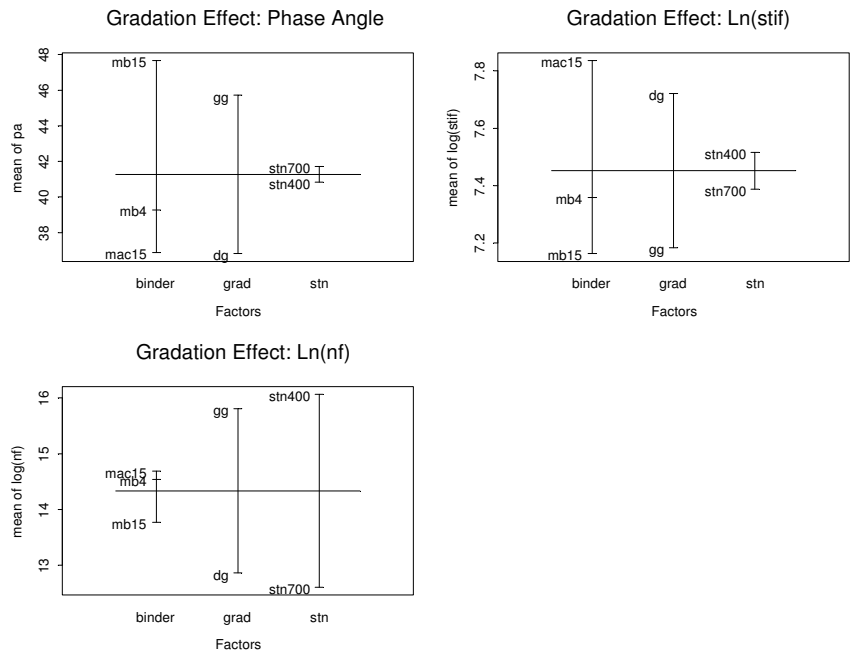

Figure 4.21: Design plots for gradation effect (6 percent AV).

A review of the data leads to the following statistical observations:

- Gradation is "very important" to all response variables, with phase angle and initial stiffness significantly affected by the binder.
- In this series of tests, the effect of binder type on fatigue performance was significant.
- Strain magnitude is "very important" to fatigue life. At a low strain there is generally more variation in the test results than at a higher strain, with dense-graded mixes showing less variation than gap-graded mixes.
- The best subsets of covariates chosen by Mallows' C_p criterion are:
    - Binder and gradation for initial stiffness
    - Gradation and strain for fatigue life

The following performance-related observations are drawn from the box plots and design plots:

- The phase angles of the MAC15-D, MB15-D, and MB4-D mixes are smaller than those of the gap-graded mixes with the same binder type. The dense-graded MB15-D and MB4-D mixes have greater phase angles than the AR4000-D and RAC-G mixes, indicating the potential for better resistance to cracking when used in thin overlays.
- As expected, the initial stiffnesses of the MAC15-D, MB15-D, and MB4-D mixes are greater than those of the gap-graded mixes with the same binder. This indicates that these mixes will likely

have smaller tensile strains compared to the gap-graded mixes when placed in overlays that are thicker than thin blankets, which will tend to increase pavement fatigue life.

- The beam fatigue lives of the MAC15-D, MB15-D, and MB4-D mixes are shorter than those of the gap-graded mixes with the same binder type. This indicates that when used in thin blanket overlays for reflective cracking they will likely have shorter fatigue lives than the gap-graded mixes with the same binder type.
- The stiffnesses of the MAC15-D, MB15-D, and MB4-D mixes are less than the stiffnesses of the AR4000-D and RAC-G mixes, except for the MAC15-D mix at 400 microstrain. The beam fatigue lives of the MAC15-D, MB15-D, and MB4-D mixes are greater than the beam fatigue lives of the AR4000D and RAC-G mixes, except for the MAC15-D mix at 700 microstrain. The net result for the predicted pavement fatigue life and the reflective cracking life of thicker overlays will depend on the interaction of the mix stiffness, greater values of which reduce tensile strains, and the beam fatigue life at a given tensile strain as explained in Section 1.1.2. The results do indicate that structural analysis calculations should be performed for various structures and loading conditions to evaluate the expected cracking performance of MAC15-D, MB15-D, and MB4-D mixes compared to typical structural mixes in structural overlay and new pavement applications.
- In general, these dense-graded mixes are likely to have greater mix rutting resistance, reduce the risk of rutting of the unbound layers, and have somewhat less low-temperature cracking resistance than the corresponding gap-graded mixes. However, performance with regard to these distresses should be evaluated using appropriate tests before drawing definitive conclusions.

The final regression models after the identification of significant factors and the iterative procedure of model building are:

$$E(\ln stif) = \underset{(0.0247)}{7.4573} - \underset{(0.0299)}{0.3121}\, binder1 - \underset{(0.0176)}{0.0665}\, binder2 - \underset{(0.0247)}{0.2639}\, grad \qquad \textbf{(4.12)}$$

$R^2 = 0.93$

and

$$E(\ln nf) = \underset{(4.9132)}{-32.7888} + \underset{(0.1770)}{1.4293}\, grad - \underset{(0.6556)}{6.2637} \ln stn \qquad \textbf{(4.13)}$$

$R^2 = 0.88$

4.7. Grouped Fatigue Tests

Analyses of grouped results were undertaken to develop comprehensive models that better describe the beam fatigue performance of the materials tested. The dataset used consisted of all 172 fatigue tests. The covariates inspected were:

- Binder type *(binder)*
- Gradation *(grad)*
- Compaction *(comp)*
- Aging *(cond)*
- Air-void content *(av)*
- Temperature *(temp)*
- Strain (*stn*)

A sample design plot is shown in Figure 4.22. The other plots, correlation matrices, and analysis of variance results are provided in Reference (3).

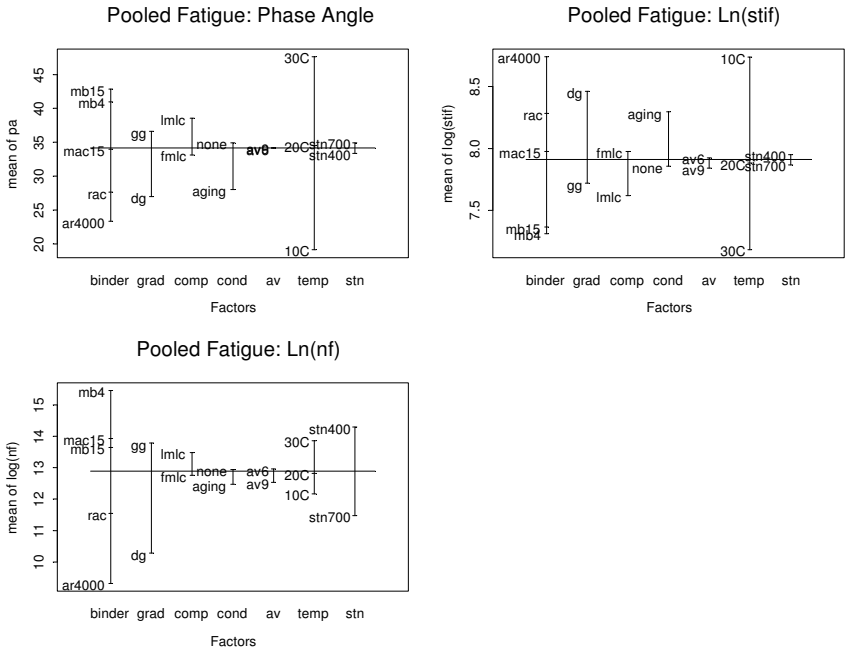

Figure 4.22: Example design plots for pooled fatigue tests.

A review of the data (summarized in Table 4.4) led to the following statistical observations:

- Temperature is "very important" to phase angle, while the covariates binder, gradation, compaction, and conditioning are "important." The air-void content and strain covariates are "less important" to phase angle.
- Initial stiffness is mainly affected by gradation and temperature, which were identified as "very important." The binder, compaction, and conditioning covariates are "important," while air-void content and strain were again "less important."

- Strain and gradation are "very important" in fatigue performance, with binder, compaction, and temperature considered "important." Air-void content was considered "less important," while conditioning had no effect on fatigue performance.
- The analysis of variance and interaction plots showed a 5 percent significance level of P-value for interactions between:
    - Binder and compaction, and binder and temperature on phase angle,
    - Binder and temperature, and temperature and strain on initial stiffness, and
    - Temperature and strain, and binder and temperature on fatigue life.
- When analyzed using mean squares and interaction plots, the interaction effects of all the response variables could be ignored when compared to the main effects.
- The best subsets of covariates chosen by Mallows' C_p criterion are:
    - For initial stiffness: binder, gradation, compaction, conditioning, and temperature, based on Mallows' C_p criterion.
    - For fatigue life: binder, gradation, compaction, air-void content, temperature, and strain, based on Mallows' C_p criterion. Although air-void content was selected based on the C_p criterion, it was excluded from the regression models, based on an analysis of all data and preliminary regression analyses.

The final regression models for grouped fatigue testing after the identification of significant factors and the iterative procedure of model building are:

$$E(\ln stif) = \underset{(0.0633)}{9.6615} - \underset{(0.0442)}{0.1105}\,binder1 - \underset{(0.0189)}{0.2409}\,binder2 - \underset{(0.0119)}{0.1338}\,binder3 + \underset{(0.0096)}{0.1178}\,binder4 - \underset{(0.0391)}{0.2805}\,grad - \underset{(0.0255)}{0.1832}\,comp - \underset{0.0255}{0.1924}\,cond - \underset{0.0027}{0.0774}\,temp \quad \textbf{(4.14)}$$

$R^2 = 0.93$

and

$$E(\ln nf) = \underset{(2.0795)}{-25.7076} + \underset{(0.2089)}{1.1699}\,binder1 + \underset{(0.0897)}{0.3658}\,binder2 + \underset{(0.0565)}{0.6024}\,binder3 - \underset{(0.0453)}{0.4411}\,binder4 + \underset{(0.1859)}{1.1629}\,grad + \underset{(0.1213)}{0.4461}\,comp + \underset{0.02128}{0.0828}\,temp - \underset{0.2723}{4.8507}\ln stn \quad \textbf{(4.15)}$$

$R^2 = 0.87$

4.8. Summary of Factor Identification

A main-effect summary table was developed based on quantitative and qualitative analyses to identify the significant factors of the study. Although this identification process is somewhat subjective, the significant factors identified closely match the covariates selected for regression analysis using Mallow's C_p criterion. A summary of the factor identification process includes:

- The temperature effect on fatigue performance is apparent on all three response variables, namely phase angle, initial stiffness, and fatigue life.
- The air-void content effect on fatigue performance is not significant for all the response variables.
- The aging effect on fatigue performance is only significant for phase angle and initial stiffness.
- The compaction effect on fatigue performance is important for all the response variables.
- The gradation effect (dense- versus gap-grading) on fatigue performance is significant for the MAC15, MB15, and MB4 mixes for all the response variables. AR4000 and ARB were excluded from this test.
- Strain has a dominant effect on fatigue life but not on phase angle and initial stiffness, as expected. It should be noted that the selection of strain levels and observations from the test are directly related to the use of thin overlays over cracked pavement, and are *not* related to structural overlays, which should be designed and analyzed using a mechanistic analysis.
- Binder type has a universal effect on all the response variables. The only exception was a limited effect on fatigue performance when comparing the effect of gradation with the MAC15, MB15, and MB4 mixes.

4.9. Summary of Regression Analysis

The regression models are summarized in Tables 4.6 and 4.7. Given that a partial factorial experimental design (172 tests selected from a full factorial of 1,440 tests) was followed, extrapolations or inferences of model predictions beyond the data range should be undertaken with caution.

4.9.1 Initial Stiffness

Figure 4.23 schematically summarizes the initial stiffness regression models listed in Table 4.6. Evaluations of these data suggest the following:

- The ranking of initial stiffness of the binders, from stiffest to least stiff, under various effects is in the order listed below for the FMLC specimens. It will be noted that the LMLC specimens with the MB4 and MB15 binders exhibit essentially the same behavior.
    1. AR4000-D
    2. RAC-G
    3. MAC15-G
    4. MB15-G
    5. MB4-G
- The values of initial stiffness increase under the following situations:
    - Specimens tested at low temperature or aging-conditioned

- Specimens prepared at low air-void content or by the field-mixed, laboratory-compacted method
- Specimens with a dense-graded gradation compared to a gap-graded gradation, for the same binder type.

- The effects of air-void content, aging, compaction, and gradation have moderate impacts on the values of initial stiffness but are not as significant as the effects of temperature and binder type.

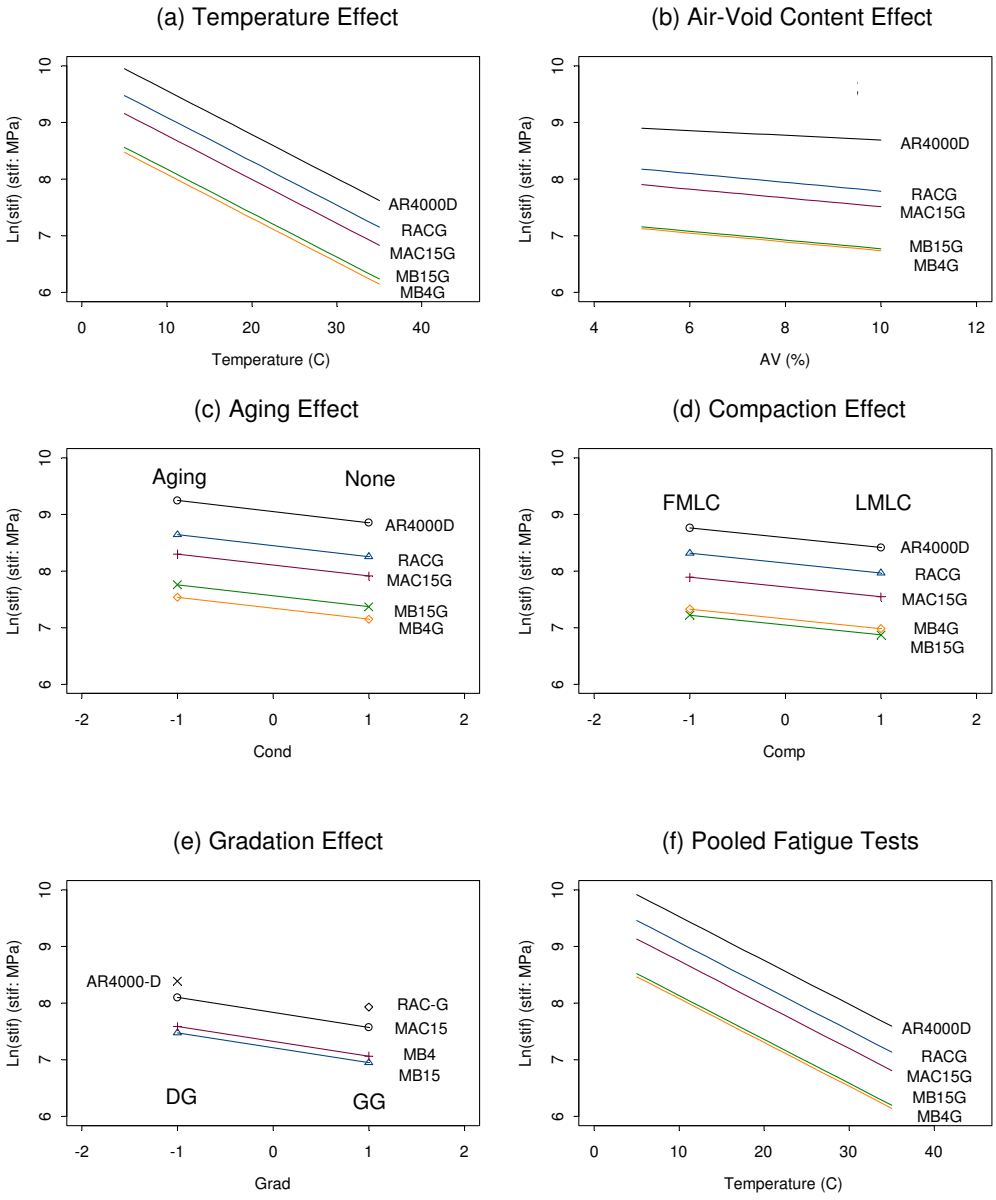

Figure 4.23: Schematic summary of initial stiffness regression models.

Table 4.6: Regression Models for Initial Stiffness

Test	Regression Model	R^2
Temperature Effect	$E(\ln stif) = \underset{(0.0682)}{9.5115} - \underset{(0.0407)}{0.3949}binder1 - \underset{(0.0235)}{0.3300}binder2 - \underset{(0.0166)}{0.1875}binder3 + \underset{(0.0129)}{0.0883}binder4 - \underset{(0.0031)}{0.0775}temp$	0.93
Air-void Content Effect	$E(\ln stif) = \underset{(0.0931)}{8.2053} - \underset{(0.0277)}{0.4120}binder1 - \underset{(0.0159)}{0.3850}binder2 - \underset{(0.0109)}{0.2007}binder3 + \underset{(0.0084)}{0.0897}binder4 - \underset{(0.0123)}{0.0425}av$	0.96
Aging Effect	$E(\ln stif) = \underset{(0.0254)}{8.1027} - \underset{(0.0390)}{0.4717}binder1 - \underset{(0.0234)}{0.3383}binder2 - \underset{(0.0160)}{0.2239}binder3 + \underset{(0.0124)}{0.0867}binder4 - \underset{(0.0254)}{0.1944}cond$	0.94
Compaction Effect	$E(\ln stif) = \underset{(0.0288)}{7.7301} - \underset{(0.0442)}{0.4353}binder1 - \underset{(0.0265)}{0.3683}binder2 - \underset{(0.0181)}{0.1576}binder3 + \underset{(0.0140)}{0.1026}binder4 - \underset{(0.0288)}{0.1733}comp$	0.92
Gradation Effect	$E(\ln stif) = \underset{(0.0247)}{7.4573} - \underset{(0.0299)}{0.3121}binder1 - \underset{(0.0176)}{0.0665}binder2 - \underset{(0.0247)}{0.2639}grad$	0.93
Pooled Fatigue Tests	$E(\ln stif) = \underset{(0.0633)}{9.6615} - \underset{(0.0442)}{0.1105}binder1 - \underset{(0.0189)}{0.2409}binder2 - \underset{(0.0119)}{0.1338}binder3 + \underset{(0.0096)}{0.1178}binder4 - \underset{(0.0391)}{0.2805}grad - \underset{(0.0255)}{0.1832}comp - \underset{0.0255}{0.1924}cond - \underset{0.0027}{0.0774}temp$	0.93

Table 4.7: Regression Models for Fatigue Life

Test	Regression Model	R^2
Temperature Effect	$E(\ln nf) = \underset{(2.8240)}{-22.7041} + \underset{(0.1629)}{2.1694}binder1 + \underset{(0.0941)}{0.7178}binder2 + \underset{(0.0696)}{0.8797}binder3 - \underset{(0.0517)}{0.3740}binder4 + \underset{(0.0127)}{0.0837}temp - \underset{(0.3711)}{4.5027}\ln stn$	0.88
Air-void Content Effect	$E(\ln nf) = \underset{(2.5359)}{-25.1119} + \underset{(0.1476)}{2.5119}binder1 + \underset{(0.0852)}{0.8216}binder2 + \underset{(0.0603)}{0.7180}binder3 - \underset{(0.0467)}{0.3696}binder4 - \underset{(0.3369)}{5.0109}\ln stn$	0.94
Aging Effect	$E(\ln nf) = \underset{(2.5566)}{-21.3729} + \underset{(0.1448)}{2.4274}binder1 + \underset{(0.0836)}{0.6077}binder2 + \underset{(0.0616)}{0.8821}binder3 - \underset{(0.0481)}{0.3062}binder4 + \underset{(0.0959)}{0.2001}cond - \underset{(0.3396)}{4.5051}\ln stn$	0.95
Compaction Effect	$E(\ln nf) = \underset{(3.1749)}{-21.4758} + \underset{(0.1842)}{2.8998}binder1 + \underset{(0.1043)}{0.6178}binder2 + \underset{(0.0734)}{0.6478}binder3 - \underset{(0.0567)}{0.3345}binder4 + \underset{(0.1175)}{0.5082}comp - \underset{(0.4222)}{4.6000}1\ln stn$	0.92
Gradation Effect	$E(\ln nf) = \underset{(4.9132)}{-32.7888} + \underset{(0.1770)}{1.4293}grad - \underset{(0.6556)}{6.2637}\ln stn$	0.88
Pooled Fatigue Tests	$E(\ln nf) = \underset{(2.0795)}{-25.7076} + \underset{(0.2089)}{1.1699}binder1 + \underset{(0.0897)}{0.3658}binder2 + \underset{(0.0565)}{0.6024}binder3 - \underset{(0.0453)}{0.4411}binder4 + \underset{(0.1859)}{1.1629}grad + \underset{(0.1213)}{0.4461}comp + \underset{0.02128}{0.0828}temp - \underset{0.2723}{4.8507}\ln stn$	0.87

4.9.2 Fatigue Life

Figure 4.24 summarizes the regression models for beam fatigue life at a given tensile strain listed in Table 4.7. The following are observed:

- The ranking of beam fatigue life of the binders under various effects, including different strains, is always in the order listed below, from longest life to shortest life. There appears to be little difference between the MAC15-G and MB15-G mixes.
    1. MB4-G
    2. MB15-G
    3. MAC15-G
    4. RAC-G
    5. AR4000-D
- Beam fatigue life at a given tensile strain generally increases under the following situations:
    - Higher temperature (regardless of strain level)
    - Lower strain levels (regardless of mix properties and testing conditions)
    - The specimen was not aged
- In this project, no significant effect of air-void content on beam fatigue life was noted.
- Laboratory-mixed, laboratory compacted specimens performed better than field-mixed, laboratory compacted specimens in fatigue life.
- Figure 4.23f shows the dense- and gap-graded beam fatigue life for the three modified binder types (MAC15, MB15, and MB4) pooled together. The dense-graded MAC15, MB15, and MB4 mixes had better beam fatigue life performance than the AR4000-D and RAC-G mixes. However, they had less stiffness than the AR4000-D and RAC-G mixes. This implies that modified binders could be considered in dense-graded applications in structural overlays. However, additional testing and a thorough mechanistic analysis of the entire pavement structure, traffic loading, and environment would need to be carried out before any recommendation could be made.
- The stiffness of the modified binder mixes, which are typically lower than conventional binder mixes, would also need to be considered in terms of rutting potential, if the dense-graded MAC15, MB15, and MB4 mixes are to be considered for thicker overlays or structural layers.

4.10. Transition from Crack Initiation to Crack Propagation

Beam fatigue tests in the constant deformation mode-of-loading can be plotted in terms of the double natural logarithm ln (ln taken twice) of the stiffness ratio (SR) versus the number of repetitions of the tensile strain in the test. Stiffness ratio is defined as the stiffness at a specific number of repetitions divided by the initial stiffness:

Stiffness Ratio (SR) = stiffness / initial stiffness

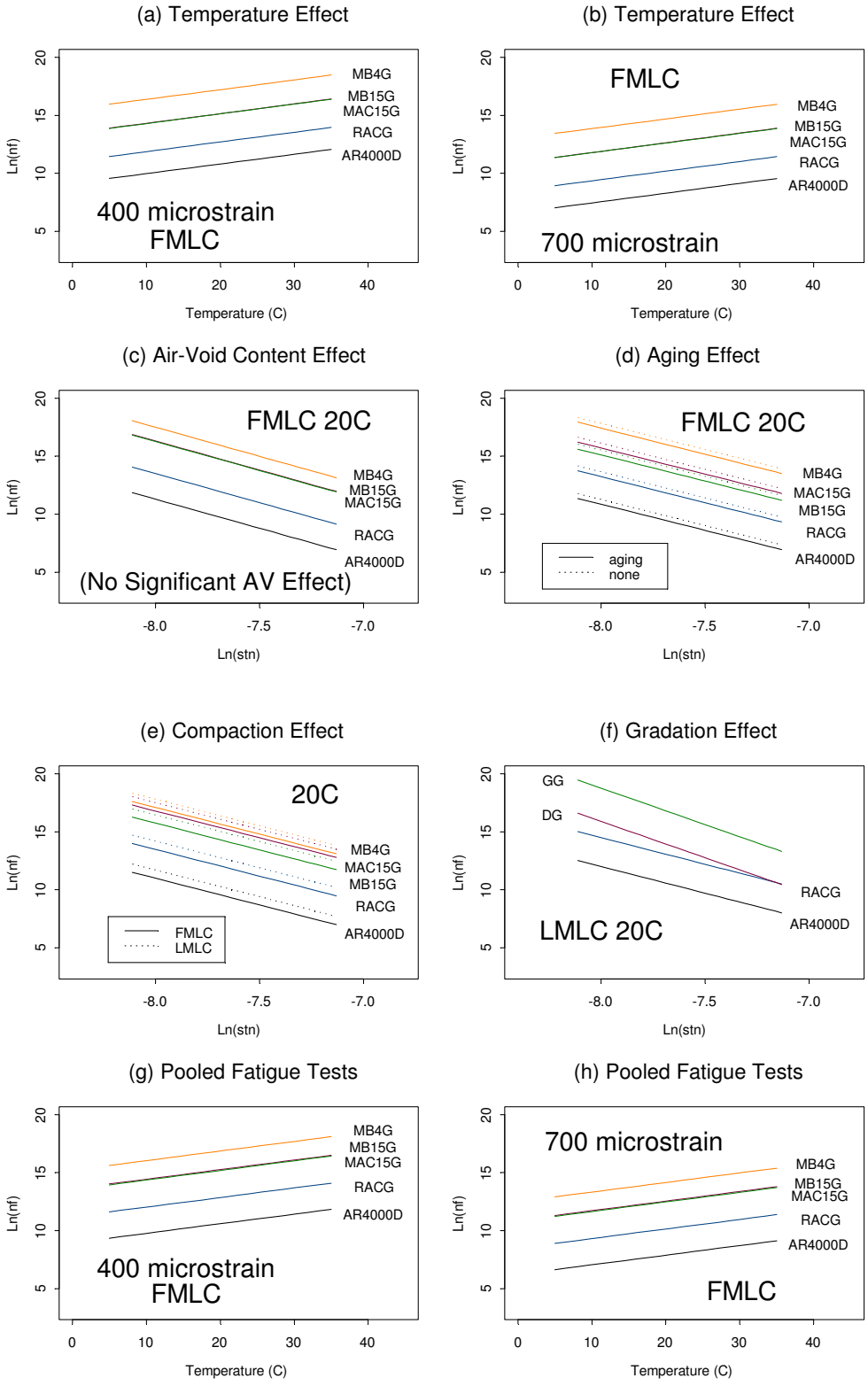

Figure 4.24: Schematic summary of fatigue life regression models.
(Figures a, b, c, d only include regression of results from each experiment, Figures g, h include regression of all results pooled together).

As a beam or pavement is subjected to more repetitions of a tensile strain it loses stiffness, i.e., it incurs fatigue damage, and the stiffness ratio is reduced from the initial value of 100 percent. A beam with an SR of zero would have a crack extending completely through it. The ln(-ln(SR)) value for approximately 100 percent (actually 99.99 percent) is about -6, and the ln(-ln(SR)) value for 10 percent stiffness ratio is 0.83.

This concept has been long recognized and is incorporated, for example, in the current Caltrans empirical design method for asphalt overlays, in which deflections are measured and compared with expected (or "tolerable") deflections for a given thickness of asphalt concrete. If the stiffness ratio of the existing asphalt concrete has been significantly reduced due to fatigue damage, the deflection will be greater and a thicker overlay will be required to restore the pavement's structural capacity.

When plotted as a double log of SR versus log of repetitions, the fatigue damage curve for a beam fatigue test typically consists of three stages (Figure 4.25), namely:

1. Stage I, an initial or warm-up stage during which the temperature of the beam increases with energy dissipation until it reaches a fairly stable temperature;
2. Stage II, crack initiation, during which there is a steady rate of stiffness reduction versus repetitions; and
3. Stage III, crack propagation, during which the rate of stiffness reduction versus repetitions is greater than in Stage II.

Based on extensive testing and use of this approach, a 50 percent stiffness ratio has been found to correlate with the end of crack initiation (Stage II) and the beginning of crack propagation (Stage III) for dense-graded mixes with conventional binders; this transition is fairly distinct in a plot of this type. A 50 percent stiffness ratio corresponds to a value of ln(-ln(SR)) of -0.36 in Figure 4.25.

These three stages can be analyzed using a three-stage Weibull equation (3, 5); in this study it was used to evaluate each fatigue test. The associated fatigue parameters that define the three-stage Weibull fatigue curve are:

- Six parameters taken directly from the curve: $\ln\alpha_1$, β_1, $\ln\alpha_2$, β_2, $\ln\alpha_3$, β_3; and
- Two parameters derived from the curve. i.e., the repetitions at which the transitions between Stages I and II, and Stage II and Stage III occur: n_1, n_2, respectively.

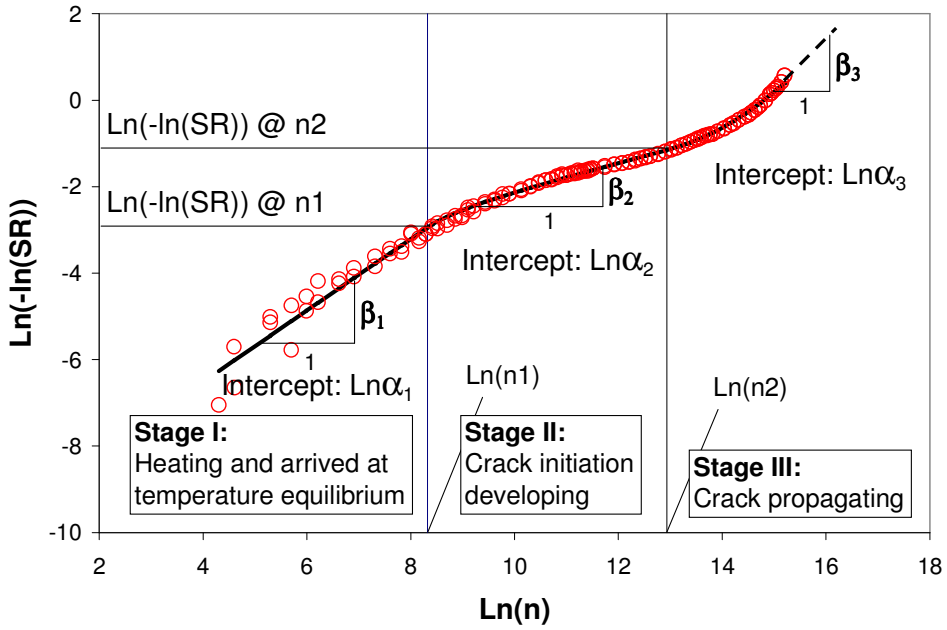

Figure 4.25: Example three-stage Weibull curve.

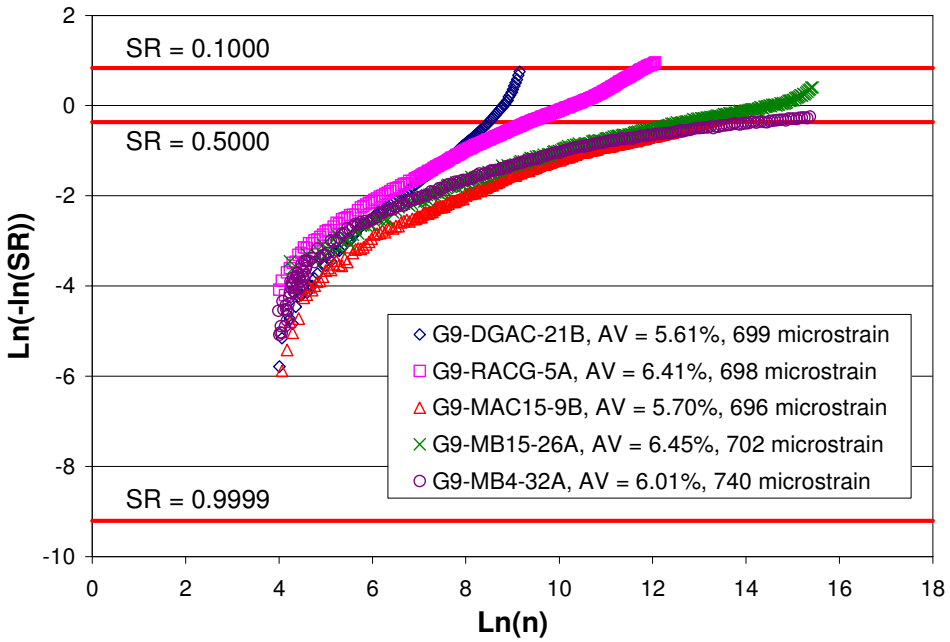

Figure 4.26: Typical results of beam fatigue test for mixes
(Figures are plotted in terms of double log of stiffness reduction versus log of strain repetition.)

A more detailed analysis of the Weibull parameters for all of the beam test results will be included in the second-level analysis report to follow. Some interesting results have already been identified. Figure 4.26 shows typical beam fatigue test results for one specimen of each of the following mixes, all tested under the same conditions of temperature and tensile strain:

- AR4000-D: specimen G9-DGAC-21B

- RAC-G: specimen G9-RACG-5A
- MAC15-G: specimen G9MAC15-9B
- MB15-G: specimen G9MB15-26A
- MB4-G: specimen G9MB4-32A

Each of these specimens is field-mixed, lab compacted, and all have air-void contents (AV) of approximately 6 percent.

Initial observations from these typical results can be summarized as follows:

- The plots for the AR4000-D show behavior that is different from that of the RAC-G mixes, and the behavior of the MAC15-G, MB15-G, and MB4-G mixes is different from that of the AR4000-D and RAC-G mixes.
- The results from the beam fatigue tests on the RAC-G, MAC15-G, MB15-G, and MB4-G mixes in this study indicate that Stage III did not always occur. Instead, the fatigue damage rate (the rate at which SR changes with each repetition) actually reduced to below that of Stage II, rather than increased as occurred with the AR4000-D mixes and as is typical of most dense-graded mixes with conventional asphalt binders. This finding should be considered in the context that the duration of a fatigue test is usually less than one week (~6 million repetitions at 10 Hz) and will need to be substantiated with HVS and long-term field performance tests. A longer testing period may also result in a characteristic Stage III condition being reached after many more repetitions.

4.11. Correlation of Phase Angle versus Stiffness versus Fatigue Life

Figure 4.27 illustrates the paired scatter plots of phase angle, initial stiffness, and fatigue life for all fatigue tests. The phase angle (*pa*) and the natural logarithm of initial stiffness (*lnstif*) are highly negative-correlated (ρ = -0.966) regardless of the mix type, and thus the higher the stiffness, the smaller the phase angle. With a correlation as high as -0.966, the phase angle (*pa*) and initial stiffness (*lnstif*) can be regarded as the same variables. Any covariates that affect one will certainly affect the other.

The relationship between the natural logarithms of initial stiffness and fatigue life, as shown in the figure, indicates that these two response variables are moderately negative-correlated (ρ = -0.604). Given that lower stiffnesses result in higher beam fatigue life at a given tensile strains, it is appropriate to infer the ranking of fatigue life based on the ranking of initial stiffness, for instances of controlled strain, applicable to thin overlays over cracked pavement.

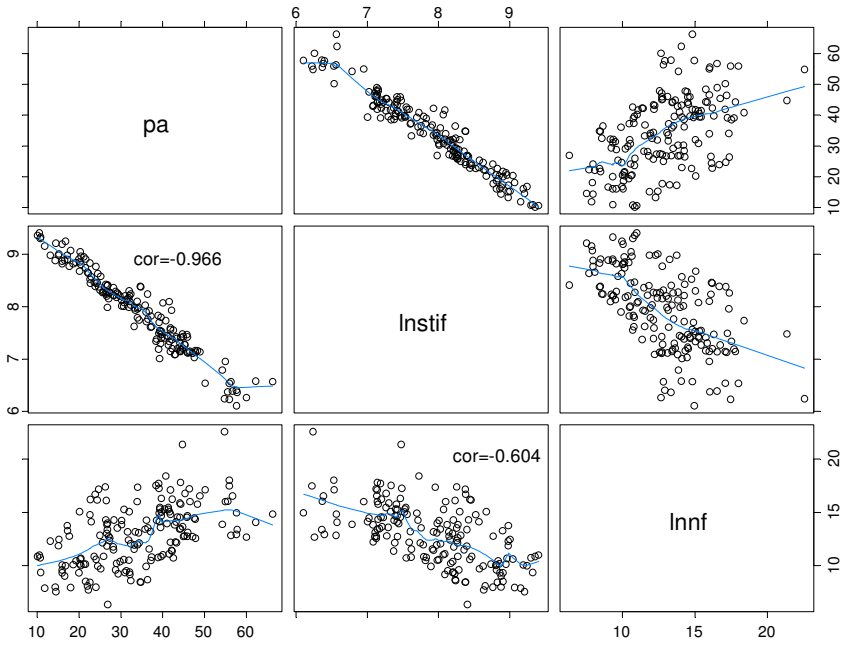

Figure 4.27: Relationships among pa, lnstif, and lnnf.

4.12. Second-Level Analysis

A second-level analysis report will be prepared on completion of all HVS testing, laboratory testing, and forensic evaluations. This report will include:

- As-built layer thicknesses of the HVS sections;
- Backcalculation of moduli from deflection measurements (RSD, MDD, and FWD);
- Verification of data collected from in-depth measurements with visual observations from test pits;
- Comparison of performance between HVS test sections;
- Comparison of performance between HVS test sections, after accounting for any differences in underlying support conditions;
- Comparisons of HVS test results with laboratory test results;
- Analysis of expected pavement fatigue life for a range of pavement structures containing dense-graded mixes with MB4, MB15, and MAC15 binders and comparison with dense-graded mixes containing conventional and other modified binders;
- Analysis of the fatigue beam results using three-stage Weibull analysis; and
- Recommendations.

5. FLEXURAL FREQUENCY SWEEP TESTING

5.1. Introduction

The complex modulus master curve (*E** master curve) obtained from flexural frequency sweep tests is useful for characterizing the effects of loading frequency and temperature on the initial stiffness of an asphalt mix. The main objective of conducting flexural frequency sweep tests in this study is to compare the loading frequency and temperature responses for various mix types under different material properties and testing conditions. The comparison is based on the following categories (Table 5.1):

- FMLC, AV= 6 percent
- FMLC, AV = 9 percent,
- FMLC, AV = 6 percent, LTOA6,
- LMLC-GG, AV = 6 percent, and
- LMLC-DG, AV = 6 percent.

Table 5.1: Summary of Categories for Comparing the *E Master Curves**

Mix[1,2]	Grading[3,4,5]				
	AR4000	ARB	MAC15	MB15	MB4
FMLC AV6	DG	GG	GG	GG	GG
FMLC AV9	DG	GG	GG	GG	GG
FMLC AV6 LTOA6	DG	GG	GG	GG	GG
LMLC AV6	DG	GG	GG	GG	GG
LMLC AV6 DG	Not tested	Not tested	DG	DG	DG

1. AV6: 6 percent air-void content; AV9: 9 percent air-void content
2. LTOA6: long-term oven aging for 6 days
3. DG: dense-graded; GG: gap-graded
4. LMLC GG - asphalt content is the same as the asphalt content of field mix.
5. LMLC DG - asphalt content is optimum binder content.

A function that describes flexural stiffness as a function of temperature and time of loading can be used for pavement design, and is referred to as a "master curve" for stiffness. The initial stiffness analyses presented in Chapter 4 of this report are for a loading frequency of 10 Hz only. With a master curve, the inferences based on stiffness of the mix and its effects on fatigue cracking, rutting, and low-temperature cracking can be extended to additional traffic loading speeds and a wider range of temperatures.

Flexural frequency sweep tests are mostly conducted from 15 to 0.01 Hz at three or four temperature levels. Under the assumption that asphalt mix is a time-temperature-rheologically simple material, the curves can be shifted horizontally relative to one of the test temperatures to obtain the full spectrum of complex moduli. With the aid of a genetic algorithm (3), the shifted horizontal distances can be determined and the master curve of the complex modulus constructed. The shifted horizontal distances

together with the temperature differences relative to the reference temperature establish the temperature-shift relationship.

Once the master curve is constructed, a Gamma nonlinear fitting is conducted to find a suitable mathematical function to represent the relationship of the complex modulus and reduced loading frequency at a reference temperature. The Gamma nonlinear fitting can also describe the temperature-shift relationship. Using these relationships, the temperature sensitivity of the initial stiffness of asphalt mix can be easily investigated at a specified loading frequency.

5.2. Results and Analysis

5.2.1 *E** Master Curves and Temperature Shift Relationships

The Gamma fitting results for the *E** master curves and temperature-shift relationships are included in Reference (3). Figures 5.1 to 5.5 plot the *E** master curve relationships for each mix; Figures 5.6 to 5.10 provide comparisons among the mixes for the different variables considered. The following observations were made:

- The complex modulus of a master curve increases exponentially as the loading frequency increases. The shapes are generally upwardly concave. The only exception is the master curve of the AR4000-D FMLC mixes, which is "S" shaped.
- The aging effect on the FMLC specimens appears to be significant for all binder/mix types except the MAC15 mixes, whereas no aging effect is observed between the FMLC AV6 and FMLC AV6 LTOA6 master curves (Figure 5.3).
- For the AR4000-D mixes, the air-void content effect is apparent only at medium-to-high loading frequencies. The air-void content effect for the RAC-G, MAC15, MB15, and MB4 mixes is negligible. For MAC15 mixes, the 9.0 percent air-void content master curve is apparently below the 6.0 percent master curve.
- For MAC15, MB15, and MB4 mixes, the master curves for dense-gradations (LMLC-DG) are well above the gap-graded master curves (LMLC-GG). This implies that binders with dense gradations will have potentially improved resistance to rutting but reduced fatigue-resistance at a wide range of temperatures and traffic speeds.

5.2.2 Mix Ranking

Figures 5.6 through 5.10 show the mix ranking of the *E** master curves for various material properties and testing conditions. Plots of temperature-shift relationships for each mix and condition are included in Reference (3). The following were observed:

- If the gradation effect (LMLC AV6 DG) is excluded, the mix ranking of master curve stiffness from the stiffest to the least stiff is generally as is listed below. As expected. this ranking is the opposite of the fatigue performance ranking observed in Chapter 4.
    1. AR4000-D
    2. RAC-G
    3. MAC15-G
    4. MB15-G
    5. MB4-G.
- The MB15 and MB4 mixes show no significant differences in their master curves for all the categories listed in Table 5.1.
- The ranking of the dense-graded mixes with MB15, MB4, and MAC15 binders (LMLC AV6 DG), from the stiffest to the least stiff, is as listed below. There is no significant difference in the master curves for the MB15-D and MB4-D mixes.
    1. MAC15-D
    2. MB4-D
    3. MB15-D

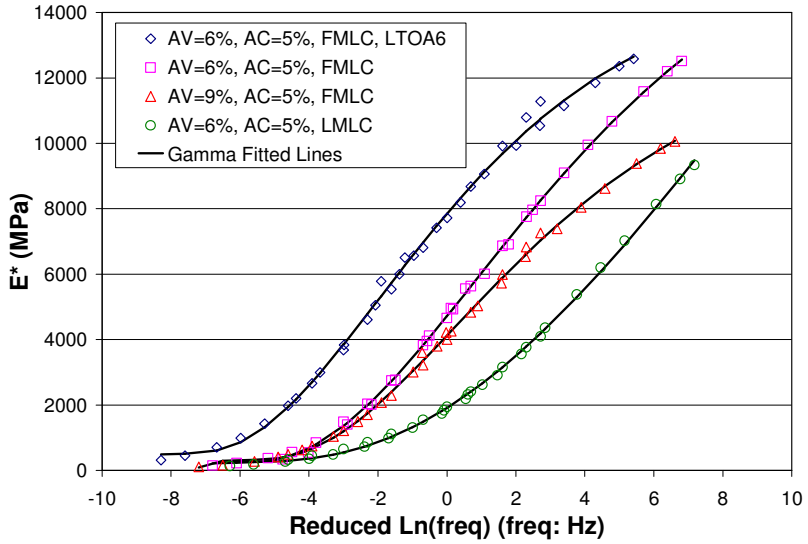

Figure 5.1: *E master curves for AR4000-D mixes.**

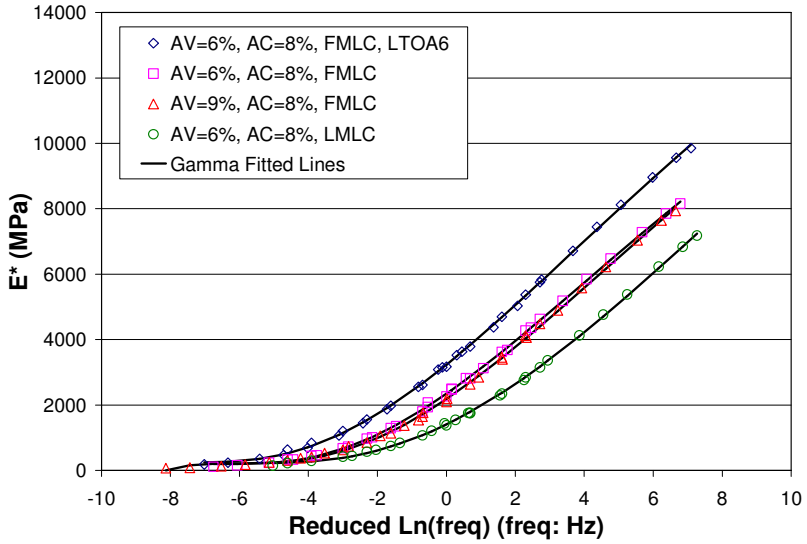

Figure 5.2: *E master curves for RAC-G mixes.**

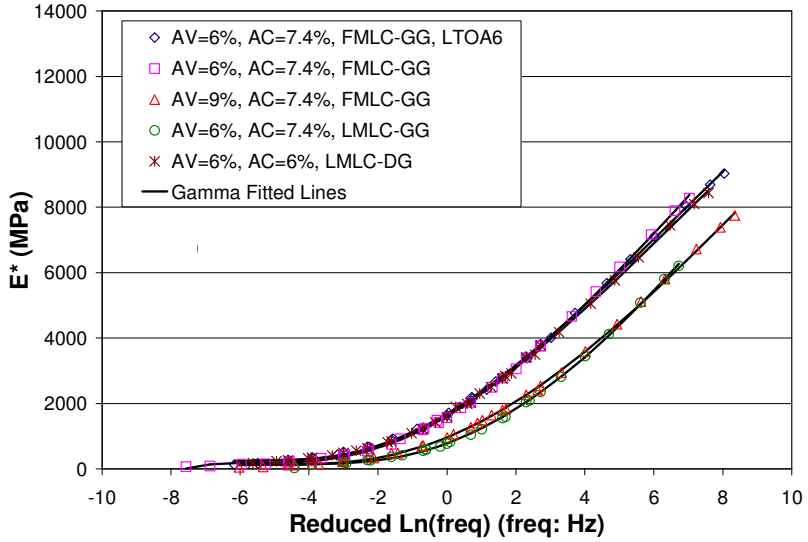

Figure 5.3: *E master curves for MAC15 mixes.**

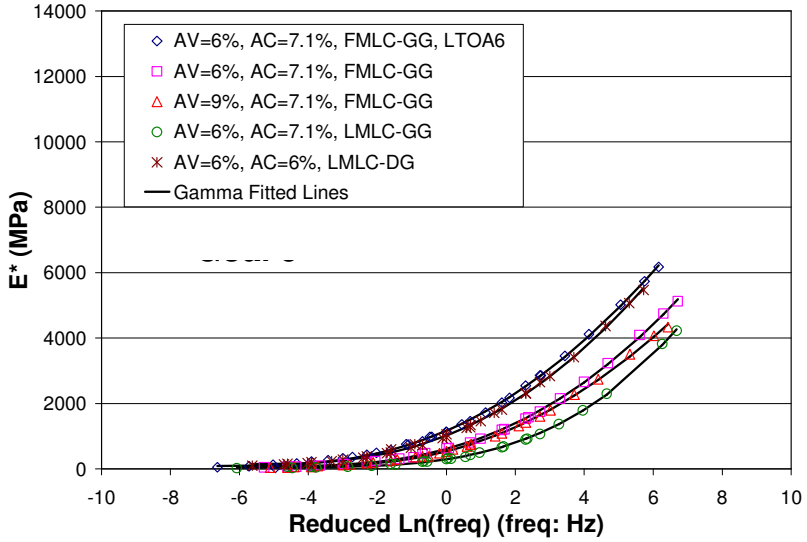

Figure 5.4: *E master curves for MB15 mixes.**

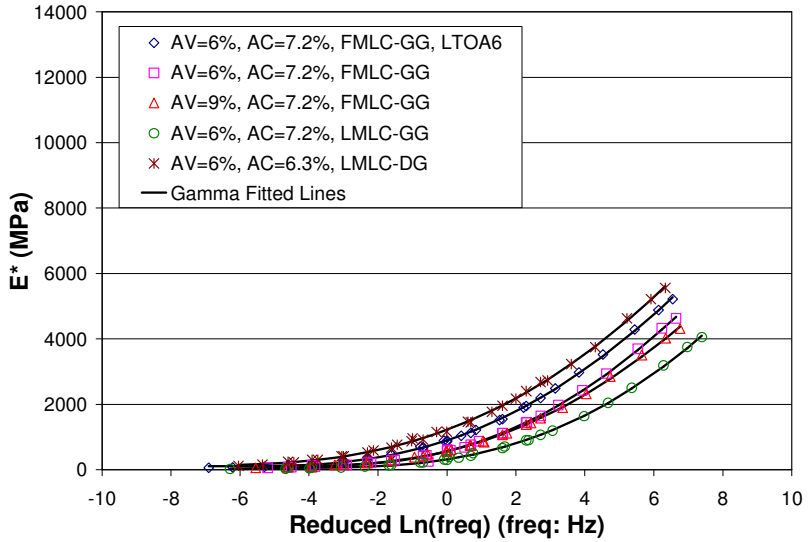

Figure 5.5: *E master curves for MB4 mixes.**

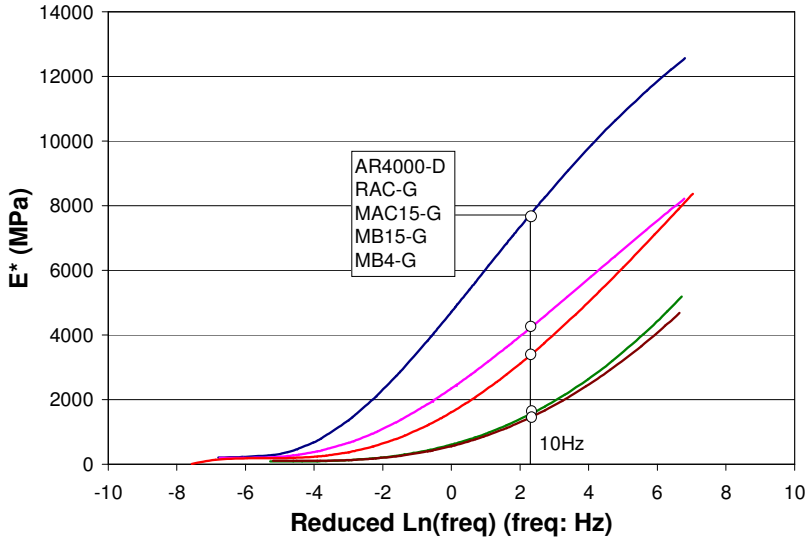

Figure 5.6: E* master curves - FMLC, 6% AV.

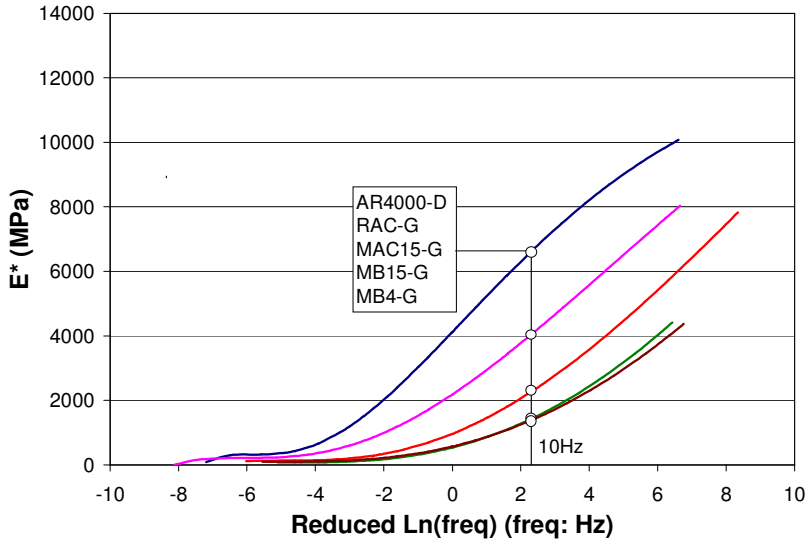

Figure 5.7: *E master curves - FMLC, 9% AV.**

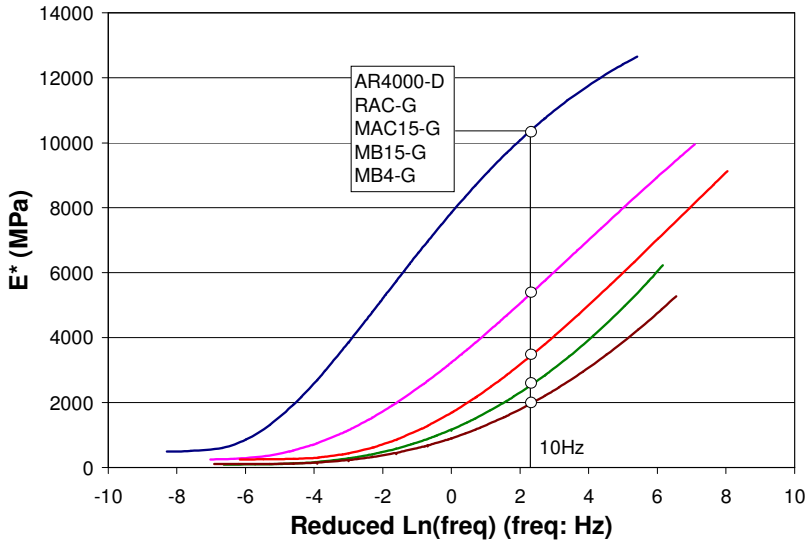

Figure 5.8: *E master curves - FMLC, 6% AV, LTOA6.**

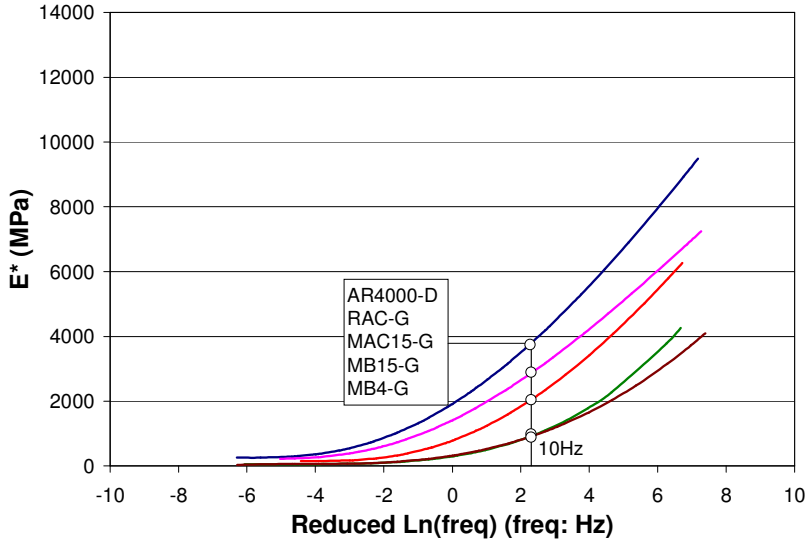

Figure 5.9: *E master curves - LMLC, 6% AV, GG.**

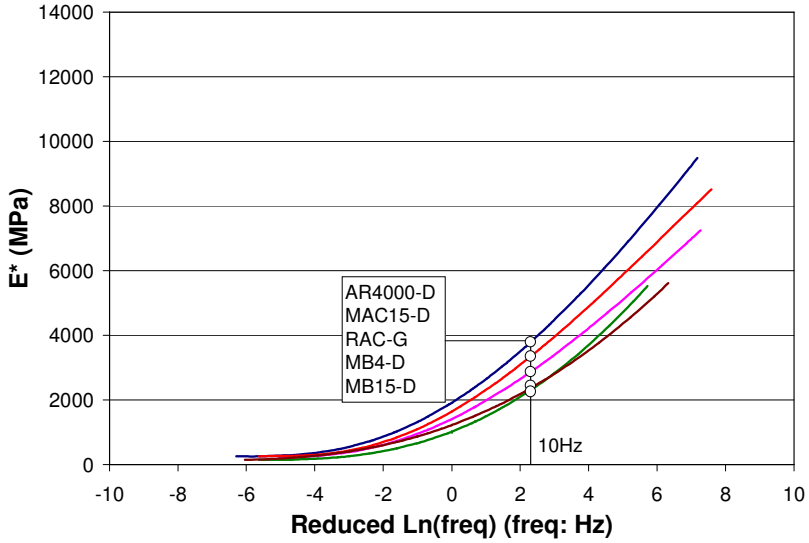

Figure 5.10: *E master curves - LMLC, 6% AV, DG.**

5.2.3 Comparison between LMLC-DG and LMLC-GG

Figure 5.11 summarizes the *E** master curves of the LMLC dense-graded (DG) and LMLC gap-graded (GG) mixes at 20°C and 6.0 percent air-void content. Asphalt contents for each mix (AC) are also shown in the figure.

The mix ranking of the *E** master curves, from the most to the least stiff is:

1. AR4000-D
2. MAC15-D
3. RAC-G
4. MB15-D
5. MB4-D
6. MAC15-G
7. MB15-G
8. MB4-G

The mix ranking for beam fatigue life at 400 microstrain shows exactly the reverse trend, except that MAC15-D and RAC-G change places:

1. MAC15-G
2. MB4-G
3. MB15-G
4. MB4-D
5. MB15-D
6. MAC15-D
7. RAC-G
8. AR4000-D

The mixes with dense-gradations have increased stiffness but poorer fatigue performance when compared to gap-graded mixes. Any improvement in rutting resistance from increased stiffness for the dense-graded mixes with MB4, MB15, and MAC15 binders will be discussed in the report on laboratory shear testing.

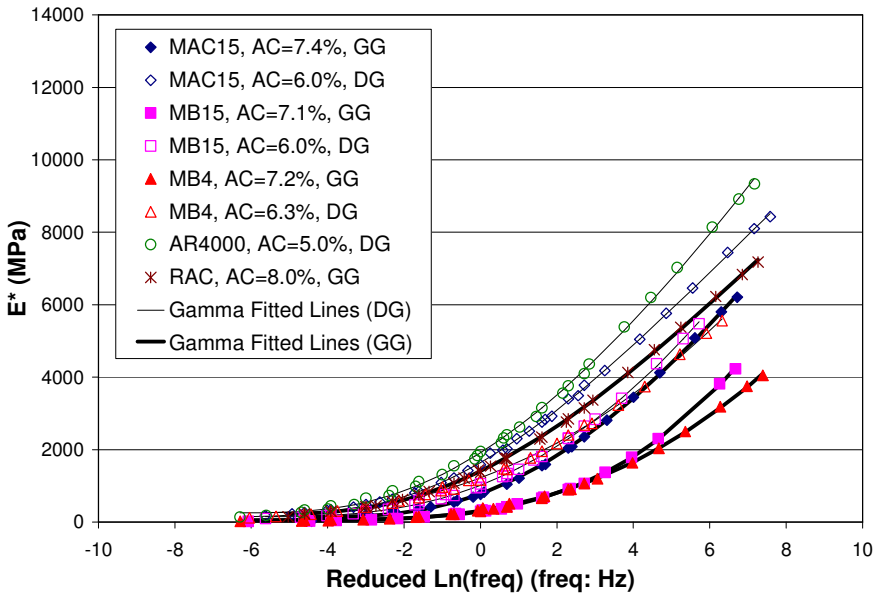

Figure 5.11: Gradation effect on *E master curves for MAC15, MB15, and MB4.**

5.2.4 Temperature Sensitivity

Temperature sensitivity, an important parameter in overlay design, is defined as the change in stiffness with change in temperature. Low temperature sensitivity results in low stiffness at low temperatures and greater stiffness at high temperatures. Low temperature sensitivity is desirable because low stiffness at low temperatures is important in limiting thermal cracking, while high stiffness at high temperatures is often important in limiting rutting. Table 5.2 and Figures 5.12 through 5.16 illustrate the sensitivity of stiffness at various temperatures for AR4000-D, RAC-G, MAC15, MB15, and MB4 mixes respectively for a frequency of 10 Hz. Figures 5.17 through 5.21 show the same mix characteristics at 0.01 Hz.

The sensitivity of stiffness at various temperatures at the 0.01 Hz frequency have been included since the development of thermal stresses occur at longer times of loading as compared to those of moving traffic. The trends shown for these curves are essentially the same as those shown in Figures 5.12 through 5.16 and the analysis summarized in Table 5.2 for the 10 Hz frequency.

The following observations were made from these plots:

- For AR4000-D mixes, the FMLC AV6 LTOA6 mix has a reversed temperature sensitivity trend when compared to that of the LMLC AV6 mix. The temperature sensitivity of aged mix is very insensitive at low temperatures but very sensitive at high temperatures for all the categories listed in Table 5.1.
- In general, the RAC-G, MAC15, MB15, and MB4 mixes are insensitive at high temperatures but very sensitive at low temperatures.

- The MAC15 mixes appear particularly temperature-sensitive at low temperatures, becoming as stiff as the AR4000 mix.
- The MB15 and MB4 mixes have similar behavior with respect to temperature sensitivity.
- The master curves indicate that the AR4000 mix will likely have the best rutting resistance, although this inference is drawn from stiffness results at 35°C, and must be checked with repeated load testing. Results from other experiments indicate that modified mixes may have lower stiffnesses but superior rutting resistance compared to conventional binder mixes.
- The results indicate that the MB4 and MB15 mixes, both gap- and dense-graded, will likely have superior low-temperature cracking resistance compared with the other mixes. They also indicate that the MAC15 mixes may become very stiff at lower temperatures, resulting in low-temperature cracking resistance similar to that of AR4000. These inferences are based on stiffness results at 5°C and would need to be verified with appropriate low-temperature cracking laboratory testing before definitive conclusions are drawn.

Table 5.2: Summary of Temperature Sensitivity of *E at 10 Hz**

Binder Type	Comp.	AV	AC	Aging	Grad.	Temperature Sensitivity (MPa/°C)		
						10C	20C	30C
AR4000	FMLC	6.0	5.0	None	DG	-485	-375	-213
		9.0	5.0	None	DG	-301	-321	-237
		6.0	5.0	LTOA6	DG	-142	-295	-565
	LMLC	6.0	5.0	None	DG	-855	-252	-80
		6.0	5.0	None	GG			
ARB	FMLC	6.0	8.0	None	GG	-466	-255	-120
		9.0	8.0	None	GG	-380	-327	-199
		6.0	8.0	LTOA6	GG	-523	-309	-155
	LMLC	6.0	8.0	None	DG			
		6.0	8.0	None	GG	-607	-219	-76
MAC15	FMLC	6.0	7.4	None	GG	-576	-318	-137
		9.0	7.4	None	GG	-1006	-182	-38
		6.0	7.4	LTOA6	GG	-896	-236	-61
	LMLC	6.0	6.0	None	DG	-910	-173	-35
		6.0	7.4	None	GG	-513	-239	-82
MB15	FMLC	6.0	7.1	None	GG	-429	-207	-63
		9.0	7.1	None	GG	-413	-140	-48
		6.0	7.1	LTOA6	GG	-426	-221	-103
	LMLC	6.0	6.0	None	DG	-419	-159	-65
		6.0	7.1	None	GG	-537	-116	-29
MB4	FMLC	6.0	7.2	None	GG	-455	-147	-48
		9.0	7.2	None	GG	-478	-114	-33
		6.0	7.2	LTOA6	GG	-440	-168	-65
	LMLC	6.0	6.3	None	DG	-338	-222	-110
		6.0	7.2	None	GG	-515	-117	-29

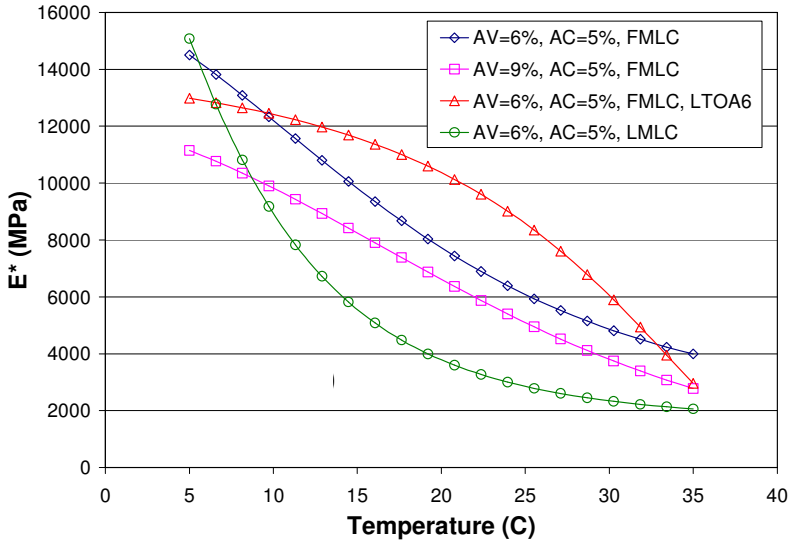

Figure 5.12: Temperature sensitivity for AR4000-D mixes, 10 Hz.

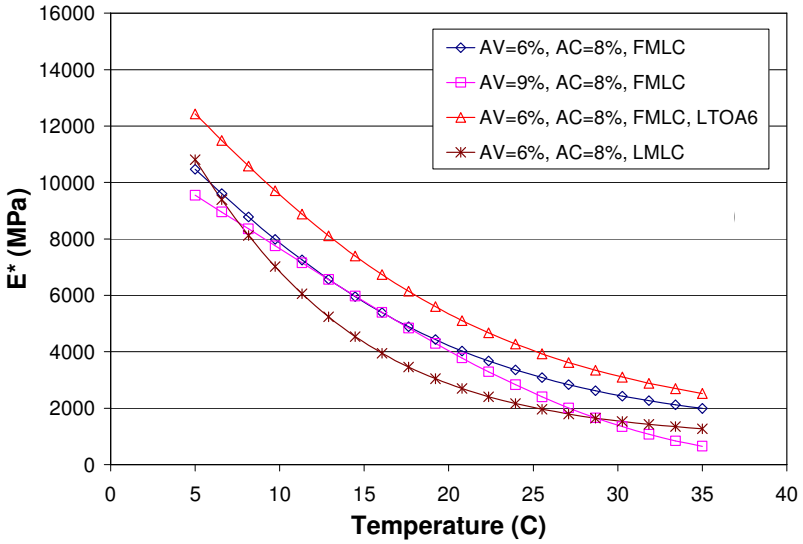

Figure 5.13: Temperature sensitivity for RAC-G mixes, 10 Hz.

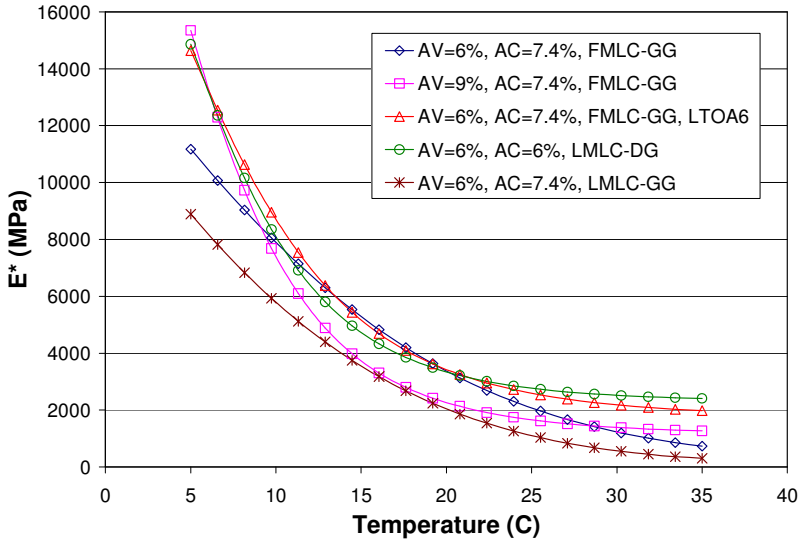

Figure 5.14: Temperature sensitivity for MAC15 mixes, 10 Hz.

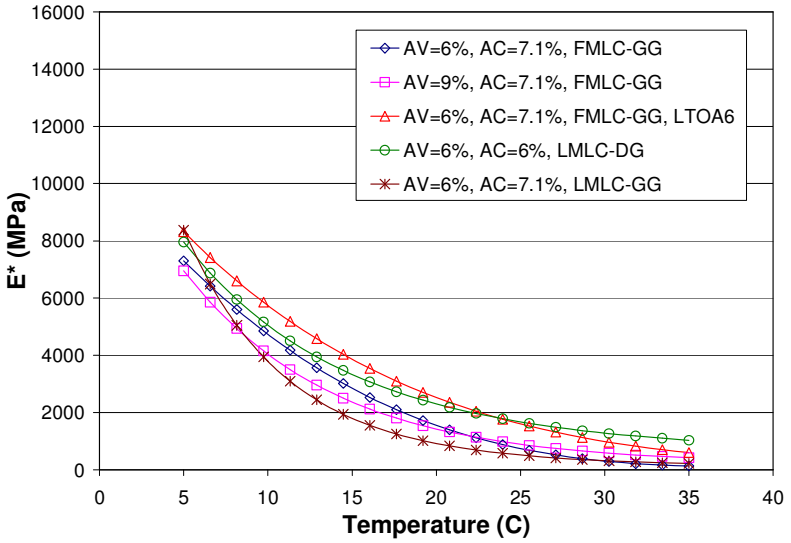

Figure 5.15: Temperature sensitivity for MB15 mixes, 10 Hz.

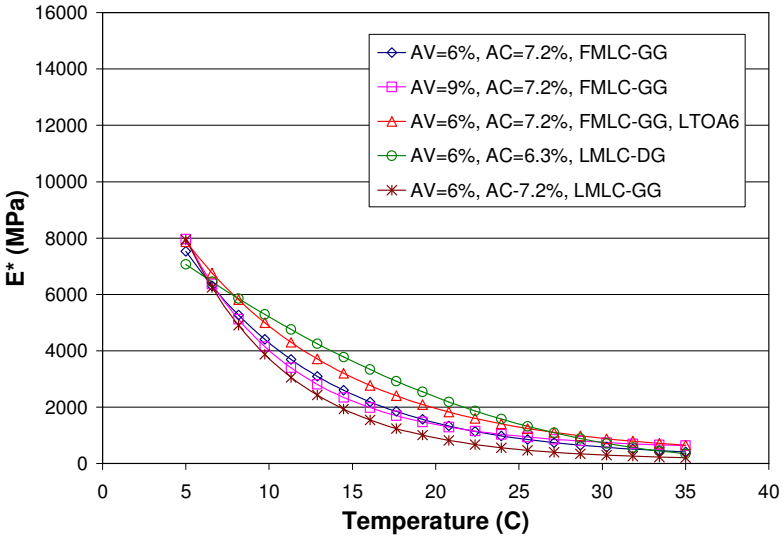

Figure 5.16: Temperature sensitivity for MB4 mixes, 10 Hz.

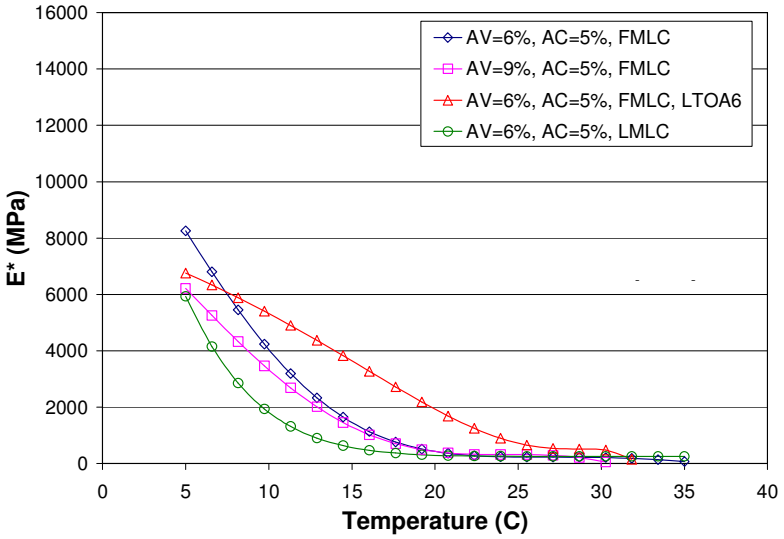

Figure 5.17: Temperature sensitivity for AR4000-D mixes, 0.01 Hz.

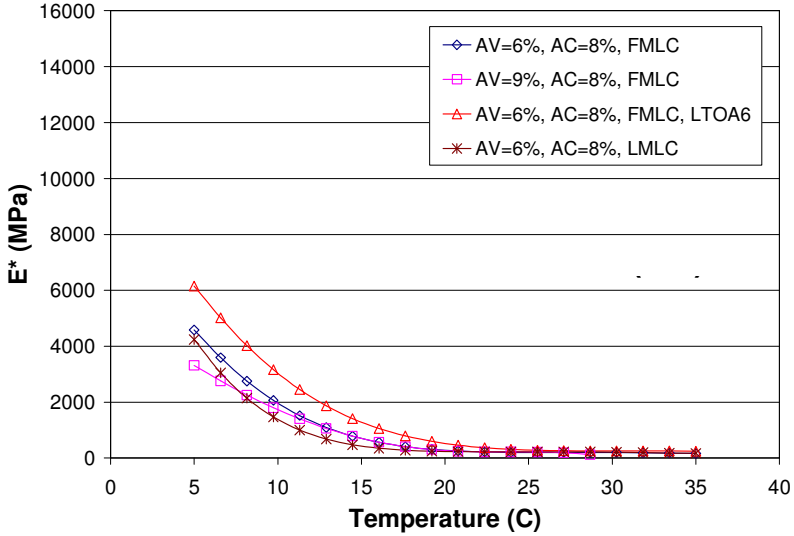

Figure 5.18: Temperature sensitivity for RAC-G mixes, 0.01 Hz.

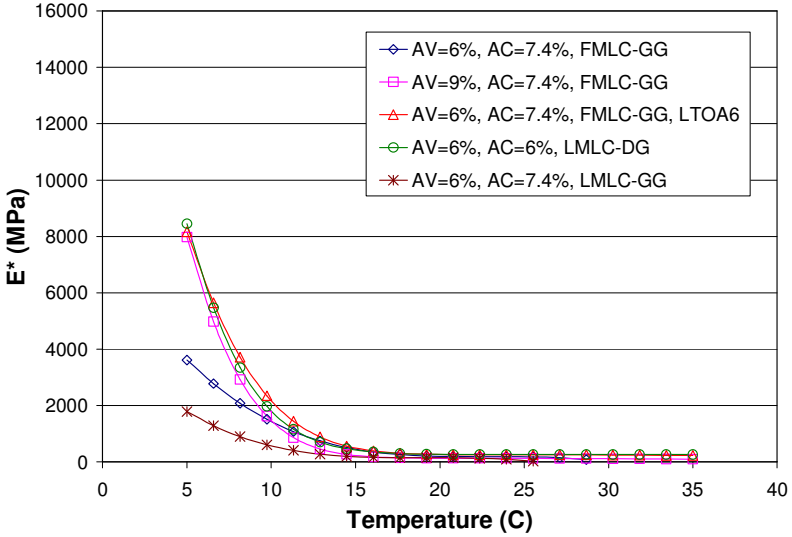

Figure 5.19: Temperature sensitivity for MAC15 mixes, 0.01 Hz.

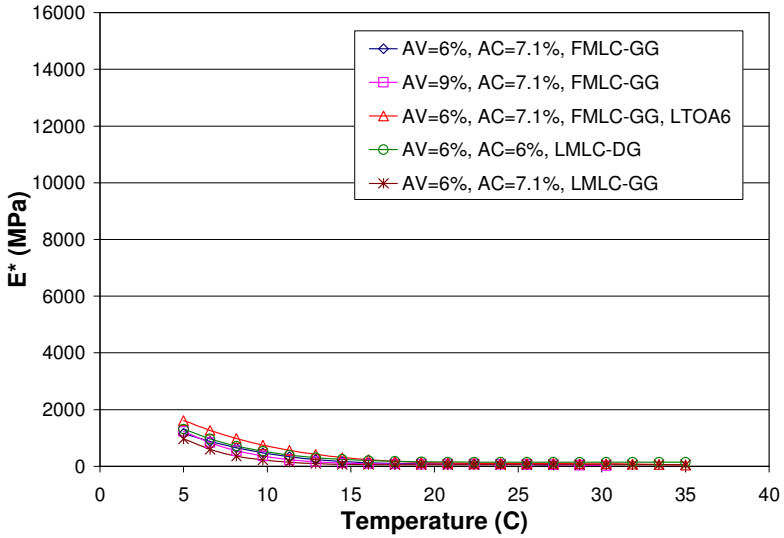

Figure 5.20: Temperature sensitivity for MB15 mixes, 0.01 Hz.

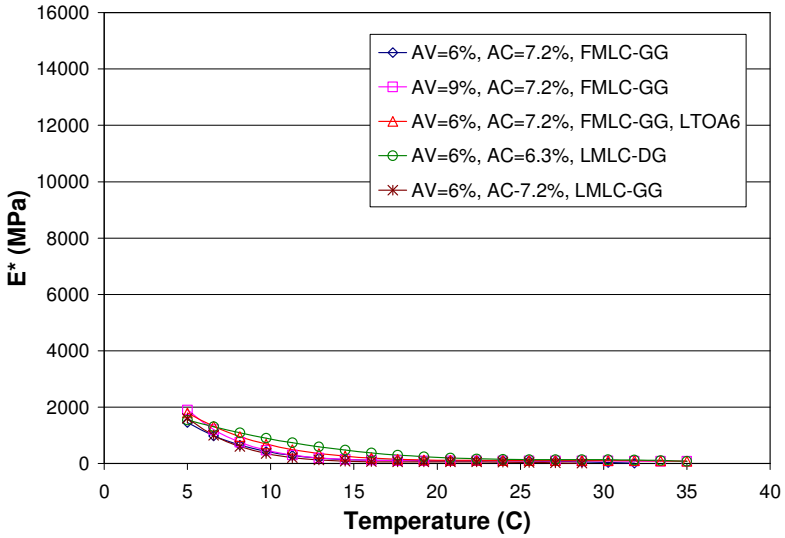

Figure 5.21: Temperature sensitivity for MB4 mixes, 0.01 Hz.

6. CONCLUSIONS

This summary report is one of a series of reports detailing the results of laboratory testing undertaken in conjunction with HVS testing to validate Caltrans overlay strategies for the rehabilitation of cracked asphalt concrete. It describes the results of the laboratory fatigue study, carried out on a variety of binders and mixes. Comparison of the laboratory and test section performance, including the results of a forensic investigation to be conducted when testing is complete, will be discussed in a second-level report once the data from all of the studies has been collected. Findings and observations based on the laboratory fatigue study are discussed below. It should be noted that the study was focused on the use of modified binders in thin overlays on existing cracked asphalt surfaces, and not in structural layers.

6.1. Findings and Observations

Summary of Binder Tests

- Based on Bending Beam Rheometer (BBR) test results conducted by FHWA, the ranking of propensity to low temperature thermal cracking is listed below, from worst to best. Asphalt rubber binder was not tested.
    1. AR4000
    2. MAC15
    3. MB15
    4. MB4.
- The order of thermal cracking potential is closely matched with the order of initial stiffness in the fatigue beam tests and flexural frequency sweep results; hence a mix with a higher initial stiffness might have a higher thermal cracking potential.
- The Dynamic Shear Rheometer (DSR) test results indicated that:
    - MAC15 failed to meet the Superpave rutting specification.
    - MB4 and MB15 binders have better rutting resistance capacities than AR4000 binder.
    - According to the Superpave specification, the ranking of fatigue resistance capacity is in the order listed below, which is the same ranking obtained for initial stiffness during laboratory mix fatigue tests.
        1. MB4
        2. MB15
        3. MAC15
        4. AR4000

Test Effects

- The binder type has an overall effect on all the response variables including initial phase angle, initial stiffness, and fatigue life. As expected, the temperature effect on all three response

variables is immediately apparent. The other effects assessed at 20°C (68°F)(for comparison with HVS testing) reveal that:

- Air-void content had a significant effect for some parts of the experiment, such as the FMLC mixes at 20°C, but the effect was not significant for many of the mixes and test conditions for all of the response variables.
- The aging effect is only significant for initial phase angle and stiffness but not for fatigue life.
- For MAC15, MB15, and MB4 mixes, all the response variables are significantly affected by the change from a gap-gradation to a dense-gradation.

Ranking of Initial Stiffness and Fatigue Performance

- The ranking of predicted initial stiffness and fatigue life under various specimen preparation and testing conditions, and specifically for the controlled strain mode of loading used in this experiment, is normally in the order listed below. For initial stiffness, no apparent differences exist between MB15-G and MB4-G mixes, while for fatigue life, no apparent differences exist between MAC15-G and MB15-G mixes. As expected, the two orders are reversed.

Initial stiffness	Fatigue life
1. AR4000-D	1. MB4-G
2. RAC-G	2. MAC15-G
3. MAC15-G	3. MB15-G
4. MB15-G	4. RAC-G
5. MB4-G	5. AR4000-D

- Fatigue test results indicate that initial stiffness (*lnstif*) and fatigue life (*lnnf*) are moderately negative-correlated (ρ = -0.604), confirming a general observation that lower stiffnesses equate to higher fatigue life at a given tensile strain under controlled-strain testing when ranking fatigue life performance against initial stiffness or vice versa. However, when using this observation, consideration must also be given to rutting, as mixes with low stiffness are generally susceptible to this distress.
- Preliminary analysis of stiffness versus strain repetition curves using three-stage Weibull analysis indicates differences in crack initiation and propagation. The AR4000-D mix has different behavior from that of the RAC-G mix, while the RAC-G mix performed differently than the MB4-G, MB15-G, and MAC15-G mixes. The results indicate that damage may slow during the propagation phase of the latter four mixes, while it accelerates for the AR4000-D mix.

Dense-Graded versus Gap-Graded Mixes

- The optimum binder contents used in the mix designs for the MAC15, MB15, and MB4 dense-graded mixes (6.0, 6.0, and 6.3 percent respectively) were lower than the optimum binder contents used in the mix designs of the gap-graded mixes (7.4, 7.1, and 7.2 percent respectively).
- Limited fatigue testing of modified binders in dense-graded mixes led to the following observations:
  - The initial stiffness of the dense-graded mixes was generally greater than those of the corresponding gap-graded mixes but less than those of the AR4000-D and RAC-G mixes. The beam fatigue life at a given tensile strain of the dense-graded mixes was generally less than those of the corresponding gap-graded mixes, but greater than those of the AR4000-D and RAC-G mixes. Any improvement in rutting resistance from increased stiffness of the dense-graded mixes with MB4, MB15, and MAC15 binders over that of the corresponding gap-graded mixes will be discussed in the report on laboratory shear testing.
  - The mix ranking of the E^* master curves, from most to least stiff, for laboratory mixed, laboratory compacted specimens at 6 percent air-voids is:
    1. AR4000-D
    2. MAC15-D
    3. RAC-G
    4. MB15-D
    5. MB4-D
    6. MAC15-G
    7. MB15-G
    8. MB4-G
  - The mix ranking for the same conditions for beam fatigue life at 400 microstrain shows exactly the reverse trend from the above except that MAC15-D and RAC-G change places:
    1. MAC15-G
    2. MB4-G
    3. MB15-G
    4. MB4-D
    5. MB15-D
    6. MAC15-D
    7. RAC-G
    8. AR4000-D

Complex Modulus (E^*) Master Curves of Mixes

- E^* master curves from flexural frequency sweep tests show mix stiffnesses for a wide range of temperature and time of loading conditions. Initial stiffnesses determined from beam fatigue tests are only for 10 Hz and the temperature at which the fatigue test was performed. Nevertheless, the

mix ranking of E^* master curves under various combinations of material properties and testing conditions is generally in the order listed below, and is comparable to the overall general ranking of beam fatigue performance in the controlled-strain testing. The MB4 and MB15 mixes show no significant difference in E^* master curves.

Initial stiffness	Fatigue life
1. AR4000-D	1. MB4-G
2. RAC-G	2. MB15-G
3. MAC15-G	3. MAC15-G
4. MB15-G	4. RAC-G
5. MB4-G	5. AR4000-D

- The ranking of E^* master curves for dense-graded mixes considering the effect of gradation is in the order below, with no significant difference between the MB4-D and MB15-D mixes:
    1. MAC15-D
    2. MB4-D
    3. MB15-D

6.2. Recommendations

No recommendations as to the use of modified binder mixes are made at this time. These recommendations will be included in the second-level analysis report that will be prepared and submitted on completion of all HVS and laboratory testing.

7. REFERENCES

1. **Generic experimental design for product/strategy evaluation - crumb rubber modified materials**. 2005. Sacramento, CA: Caltrans, Materials and Engineering Testing Services, Office of Flexible Pavement Materials. Sacramento, CA. 55 pp.
2. **Reflective Cracking Study: Workplan for the Comparison of MB, RAC-G, and DGAC Mixes Under HVS and Laboratory Testing.** 2003. Davis and Berkeley, CA: University of California Pavement Research Center. (UCPRC-WP-2003-01).
3. TSAI, B.W., Guada, I. and Lu, Q. 2006. **Reflective Cracking Study: Detailed Results of Laboratory Fatigue Testing**. Davis and Berkeley, CA: University of California Pavement Research Center. (UCPRC-2006-09).
4. BELL, C.A. and Sosnovske, D. 1994. **Aging: Binder Validation.** SHRP-A-384, Strategic Highway Research Program, National Research Council, Washington, D.C.
5. TSAI, B.W., Harvey, J. and Monismith, C. 2005. Characterization of Mix Fatigue Damage Process Using a Three-Stage Weibull Equation and a Tree-Based Model. **Transportation Research Record 1929.** Washington, D.C.: Transportation Research Board. pp. 227-237.
6. REESE, R.E. 1997. Properties of Aged Binder Related to Asphalt Concrete Fatigue Life. ***Journal* Association of Asphalt Paving Technologists**, Vol. 66, 1997, pp. 604-632.
7. MALLOWS, C.L. 1973. Some comments on C_p. **Technometrics**. Vol.15, pp. 661 – 675.
8. SEBER, G.A.F. 1977. **Linear Regression Analysis.** New York, NY: John Wiley & Sons.
9. CHAMBERS, J.M. and Hastie, T.J. 1993. **Statistical Models in S**. London: Chapman & Hall.
10. SEN, A. and Srivastava, M. 1990. **Regression Analysis: Theory, Methods, and Applications.** Springer-Verlag.

APPENDIX A: SUMMARY OF RESULTS

Summary results are presented as follows:

Table A.1: Summary of fatigue test results for AR4000-D mixes
(Temperature effect, FMLC, AV = 6.0 %, AC=5.0 %)

Table A.2: Summary of fatigue test results for RAC-G mixes
(Temperature effect, FMLC, AV = 6%, AC = 8.0%)

Table A.3: Summary of fatigue test results for MAC15-G mixes
(Temperature effect, FMLC, AV = 6.0 %, AC = 7.4 %)

Table A.4: Summary of fatigue test results for MB15-G mixes
(Temperature effect, FMLC, AV = 6.0 %, AC = 7.1 %)

Table A.5: Summary of fatigue test results for MB4-G mixes
(Temperature effect, FMLC, AV = 6%, AC = 7.2%)

Table A.6: Summary of fatigue test results
(Air-void content effect, FMLC, AV = 9.0 %)

Table A.7: Summary of fatigue test results
(Aging effect, FMLC, AV = 6.0 %, 20C, LTOA6)

Table A.8: Summary of fatigue test results
(Compaction effect, LMLC, AV = 6%, 20C, GG)

Table A.9: Summary of fatigue test results
(Gradation effect, LMLC, AV = 6%, 20C, DG)

Table A.1: Summary of Fatigue Test Results for AR4000-D Mixes

(Temperature effect, FMLC, AV = 6.0 %, AC=5.0 %)

Specimen Designation	Mix Type	AV (%)	AC (%)	Test Temp. (C)	Test Strain Level	Initial Phase Angle (Deg.)	Initial Stiffness (MPa)	Fatigue Life Nf
G9-DGAC-17B	AR4000-D	6.26	5.0	10.40	0.000398	10.11	11588	51,204
G9-DGAC-12B	AR4000-D	6.41	5.0	10.27	0.000398	10.72	10915	45,566
G9-DGAC-4A	AR4000-D	6.11	5.0	9.97	0.000396	10.55	12147	58,924
G9-DGAC-11B	AR4000-D	6.50	5.0	9.88	0.000710	11.81	9463	2,626
G9-DGAC-17A	AR4000-D	6.43	5.0	10.75	0.000702	10.86	11215	11,345
G9-DGAC-20B	AR4000-D	5.70	5.0	9.96	0.000712	14.35	7176	2,887
G9-DGAC-8A	AR4000-D	6.11	5.0	19.88	0.000400	19.99	7372	11,233
G9-DGAC-15A	AR4000-D	5.58	5.0	19.90	0.000390	20.35	8479	40,131
G9-DGAC-22A	AR4000-D	6.07	5.0	19.91	0.000398	21.20	7700	24,895
G9-DGAC-13B	AR4000-D	5.91	5.0	19.94	0.000695	22.63	6829	4,543
G9-DGAC-21B	AR4000-D	5.61	5.0	19.91	0.000699	21.62	7385	4,853
G9-DGAC-14B	AR4000-D	6.53	5.0	19.86	0.000697	24.08	6402	2,871
G9-DGAC-15B	AR4000-D	5.68	5.0	29.93	0.000408	41.59	3268	65,015
G9-DGAC-18B	AR4000-D	6.43	5.0	29.89	0.000408	42.16	2777	92,330
G9-DGAC-16A	AR4000-D	5.70	5.0	29.95	0.000407	40.11	3190	61,006
G9-DGAC-14A	AR4000-D	6.39	5.0	30.95	0.000714	34.81	4335	4,554
G9-DGAC-6A	AR4000-D	6.47	5.0	30.73	0.000712	36.41	3779	5,748
G9-DGAC-8B	AR4000-D	6.21	5.0	30.87	0.000711	34.67	4372	4,761

Table A.2: Summary of Fatigue Test Results for RAC-G Mixes

(Temperature effect, FMLC, AV = 6%, AC = 8.0%)

Specimen Designation	Mix Type	AV (%)	AC (%)	Test Temp. (°C)	Test Strain Level	Initial Phase Angle (Deg.)	Initial Stiffness (MPa)	Fatigue Life Nf
G9-RACG-6A	RAC-G	5.50	8.0	10.09	0.000396	15.10	7930	141,141
G9-RACG-3A	RAC-G	5.92	8.0	10.38	0.000387	15.24	8129	253,404
G9-RACG-5B	RAC-G	5.92	8.0	9.90	0.000393	13.20	7928	215,076
G9-RACG-6B	RAC-G	6.30	8.0	10.70	0.000705	16.62	7201	8,245
G9-RACG-18B	RAC-G	6.27	8.0	10.06	0.000715	15.99	6745	14,459
G9-RACG-4A	RAC-G	5.48	8.0	10.42	0.000709	16.00	7076	11,216
G9-RACG-14A	RAC-G	6.46	8.0	19.93	0.000403	26.67	3638	453,380
G9-RACG-1B	RAC-G	6.15	8.0	20.62	0.000417	26.71	4436	136,983
G9-RACG-12B	RAC-G	6.00	8.0	20.59	0.000416	26.79	4450	637,582
G9-RACG-16A	RAC-G	5.54	8.0	20.43	0.000723	28.78	3961	14,532
G9-RACG-4B	RAC-G	5.77	8.0	19.94	0.000704	29.01	3549	27,070
G9-RACG-5A	RAC-G	6.41	8.0	19.92	0.000698	32.12	3660	11,755
G9-RACG-16B	RAC-G	5.87	8.0	29.60	0.000401	36.49	2344	752,449
G9-RACG-19B	RAC-G	5.78	8.0	29.55	0.000400	36.16	2236	1,562,551
G9-RACG-10B	RAC-G	6.40	8.0	29.57	0.000404	37.15	2007	538,708*
G9-RACG-13A	RAC-G	5.60	8.0	30.35	0.000725	38.93	2513	46,845
G9-RACG-1A	RAC-G	6.41	8.0	30.20	0.000737	42.56	1901	44,642
G9-RACG-13B	RAC-G	5.75	8.0	30.67	0.000728	39.61	2424	49,882

Table A.3: Summary of Fatigue Test Results for MAC15-G Mixes

(Temperature effect, FMLC, AV = 6.0 %, AC = 7.4 %)

Specimen Designation	Mix Type	AV (%)	AC (%)	Test Temp. (°C)	Test Strain Level	Initial Phase Angle (Deg.)	Initial Stiffness (MPa)	Fatigue Life Nf
G9-MAC15-25A	MAC15-G	5.89	7.4	9.99	0.000388	17.20	7949	932,673
G9-MAC15-2B	MAC15-G	6.33	7.4	10.31	0.000400	17.72	6426	345,709
G9-MAC15-19A	MAC15-G	6.50	7.4	10.13	0.000400	17.30	7345	571,417
G9-MAC15-11A	MAC15-G	6.24	7.4	10.02	0.000706	21.59	6239	25,360
G9-MAC15-4B	MAC15-G	5.53	7.4	10.22	0.000698	18.62	6737	23,920
G9-MAC15-15B	MAC15-G	6.53	7.4	9.60	0.000706	19.30	6897	34,249
G9-MAC15-24B	MAC15-G	6.45	7.4	19.92	0.000408	41.36	1675	4,167,967
G9-MAC15-13B	MAC15-G	5.70	7.4	19.90	0.000399	33.94	3297	8,853,486*
G9-MAC15-1B	MAC15-G	5.73	7.4	20.62	0.000419	32.02	4019	3,405,270
G9-MAC15-26A	MAC15-G	6.53	7.4	19.94	0.000704	44.97	1678	331,919
G9-MAC15-9B	MAC15-G	5.70	7.4	19.94	0.000696	33.51	2782	519,505
G9-MAC15-13A	MAC15-G	6.11	7.4	19.94	0.000696	35.86	3065	664,993
G9-MAC15-10A	MAC15-G	6.23	7.4	29.72	0.000405	43.53	1333	2,062,190*
G9-MAC15-11B	MAC15-G	6.44	7.4	29.79	0.000408	46.57	1265	8,847,719*
G9-MAC15-20B	MAC15-G	5.90	7.4	30.75	0.000422	48.91	1254	15,136,954*
G9-MAC15-1A	MAC15-G	5.49	7.4	29.72	0.000714	44.33	1649	6,982,693*
G9-MAC15-25B	MAC15-G	6.34	7.4	30.84	0.000726	45.85	1745	2,025,612
G9-MAC15-8B	MAC15-G	6.20	7.4	30.79	0.000733	48.38	1281	7,014,195*

Note
*: extrapolation.

Table A.4: Summary of Fatigue Test Results for MB15-G Mixes

(Temperature effect, FMLC, AV = 6.0 %, AC = 7.1 %)

Specimen Designation	Mix Type	AV (%)	AC (%)	Test Temp. (°C)	Test Strain Level	Initial Phase Angle (Deg.)	Initial Stiffness (MPa)	Fatigue Life Nf
G9-MB15-20B	MB15-G	6.43	7.1	10.20	0.000407	26.55	3770	9,803,239*
G9-MB15-27A	MB15-G	6.44	7.1	9.93	0.000406	22.72	4640	10,728,429*
G9-MB15-23B	MB15-G	5.50	7.1	10.26	0.000403	24.35	4708	10,352,525*
G9-MB15-32B	MB15-G	6.40	7.1	10.20	0.000705	24.10	4637	38,892
G9-MB15-29B	MB15-G	6.48	7.1	9.96	0.000706	23.65	4764	51,073
G9-MB15-9A	MB15-G	5.53	7.1	10.19	0.000699	27.40	3912	292,775
G9-MB15-20A	MB15-G	6.04	7.1	20.52	0.000424	43.24	1673	1,303,284
G9-MB15-1A	MB15-G	6.46	7.1	19.92	0.000405	41.69	1522	3,406,799
G9-MB15-30B	MB15-G	6.24	7.1	19.91	0.000408	30.79	3209	4,191,041
G9-MB15-25B	MB15-G	6.31	7.1	19.92	0.000702	45.28	1446	355,412
G9-MB15-34A	MB15-G	5.86	7.1	19.91	0.000701	47.88	1244	286,651
G9-MB15-26A	MB15-G	6.45	7.1	19.93	0.000702	45.92	1248	337,904
G9-MB15-19B	MB15-G	6.41	7.1	30.33	0.000431	62.30	717	1,273,806
G9-MB15-5A	MB15-G	6.23	7.1	30.68	0.000433	66.30	712	2,760,082
G9-MB15-7A	MB15-G	6.02	7.1	29.95	0.000402	57.72	448	3,122,129
G9-MB15-12A	MB15-G	6.54	7.1	30.80	0.000746	57.85	579	628,905
G9-MB15-26B	MB15-G	6.11	7.1	30.06	0.000748	60.07	523	318,278
G9-MB15-33A	MB15-G	6.49	7.1	30.74	0.000747	57.64	602	408,079

Note
*: extrapolation.

Table A.5: Summary of Fatigue Test Results for MB4-G Mixes

(Temperature effect, FMLC, AV = 6%, AC = 7.2%)

Specimen Designation	Mix Type	AV (%)	AC (%)	Test Temp. (°C)	Test Strain Level	Initial Phase Angle (Deg.)	Initial Stiffness (MPa)	Fatigue Life Nf
G9-MB4-13A	MB4-G	5.50	7.2	9.91	0.000402	23.88	4372	17,664,495*
G9-MB4-17A	MB4-G	5.83	7.2	9.94	0.000404	26.33	3850	35,231,219*
G9-MB4-17B	MB4-G	5.50	7.2	9.97	0.000402	24.69	4350	27,633,563*
G9-MB4-5B	MB4-G	6.07	7.2	9.81	0.000699	24.99	4070	372,928
G9-MB4-12B	MB4-G	5.58	7.2	9.80	0.000701	25.66	3893	186,987
G9-MB4-11A	MB4-G	6.40	7.2	10.13	0.000700	26.72	3921	1,019,530
G9-MB4-30B	MB4-G	6.27	7.2	20.49	0.000424	45.37	1429	18,774,076*
G9-MB4-8B	MB4-G	6.37	7.2	20.56	0.000427	46.40	1243	29,211,530*
G9-MB4-26B	MB4-G	5.84	7.2	20.65	0.000424	44.15	1483	7,725,081*
G9-MB4-14A	MB4-G	5.86	7.2	20.44	0.000737	42.28	1590	85,028
G9-MB4-32A	MB4-G	6.01	7.2	20.60	0.000740	47.82	1279	1,682,779
G9-MB4-7B	MB4-G	5.80	7.2	20.55	0.000742	46.02	1226	492,375
G9-MB4-20B	MB4-G	5.47	7.2	29.47	0.000406	54.82	512	6,241,325,854*
G9-MB4-11B	MB4-G	5.50	7.2	29.36	0.000405	50.19	689	26,790,763*
G9-MB4-30A	MB4-G	5.70	7.2	30.12	0.000430	55.96	686	66,007,390*
G9-MB4-21B	MB4-G	5.96	7.2	29.29	0.000706	55.61	584	9,169,275*
G9-MB4-26A	MB4-G	5.50	7.2	29.51	0.000712	55.95	505	38,534,397*
G9-MB4-25A	MB4-G	5.68	7.2	30.76	0.000739	56.73	593	14,971,040*

Note
*: extrapolation.

Table A.6: Summary of Fatigue Test Results for Air-Void Content

(Air-void content effect, FMLC, AV = 9.0 %)

Specimen Designation	Mix Type	AV (%)	AC (%)	Test Temp. (C)	Test Strain Level	Initial Phase Angle (Deg.)	Initial Stiffness (MPa)	Fatigue Life Nf
G9-DGAC-12A	AR4000-D	8.09	5.0	19.75	0.000406	20.50	7805	42,335
G9-DGAC-5A	AR4000-D	7.96	5.0	20.64	0.000409	20.26	6997	25,461
G9-DGAC-10A	AR4000-D	8.79	5.0	19.92	0.000399	20.47	6665	22,074
G9-DGAC-3A	AR4000-D	7.97	5.0	20.19	0.000723	26.88	4484	566
G9-DGAC-2B	AR4000-D	8.05	5.0	19.90	0.000704	22.06	5755	3,262
G9-DGAC-1B	AR4000-D	8.96	5.0	20.67	0.000717	22.28	5632	2,202
G9-RACG-22A	RAC-G	9.70	8.0	19.75	0.000411	27.27	3863	231,682
G9-RACG-25A	RAC-G	9.92	8.0	19.92	0.000400	27.12	3455	343,953
G9-RACG-20A	RAC-G	9.26	8.0	20.63	0.000413	28.16	3704	125,409
G9-RACG-23A	RAC-G	8.84	8.0	19.68	0.000709	29.87	3643	32,123
G9-RACG-20B	RAC-G	9.17	8.0	19.93	0.000694	30.99	3646	11,344
G9-RACG-24B	RAC-G	9.81	8.0	20.51	0.000726	31.35	3399	13,447
GR-MAC15-3A	MAC15-G	8.38	7.4	19.93	0.000415	30.24	3368	1,011,990
G9-MAC15-1B	MAC15-G	8.14	7.4	19.92	0.000399	34.03	2849	33,987,640*
G9-MAC15-18A	MAC15-G	9.31	7.4	20.76	0.000418	39.76	1855	3,324,576
GR-MAC15-4B	MAC15-G	9.02	7.4	20.01	0.000710	32.40	3076	170,744
G9-MAC15-29B	MAC15-G	9.50	7.4	19.92	0.000696	34.40	2304	186,137
G9-MAC15-16A	MAC15-G	8.79	7.4	20.74	0.000728	36.78	2735	103,599
G9-MB15-17B	MB15-G	8.54	7.1	20.01	0.000426	40.54	1639	4,353,301
G9-MB15-2A	MB15-G	8.50	7.1	19.94	0.000401	41.39	1426	5,049,641
G9-MB15-21A	MB15-G	8.36	7.1	20.91	0.000423	44.17	1372	2,003,311*
G9-MB15-18A	MB15-G	8.16	7.1	19.92	0.000741	44.79	1349	839,731
G9-MB15-16B	MB15-G	8.16	7.1	19.98	0.000695	43.09	1193	201,789
G9-MB15-11B	MB15-G	8.15	7.1	20.68	0.000736	47.17	1220	328,634
G9-MB4-35B	MB4-G	8.85	7.2	20.76	0.000410	39.07	1321	48,334,981*
G9-MB4-35A	MB4-G	8.15	7.2	19.92	0.000400	41.90	1261	26,496,683*
G9-MB4-37A	MB4-G	8.90	7.2	20.67	0.000415	42.30	1335	10,935,169*
G9-MB4-38B	MB4-G	8.29	7.2	20.50	0.000737	39.54	1472	788,798*
G9-MB4-37B	MB4-G	8.49	7.2	19.94	0.000697	44.27	1306	705,515
G9-MB4-38A	MB4-G	8.22	7.2	20.72	0.000736	44.12	1265	669,923

Note
*: extrapolation.

Table A.7: Summary of Fatigue Test Results for Aging Effect

(Aging effect, FMLC, AV = 6.0 %, 20C, LTOA6)

Specimen Designation	Mix Type	AV (%)	AC (%)	Test Temp. (°C)	Test Strain Level	Initial Phase Angle (Deg.)	Initial Stiffness (MPa)	Fatigue Life Nf
G9-DGAC-9B	AR4000-D	5.58	5.0	19.98	0.000410	16.02	9794	22,963
G9-DGAC-21A	AR4000-D	6.05	5.0	20.03	0.000408	16.80	10333	21,445
G9-DGAC-6B	AR4000-D	6.55	5.0	20.45	0.000709	14.52	9979	1,860
G9-DGAC-20A	AR4000-D	5.57	5.0	19.89	0.000697	18.04	8681	2,788
G9-RACG-7A	RAC-G	6.48	8.0	20.83	0.000400	20.18	5840	3,428,264*
G9-RACG-17A	RAC-G	6.47	8.0	19.94	0.000398	22.95	5263	1,334,858
G9-RACG-15B	RAC-G	5.69	8.0	20.05	0.000725	25.24	5307	16,223
G9-RACG-15A	RAC-G	6.53	8.0	20.03	0.000705	24.54	5583	20,898
GR-MAC15-28A	MAC15-G	6.41	7.4	20.83	0.000402	22.64	5032	2,577,541
GR-MAC15-10A	MAC15-G	6.23	7.4	19.95	0.000398	26.43	4546	1,611,280
GR-MAC15-5A	MAC15-G	6.50	7.4	20.68	0.000728	31.86	3511	243,046
GR-MAC15-9B	MAC15-G	6.52	7.4	20.27	0.000709	28.25	4270	96,394
G9-MB15-33B	MB15-G	6.07	7.1	20.59	0.000407	30.24	3012	1,492,524
G9-MB15-7B	MB15-G	5.67	7.1	20.71	0.000421	34.26	2917	474,502
G9-MB15-10A	MB15-G	5.66	7.1	19.99	0.000692	37.21	2485	35,099
G9-MB15-27B	MB15-G	6.52	7.1	20.11	0.000717	34.02	2409	153,375
G9-MB4-22A	MB4-G	6.11	7.2	19.91	0.000399	39.14	1785	30,661,062*
G9-MB4-18A	MB4-G	5.98	7.2	20.86	0.000422	39.71	1747	11,997,565*
G9-MB4-25B	MB4-G	6.32	7.2	20.84	0.000719	38.60	1601	1,534,331
G9-MB4-7A	MB4-G	6.02	7.2	19.95	0.000731	39.67	1626	2,343,174

Note
*: extrapolation.

Table A.8: Summary of Fatigue Test Results for Compaction Effect

(Compaction effect, LMLC, AV = 6%, 20C, GG)

Specimen Designation	Mix Type	AV (%)	AC (%)	Test Temp. (°C)	Test Strain Level	Initial Phase Angle (Deg.)	Initial Stiffness (MPa)	Fatigue Life Nf
G9L-RACG-4A1	RAC-G	5.61	8.0	20.65	0.000410	26.82	2927	1,171,604*
G9L-RACG-6A2	RAC-G	5.73	8.0	19.81	0.000414	31.66	3452	520,228
G9L-RACG-6A1	RAC-G	6.46	8.0	19.95	0.000693	31.96	2938	36,322
G9L-RACG-3A1	RAC-G	5.81	8.0	19.97	0.000722	33.27	2910	151,182
G9L-MAC15G-3A2	MAC15-G	6.08	7.4	19.96	0.000420	44.78	1765	1,860,333,570*
G9L-MAC15G-2A1	MAC15-G	6.30	7.4	20.19	0.000411	40.76	2269	96,539,623*
G9L-MAC15G-3A1	MAC15-G	6.39	7.4	20.61	0.000708	39.18	2203	2,979,048*
G9L-MAC15G-5A2	MAC15-G	6.55	7.4	19.96	0.000700	45.95	1668	2,322,056
G9L-MB15G-1A1	MB15-G	6.39	7.1	20.78	0.000407	47.57	1127	1,896,344*
G9L-MB15G-6A1	MB15-G	5.54	7.1	20.08	0.000428	55.00	1044	8,815,565*
G9L-MB15G-2A1	MB15-G	6.34	7.1	19.96	0.000699	56.35	708	370,451
G9L-MB15G-6A2	MB15-G	5.93	7.1	20.35	0.000711	54.26	886	1,046,590
G9L-MB4G-2A1	MB4-G	5.47	7.2	20.55	0.000423	44.27	1264	53,953,532*
G9L-MB4G-1A1	MB4-G	5.59	7.2	19.98	0.000420	38.47	1536	40,412,562*
G9L-MB4G-3A1	MB4-G	5.97	7.2	20.25	0.000723	39.29	1102	1,348,690
G9L-MB4G-4B1	MB4-G	5.52	7.2	19.93	0.000696	42.87	1189	996,318

Note
*: extrapolation.

Table A.9: Summary of Fatigue Test Results for Gradation Effect

(Gradation effect, LMLC, AV = 6%, 20C, DG)

Specimen Designation	Mix Type	AV (%)	AC (%)	Test Temp. (°C)	Test Strain Level	Initial Phase Angle (Deg.)	Initial Stiffness (MPa)	Fatigue Life Nf
G9L-DGAC6-5A2	AR4000-D	5.71	5.0	19.71	0.000403	25.92	3911	51,896
G9L-DGAC6-2B2	AR4000-D	6.49	5.0	20.41	0.000420	32.17	3266	9,680
G9L-DGAC6-4B2	AR4000-D	5.52	5.0	19.94	0.000701	32.44	3796	5,313
G9L-DGAC6-6B2	AR4000-D	5.49	5.0	20.02	0.000719	29.36	3748	10,187
G9L-MAC15D6-1C1	MAC15-D	5.77	6.0	20.48	0.000418	29.20	3859	738,408
G9L-MAC15D6-4D1	MAC15-D	5.71	6.0	19.91	0.000402	28.41	3672	1,564,754
G9L-MAC15D6-1C2	MAC15-D	6.48	6.0	20.35	0.000707	30.71	2998	37,569
G9L-MAC15D6-3C2	MAC15-D	6.17	6.0	20.50	0.000728	36.05	2683	20,082
G9L-MB15D6-4B1	MB15-D	6.22	6.0	19.96	0.000407	41.02	1709	1,130,268*
G9L-MB15D6-5A2	MB15-D	5.84	6.0	20.17	0.000421	41.90	1919	2,713,330
G9L-MB15D6-5A1	MB15-D	5.81	6.0	19.95	0.000704	43.35	1614	187,478
G9L-MB15D6-1A2	MB15-D	5.53	6.0	19.94	0.000731	41.89	1980	193,472
G9L-MB4D6-9A1	MB4-D	5.69	6.3	19.92	0.000405	39.38	1863	4,446,984
G9L-MB4D6-9A2	MB4-D	6.14	6.3	20.35	0.000421	39.37	1886	5,029,498*
G9L-MB4D6-6B1	MB4-D	5.68	6.3	20.53	0.000726	37.38	2028	48,541
G9L-MB4D6-6B2	MB4-D	5.81	6.3	20.53	0.000713	33.20	2037	102,211

Note
*: extrapolation.

APPENDIX B: PROCEDURE FOR REGRESSION ANALYSIS

This Appendix includes the process followed to develop the equations discussed in Chapter 4, as well as a worked example.

B.1 Model Selection

Model selection includes two phases, namely model identification and model building. In the first phase, the objective is to identify the significant covariates (or factors) that affect the response variables, a process that uncovers the significant factors that are embedded in a data structure. In the second phase, a best fitting regression model is selected that appropriately represents the response variables as a function of correctly-selected covariates, and includes fitting and overfitting, and residual analysis.

The conventional fatigue analysis discussed below is primarily the model selection of initial stiffness and fatigue life. It should be noted that the model selection of fatigue life and stiffness is a trade-off procedure between engineering judgment and theoretical considerations.

B.1.1 Phase I: Model Identification

Model identification includes the following components:

- Summary boxplots: Boxplots provide an immediately visual investigation of test results in the underlying trends of dataset and in the data variation.
- Pairs diagram: Paired scatter plots with smoothed lines among the variables (covariates and response variables) provide an instantly visual examination of possible relationships amongst paired variables.
- Design plots and factor plots: The design plot shows the relative locations of means of factor levels. The factor plot utilizes the boxplot to present the data variation of each factor level.
- Correlation matrix: The correlation matrix measures the strength of linear relationship between the pairs of variables. The threshold of correlation to judge the strength is set at 0.4 in this report.
- Interaction plots: These plots are used to investigate the two-term interaction effects on response variables.
- ANOVA table: The analysis of variance (ANOVA) table is used to identify the significant covariates that affect the response variables. Normally, the 5 percent significance level of P-values is used to judge the importance of covariates.

B.1.2 Phase II: Model Building

Model building includes the following components:

- Mallow's C_p Criterion: The Mallow's C_p criterion selects the best subset of covariates to give a good balance between the number of covariates and the penalty caused by overfitting. This analysis is discussed in detail in References 7 and 8
- Regression analysis: This estimates the regression coefficients of a specified model specification and provides the R^2 value, which is used for the judgment of model fitting.
- Residual analysis: Residual plots are used to verify the Gauss-Markov assumptions of normality, independence, and constant variance (homoscedasticity) and to detect the possible outliers.
- Engineering judgment.

B.2 Example of Regression Analysis: Temperature Effect

B.2.1 Summary Boxplots of Test Results

Figures B.1 through B.3 summarize the fatigue test results of temperature effect for phase angle (*pangle*), initial stiffness (*lnstif*), and fatigue life (*lnnf*) respectively. The data is presented in terms of boxplots categorized by binder/mix types, strain levels, and temperatures. Each box contains three data points (three replicates): two data points are numerically located on the top and bottom edges of the box and the middle data point is located and presented as the short white strap in the box. The height of the box indicates the data variation. Interpretation of the box plots includes:

- It is apparent that the temperature is highly positive-correlated with *pangle* and negative-correlated with *lnstif* per binder/mix type and strain level. As for the temperature effect on *lnnf*, the increase of temperature generally results in an increase of fatigue life per binder type and strain level. The only exception is the MB15-G mixes at 400 microstrain. Fatigue lives at 400 microstrain and 10°C were obtained by extrapolation. Note that the *lnnf* values of MB4-G scatter widely at 400 microstrain and 30°C due to the extrapolation and might indicate the presence of possible outliers in the regression analysis.
- The strain level shows no effects on *pangle* and *lnstif* per binder type and temperature. On the contrary, the effect of strain level on *lnnf* is evident.
- It is obvious that the three response variables are significantly affected by the binder/mix types.

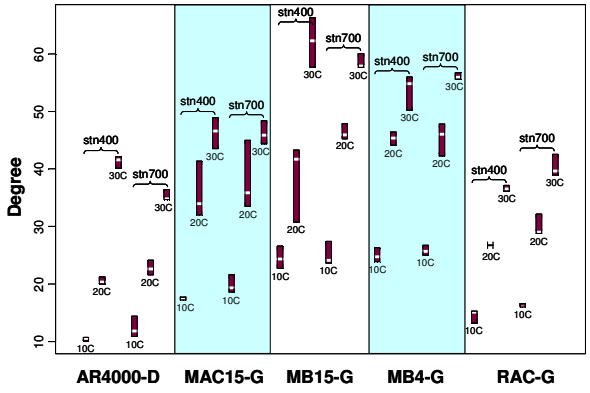

Figure B.1: Summary boxplots of phase angle.
(Temperature effect, FMLC, AV = 6%).

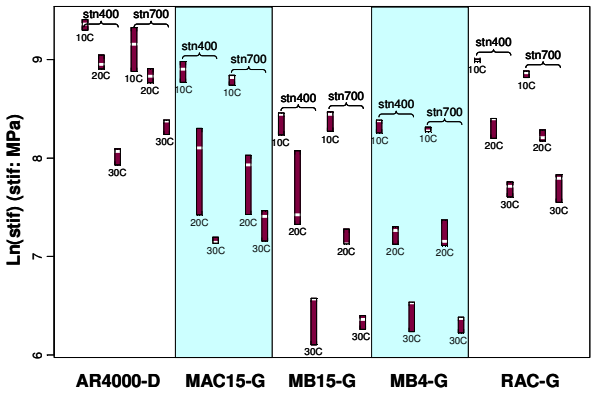

Figure B.2: Summary boxplots of *ln(stif)*.
(Temperature effect, FMLC, AV = 6%).

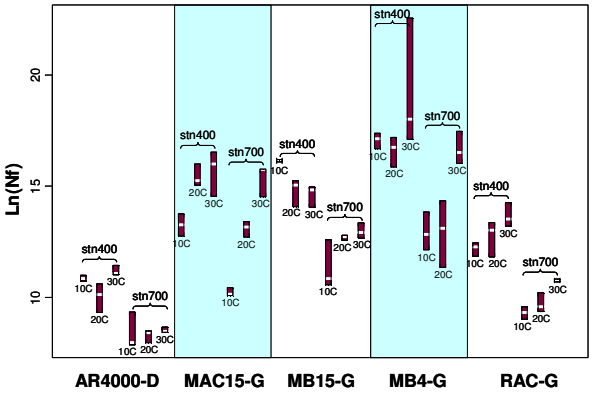

Figure B.3: Summary boxplots of *ln(Nf)*.
(Temperature effect, FMLC, AV = 6%).

B.2.2 Identification of Significant Factors

Pairs Diagram and Correlation Matrix

Figure B.4 is the pairs diagram with smoothed lines that is used to explore the relationships among variables. The information presented in Figure B.4 for *pa*, *lnstif*, and *lnnf* clearly demonstrates the following:

- The *temp* has obvious effects on *pangle* and *lnstif* and less effect on *lnnf*.
- The *stn* has significant effect on *lnnf* but not on *pangle* and *lnstif*.
- The *binder/mix* effect is apparent on *pa*, *lnstif*, and *lnnf*.
- There is a strong linear relationship between *pangle* and *lnstif*.

The correlation matrix shown in Table B.1 measures the strength of linear relationship between the pairs of variables. Figure B.5 presents a series of scatter plots of 500 independent pairs of bivariate normal random variables with various correlation coefficients, which gives an indication of how the scatter plots

appear if two normal random variables exist with a certain correlation coefficient. Note that the "clouds" of points are roughly elliptical in shape. From Figure B.5, it appears that there is a slight visually recognizable pattern when the correlation coefficient is set at a value of 0.4. Based on these subjective criteria, several findings from the scatter plots and correlation matrix are apparent:

- The *lnstn* (strain in natural logarithm) is negatively correlated with *lnnf*; which implies that a higher strain level will significantly reduce the fatigue life. There is no correlation with *pangle* and *lnstif*.
- The *binder* shows no strong correlation with any of the response variables if the correlation coefficient criterion is set at 0.4. However, in the pairs diagram, it is apparent that all the response variables are visually affected by the binder type.
- The *temp* is highly positive-correlated with *pa*, highly negative-correlated with *lnstif*, and has no apparent correlation with *lnnf*. Thus, higher temperature causes higher initial phase angle and lower initial stiffness.
- The correlation coefficients among the covariates are extremely low (i.e., the covariates are nearly independent).
- The *pangle* is highly negative-correlated with *lnstif*.

Figure B.4: Pairs diagram.
(Temperature effect, FMLC, AV = 6%).

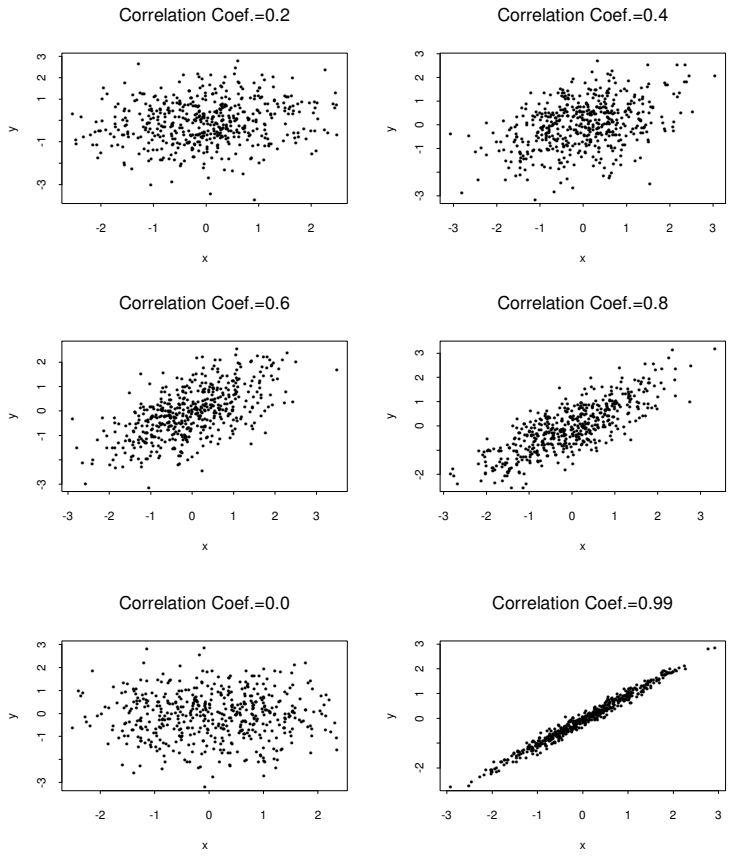

Figure B.5: Scatterplots of 500 independent pairs of bivariate normal random variables.
(With correlation coefficients ρ = 0.2, ρ = 0.4, ρ = 0.6, ρ = 0.8, ρ = 0.0, and ρ = 0.99)

Table B.1: Correlation Matrix and ANOVA Results

(Temperature effect, FMLC, AV = 6%).

(a) correlation matrix

	binder	temp	lnstn	pa	lnstif	lnnf
binder	1.0000000000	-0.0008052731	0.01785547	0.1498805	-0.26212596	0.2829874
temp	-0.0008052731	1.0000000000	0.05373812	0.8154776	-0.72451512	0.2314170
lnstn	0.0178554701	0.0537381228	1.00000000	0.1049903	-0.09380779	-0.4349115
pa	0.1498805339	0.8154776111	0.10499028	1.0000000	-0.97005572	0.5295507
lnstif	-0.2621259643	-0.7245151231	-0.09380779	-0.9700557	1.00000000	-0.6193047
lnnf	0.2829874359	0.2314169772	-0.43491147	0.5295507	-0.61930475	1.0000000

(b) ANOVA result of pa

	Df	Sum of Sq	Mean Sq	F Value	Pr(F)
binder	4	5086.28	1271.57	128.996	0.0000000
temp	1	12266.40	12266.40	1244.376	0.0000000
stn	1	33.51	33.51	3.399	0.0692335
binder:temp	4	226.10	56.52	5.734	0.0004474
binder:stn	4	28.81	7.20	0.731	0.5739031
temp:stn	1	38.08	38.08	3.863	0.0531171
Residuals	74	729.45	9.86		

(c) ANOVA result of lnstif

	Df	Sum of Sq	Mean Sq	F Value	Pr(F)
binder	4	27.65701	6.91425	199.916	0.0000000
temp	1	36.32274	36.32274	1050.220	0.0000000
stn	1	0.07740	0.07740	2.238	0.1389228
binder:temp	4	2.12373	0.53093	15.351	0.0000000
binder:stn	4	0.05672	0.01418	0.410	0.8008904
temp:stn	1	0.18325	0.18325	5.298	0.0241614
Residuals	74	2.55935	0.03459		

(d) ANOVA result of lnnf

	Df	Sum of Sq	Mean Sq	F Value	Pr(F)
binder	4	435.3588	108.8397	133.4643	0.00000000
temp	1	41.0334	41.0334	50.3170	0.00000000
stn	1	166.2617	166.2617	203.8779	0.00000000
binder:temp	4	31.7430	7.9358	9.7312	0.00000222
binder:stn	4	7.1785	1.7946	2.2007	0.07710575
temp:stn	1	8.5946	8.5946	10.5391	0.00175711
Residuals	74	60.3467	0.8155		

Design Plots, Factor Plots, Interaction Plots, and ANOVA Results

According to the experimental design, the covariate *binder* was categorized into five factor levels of AR4000, ARB, MAC15, MB15, and MB4; the factor *stn* was separated into two factor levels of *stn400* and *stn700*, and the factor *temp* was classified by three factor levels, namely *10C*, *20C*, and *30C*. A series of design plots based on the factor levels described above are presented in Figure B.6 for *pa*, *lnstif*, and *lnnf* respectively. In the figure, the horizontal line represents the grand mean of the response variable, and the vertical line marked with short ticks indicates the means of factor levels for a specific factor. Therefore, the further apart the marked factor levels in the vertical line, the more significant the effect of the factor on the response variable. It should be noted that the recognition of importance of factors using design plots is also subjective. Several findings are relevant:

- The *pangle* is primarily affected by the *temp* and *binder* and insensitive to *stn*. Note that the higher the temperature the bigger the initial phase angle.
- The *lnstif* is mainly affected by the *binder* and *temp* but not by the *stn*. Thus the lower the temperature the higher the stiffness.
- The *stn* has a significantly greater effect on the fatigue life than it does on stiffness, while *temp* has a minor effect on fatigue life. The difference of fatigue performance is evident among various binder/mix types.
- The ranking of fatigue life is MB4 > MAC15 > MB15 > ARB > AR4000 whereas the ranking of initial stiffness is roughly reversed as AR4000 > ARB > MAC15 > MB15 > MB4. Therefore, higher mix stiffnesses will result in lower fatigue life and vice versa.

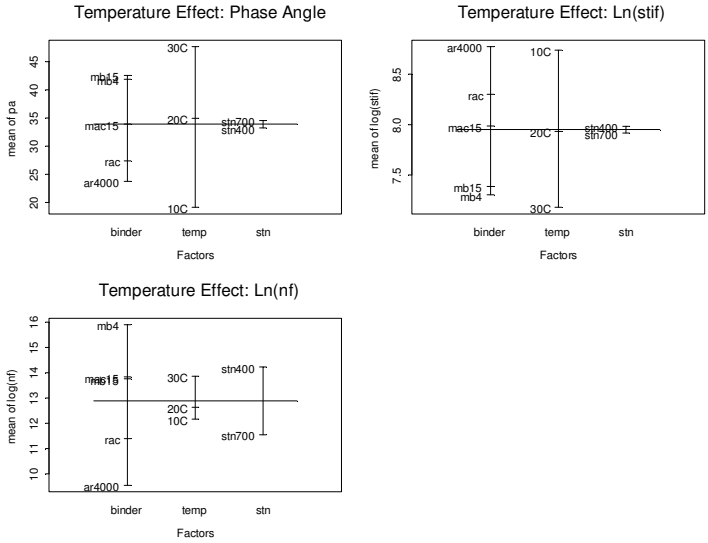

Figure B.6: Design plots of *pa*, *lnstif*, and *lnnf*.
(Temperature effect, FMLC, AV = 6%).

In addition to the design plots, Figures B.7 through B.9 present the factor plots showing the box-and-whisker plots (boxplots) used for inspecting the effect of factors on the response variables. The boxplots illustrate the variation of the response variables at various factor levels and identify the possible outliers.

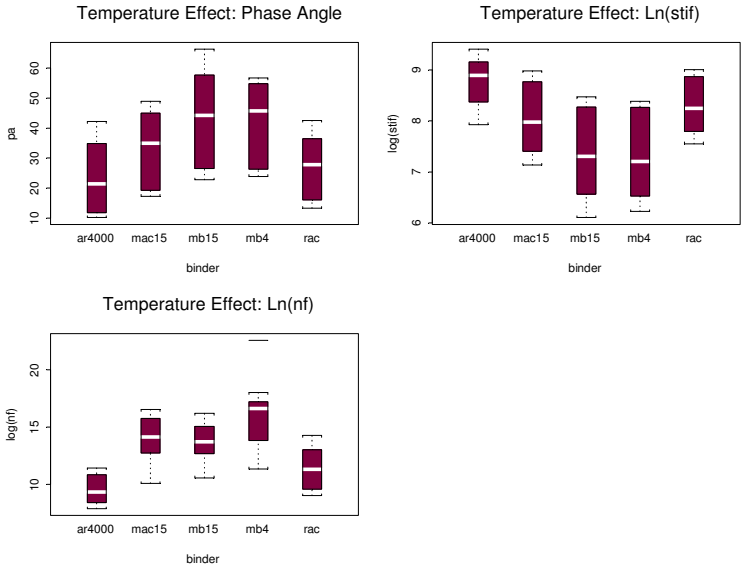

Figure B.7: Boxplots for factor *binder*.
(Temperature effect, FMLC, AV = 6%).

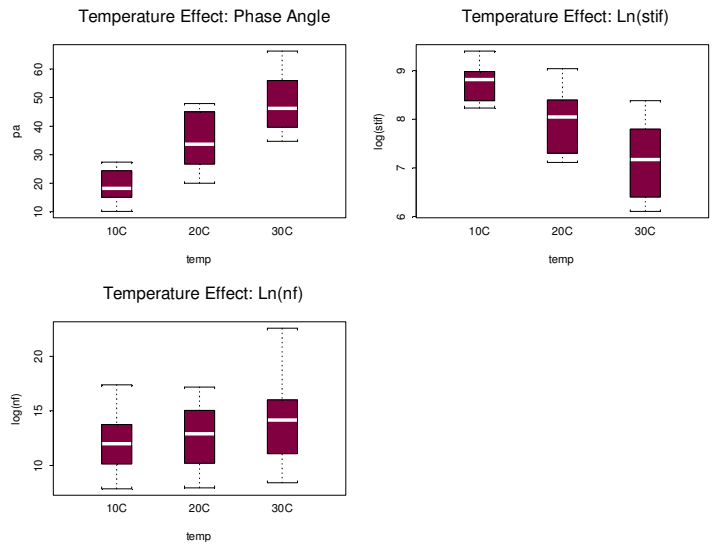

Figure B.8: Boxplots for factor *temp*.
(Temperature effect, FMLC, AV = 6%).

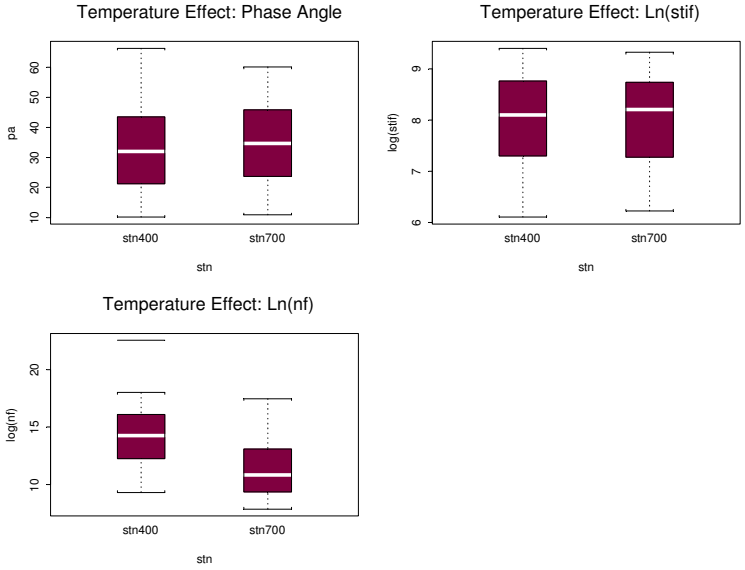

Figure B.9: Boxplots for factor *stn*.
(Temperature effect, FMLC, AV = 6%).

Examining the analysis of variance (ANOVA) results listed in Table B.1 provides a quantitative way to identify significant factors that affect the response variables. The main effects and interaction effects on response variables are summarized below accompanied with the ANOVA table. The criterion of assessing the importance of effect is set at a 5 percent significance level of P-value. The covariates beside the response variables are identified as the significant factors.

- *Pa*: *binder*, *temp*, and *binder*temp*.

	Df	Sum of Sq	Mean Sq	F Value	Pr(F)
binder	4	5086.28	1271.57	128.996	0.0000000
temp	1	12266.40	12266.40	1244.376	0.0000000
stn	1	33.51	33.51	3.399	0.0692335
binder:temp	4	226.10	56.52	5.734	0.0004474
binder:stn	4	28.81	7.20	0.731	0.5739031
temp:stn	1	38.08	38.08	3.863	0.0531171
Residuals	74	729.45	9.86		

- *Lnstif*: *binder*, *temp*, and *binder*temp*.

	Df	Sum of Sq	Mean Sq	F Value	Pr(F)
binder	4	27.65701	6.91425	199.916	0.0000000
temp	1	36.32274	36.32274	1050.220	0.0000000
stn	1	0.07740	0.07740	2.238	0.1389228
binder:temp	4	2.12373	0.53093	15.351	0.0000000
binder:stn	4	0.05672	0.01418	0.410	0.8008904
temp:stn	1	0.18325	0.18325	5.298	0.0241614
Residuals	74	2.55935	0.03459		

- *Lnnf*: *binder*, *temp*, *stn*, *binder*temp*, and *temp*stn*.

	Df	Sum of Sq	Mean Sq	F Value	Pr(F)
binder	4	435.3588	108.8397	133.4643	0.00000000
temp	1	41.0334	41.0334	50.3170	0.00000000
stn	1	166.2617	166.2617	203.8779	0.00000000
binder:temp	4	31.7430	7.9358	9.7312	0.00000222
binder:stn	4	7.1785	1.7946	2.2007	0.07710575
temp:stn	1	8.5946	8.5946	10.5391	0.00175711
Residuals	74	60.3467	0.8155		

According to the criterion of 5 percent significance level of P-value, the above ANOVA results indicate possible interaction effects exist for all the response variables. However, if the mean squares of ANOVA results are examined, the identified interaction effects based on a 5 percent significance level of P-value might be not inappropriate to ignore when compared with the mean squares of the main effects. The interaction plots in Figures B.10 through B.12 show no considerable interaction effects among covariates for this dataset.

In accordance with the identification procedure discussed above, a summary table of main effects (Table B.2) was prepared for evaluating various effects on fatigue performance. The criteria used to mark the significant factors consist of two qualitative methods (design plots and factor plots), and two quantitative methods (correlation matrix and ANOVA results). The threshold correlation of identifying a significant factor from the correlation matrix is 0.4. A 5 percent significance level of P-value is set for the ANOVA results. If all four criteria are check-marked in one independent variable, then this independent

variable is considered as a "very important" factor. If three criteria are check-marked, the factor is considered as being "important". If only one or two criteria are matched, it is deemed "less important".

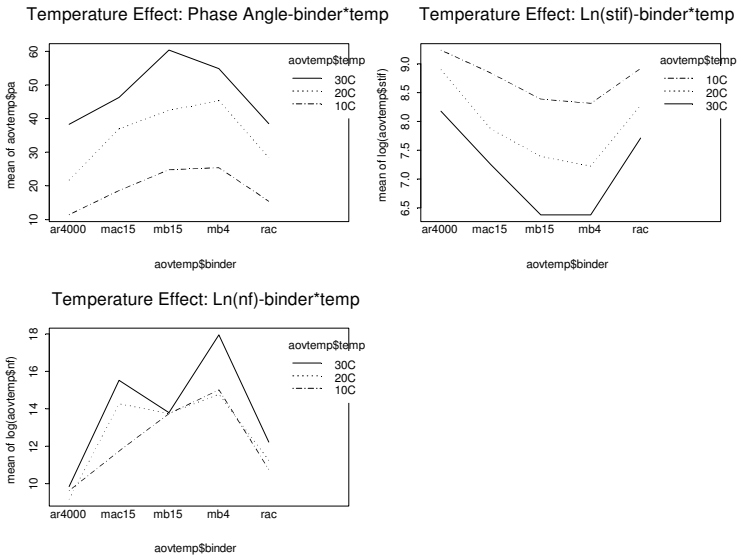

Figure B.10: Interaction plots of *binder*temp*.
(Temperature effect, FMLC, AV = 6%).

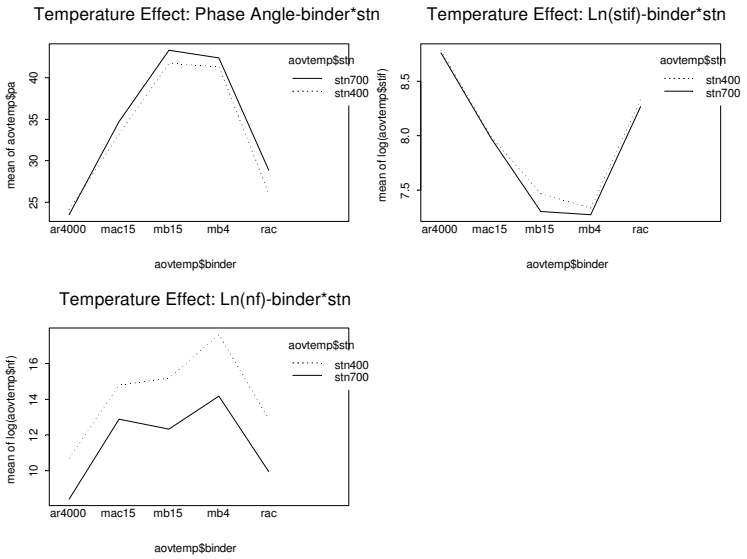

Figure B.11: Interaction plots of *binder*stn*.
(Temperature effect, FMLC, AV = 6%).

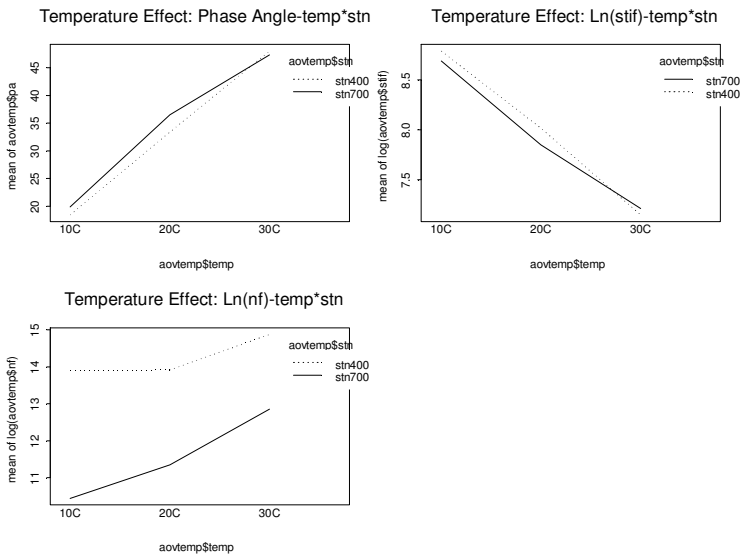

Figure B.12: Interaction plots of *temp*stn*.
(Temperature effect, FMLC, AV = 6%).

Using the above mentioned criteria for this dataset of temperature susceptibility fatigue tests, several findings are apparent:

- The *binder* is "important" to all three response variables, *pangle*, *lnstif* and *lnnf*.
- The *temp* is "very important" to both *pangle* and *lnstif* and "important" to *lnnf*.
- The *stn* is "very important" to *lnnf* and has no impacts on the *pangle* and *lnstif*.

B.2.3 Regression Analysis

Fitting, overfitting and residual analysis are important issues that have to be considered in regression analysis. Overfitting occurs when the regression model attempts to match a particular dataset too closely. It is recognized that most datasets contain a certain amount of "noise" or inherent randomness. As a consequence of overfitting, both the underlying trend and the noise are modelled. The Mallow's C_p criterion provides an effective tool for balancing the number of covariates and the penalty caused by overfitting. Residual analysis is used to verify the Gauss-Markov assumptions of normality, independence, and constant variance (homoscedasticity). Violations of any assumptions are normally corrected by variable transformation, such as taking the logarithm of the variable, or by modifying the model specification.

Inclusion of more covariates (main effects and interaction effects) in a regression model results in a higher value of R^2 but the risk of overfitting increases simultaneously. Hence, the regression analyses used in this study were iterative, but only the final models are presented.

Table B.2: Summary Statistics of Main Effects of Fatigue Tests.

Type of Test	Response Variables	Covariates																													
		binder				*grad*				*comp*				*cond*				*ac*				*av*				*temp*				*stn*			
		C	D	F	A	C	D	F	A	C	D	F	A	C	D	F	A	C	D	F	A	C	D	F	A	C	D	F	A	C	D	F	A
Temperature Effect (FMLC)	*pangle*		✓	✓	✓																					✓	✓	✓	✓				
	lnstif		✓	✓	✓																					✓	✓	✓	✓				
	lnnf		✓	✓	✓																						✓	✓	✓	✓	✓	✓	✓
Air-Void Content Effect (FMLC)	*pangle*		✓	✓	✓																												✓
	lnstif	✓	✓	✓	✓																				✓								✓
	lnnf		✓	✓	✓																									✓	✓	✓	✓
Aging Effect (FMLC)	*pangle*		✓	✓	✓										✓	✓	✓														✓	✓	✓
	lnstif	✓	✓	✓	✓										✓	✓	✓																✓
	lnnf		✓	✓	✓																									✓	✓	✓	✓
Compaction Effect (FMLC+LMLC)	*pangle*		✓	✓	✓						✓	✓	✓																				✓
	lnstif		✓	✓	✓						✓	✓	✓																				✓
	lnnf		✓	✓	✓						✓	✓	✓																	✓	✓	✓	✓
Gradation Effect (LMLC)	*pangle*		✓	✓	✓	✓	✓	✓	✓																								
	lnstif	✓	✓	✓	✓	✓	✓	✓	✓																						✓		✓
	lnnf		✓	✓	✓	✓	✓	✓	✓																					✓	✓	✓	✓
Pooled Fatigue Tests (FMLC+LMLC)	*pangle*		✓	✓	✓		✓	✓	✓		✓	✓	✓		✓	✓	✓									✓	✓	✓	✓				✓
	lnstif		✓	✓	✓	✓	✓	✓	✓		✓	✓	✓		✓	✓	✓								✓	✓	✓	✓	✓				✓
	lnnf		✓	✓	✓	✓	✓	✓	✓		✓	✓	✓												✓		✓	✓	✓	✓	✓	✓	✓

Note: 1. C: correlation matrix; D: design plot; F: factor plot; A: ANOVA result.

2. The four-in-a-row diagonal shaded area means the covariate is "very important" to the corresponding response variable.

Initial Stiffness

From the summary table of main effects (Table B.2), the *temp* and *binder* are the two major factors that have the main effects on the *lnstif*. Figure B.10 shows no obvious interaction effect of *binder* and *temp* on *lnstif*; however, the ANOVA result (Table B.1) indicates a possible interaction effect between *binder* and *temp*. To keep the model as simple and acceptable as possible, the *binder* and *temp* interaction were excluded.

The *leaps()* function of *Splus*®, based on the Mallows' C_p criterion, selected *binder* and *temp* as being the best subset of covariates. The selected subset with size 3 (including the intercept term) has C_p=*2.538*, which closely complies with the Mallows' C_p criterion that $C_p \cong p$.

The final model chosen for initial stiffness is:

$$E(\ln stif) = \underset{(0.0682)}{9.5115} - \underset{(0.0407)}{0.3949}\,binder1 - \underset{(0.0235)}{0.3300}\,binder2 - \underset{(0.0166)}{0.1875}\,binder3 + \underset{(0.0129)}{0.0883}\,binder4 - \underset{(0.0031)}{0.0775}\,temp \qquad \textbf{(B.1)}$$

$$R^2 = 0.93$$

where *stif* has the unit MPa and the *temp* is in °C. Note that the $E(\ln stif)$ term is the expected value of ln*stif* and the number in parentheses is the standard error of the estimate of regression coefficient.

The residual standard error is 0.244 on 84 degrees of freedom, $R^2 = 0.93$ (i.e. the regression line explains as high as 93 percent of the variation in the data) and the F-statistic pertaining to the test of the hypothesis that all parameters equal zero is 215 on 5 and 84 degrees of freedom, resulting in a p-value of 0. Accordingly, the hypothesis that all regression coefficients are zeros can be rejected.

It should be recognized that the *binder* term in the formulation is a category covariate. The category covariate (or factor) needs to be coded (or parameterized) by contrasts so as to be manipulative with numeric covariates in the linear regression. The default contrasts utilized in *Splus*® is the Helmert parameterization (9). Table B.3 lists the Helmert contrasts for all the category covariates utilized in this project. For example, to determine the regression equation of *lnstif* for MB4, according to the contrast, the values need to be set as follows:

binder1 as 0, *binder2* as 0, *binder3* as 3, and *binder4* as -1.

This results in the following *lnstif* regression equation for the MB4 mixes:

$$E(\ln stif) = 8.8607 - 0.0775\,temp \qquad \textbf{(B.2)}$$

Table B.3: Contrast Tables of Category Covariates used in the Regression Analysis

(a) Factor *binder*: for all the effects other than gradation effect				
Binder	*binder1*	*binder2*	*binder3*	*binder4*
AR4000	-1	-1	-1	-1
MAC15	1	-1	-1	-1
MB15	0	2	-1	-1
MB4	0	0	3	-1
ARB	0	0	0	4
(b) Factor binder: for gradation effect				
Binder	*binder1*	*binder2*		
MAC15	-1	-1		
MB15	1	-1		
MB4	0	2		
(b) Factor cond: for aging effect				
Aging	*cond*			
aging	-1			
none	1			
(b) Factor comp: for compaction effect				
Compaction	*comp*			
FMLC	-1			
LMLC	1			
(b) Factor *grad*: for gradation effect				
Gradation	*grad*			
DG	-1			
GG	1			

A graphical representation of the residual analysis of the fit is summarized in Figure B.13. Figure B.13a shows a plot of estimated residuals versus fitted values. A slight parabolic trend can be seen in this figure. An inclusion of the interaction term *binder*temp* will correct this problem. However, the increasing complexity of model specification outweighs the increase of R^2. Hence, the main effect model is preferable to the model including the interaction effect. The assumption of homoskedasticity appears reasonable. Figure B.13c plots the cook's distances (10), which is frequently used as a measure of influence in linear regression. It suggests that the specimens G9-DGAC-20B, G9-MB15-30B, and G9-MB15-7A are three influential tests in the linear regression analysis. The Cook's distance accompanied with the normal probability plot, or quantile-quantile plot (QQplot), or the histogram of residuals can be used to identify the influential points and the possible outliers. Figures B.13b and B.13d show the QQplot and histogram of residuals and indicate an appropriate normal distribution. The distribution of estimated residuals is generally close to a normal distribution (i.e. the Gauss-Markov assumption of a normal distribution of the estimated residuals is confirmed).

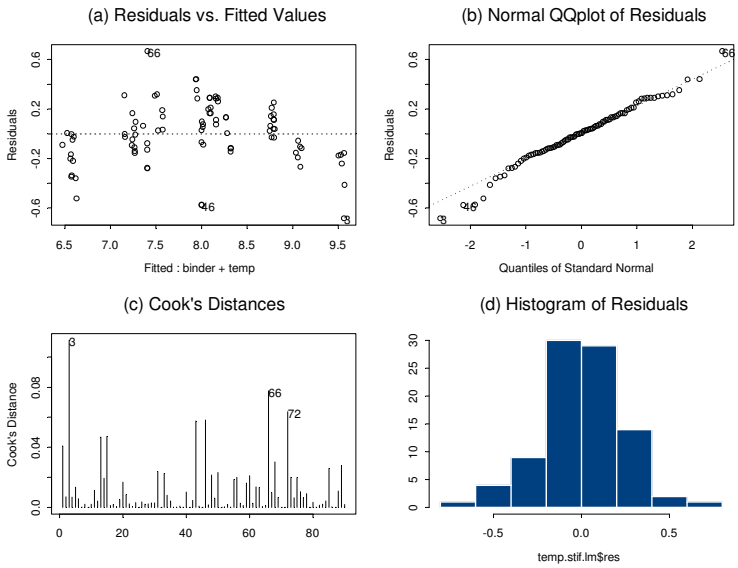

Figure B.13: Residual plots of *lnstif*.
(Temperature effect, FMLC, AV = 6%).

Fatigue Life

From the summary table of main effects for the temperature effect listed in Table B.2, the factors *binder* and *temp* are "important" to *lnnf*; and the *stn* is "very important" to *lnnf*. The ANOVA result shows the possible two-term interaction existed in *binder*temp* and *temp*stn*. However, the interaction plots shown in Figures B.10 through B.12 are less evident. Using *Splus*®, the best subset chosen based on the Mallows' C_p criterion was the full set of *binder*, *temp*, and *lnstn* (including the intercept term), with a C_p value of 4.0.

A compromise made according to previous discussions and regression fitting leads to the following final regression model of fatigue life:

$$E(\ln nf) = \underset{(2.8240)}{-22.7041} + \underset{(0.1629)}{2.1694}\,binder1 + \underset{(0.0941)}{0.7178}\,binder2 + \underset{(0.0696)}{0.8797}\,binder3 - \underset{(0.0517)}{0.3740}\,binder4 + \underset{(0.0127)}{0.0837}\,temp - \underset{(0.3711)}{4.5027}\ln stn \qquad \textbf{(B.3)}$$

$$R^2 = 0.88$$

Care needs to be taken in interpreting the coefficient of *binder*, and the contrast scheme in Table B.3 should be followed.

The residual standard error of the fit is 0.9774 on 81 degrees of freedom, R^2 = 0.88, and the F-statistic associated with the test of the hypothesis that all the parameters equal zeros is 100.6 on 6 and 81 degrees of freedom, resulting in a p-value of 0, which rejects the hypothesis. Note that in this regression two

outliers, G9-MB4-14A and G9-MB4-20B (extremes of fatigue tests in Appendix A: Table A.5), were eliminated according to the Cook's distance.

Figure B.14 plots the residual analysis of the fatigue life fit. No strong pattern is perceived in Figure B.14a indicating that the suggested model is appropriate. In Figure B.14c, the Cook's distance shows a number of influential points. Both the QQ plot in Figure B.14b and the histogram of residuals in Figure B.14d are acceptable by complying with the Gauss-Markov assumptions.

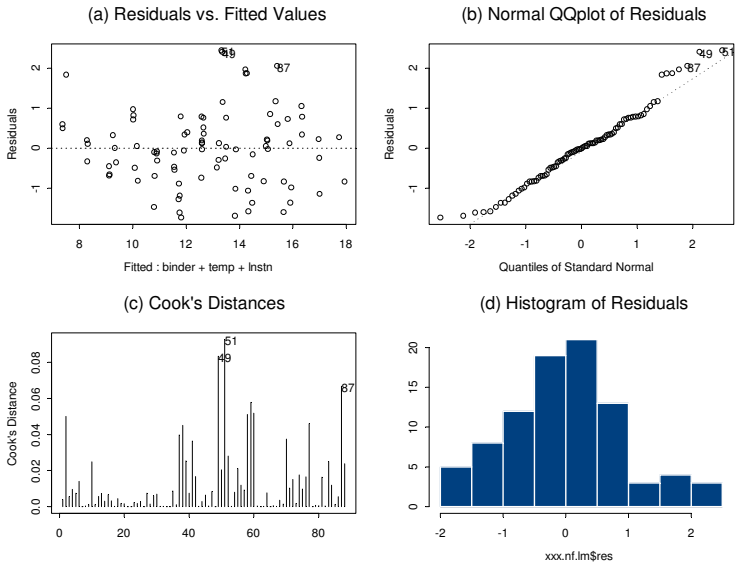

Figure B.14: Residual plots of *lnnf*.
(Temperature effect, FMLC, AV = 6%).